STRUCTURAL SYSTEMS
RESEARCH PROJECT

Report No.
SSRP – 2003/12

SEISMIC QUALIFICATION REQUIREMENTS FOR TRANSFORMER BUSHINGS

by

Howard Matt

André Filiatrault

Final Report to the Pacific Earthquake Engineering Research Center (PEER) for Task 406 of the PEER Lifeline Directed Studies Program

May 2004

Department of Structural Engineering
University of California, San Diego
La Jolla, California 92093-0085

University of California, San Diego
Department of Structural Engineering
Structural Systems Research Project

Report No. SSRP-2003/12

SEISMIC QUALIFICATION REQUIREMENTS FOR TRANSFORMER BUSHINGS

by

Howard Matt

Graduate Student Researcher

André Filiatrault

Professor of Structural Engineering

Department of Structural Engineering
University of California, San Diego
La Jolla, California 92093-0085

May 2004

DISCAIMER

Opinions, findings, conclusions and recommendations expressed in this report are those of the authors and do not necessarily reflect views of the Pacific Earthquake Engineering Research Center (PEER).

ACKNOWLEDGEMENTS

This project was sponsored by the Pacific Earthquake Engineering Research Center's Program of Applied Earthquake Engineering Research of Lifeline Systems supported by the California Energy Commission, California Department of Transportation, and the Pacific Gas & Electric Company.

This work made use of Earthquake Engineering Research Centers Shared Facilities supported by the National Science Foundation under Award Number EEC-9701568.

We greatly appreciated the input and coordination provided by Dr. Michael Riemer from PEER and Mr. Eric Fujisaki from the Pacific Gas and Electric Company (PG&E) during the development of this research project. The support of Mr. David Chambers from the California Energy Commission is also gratefully acknowledged.

Special thanks must be also given to Mr. Bill Gundy for supplying two of the original transformer models, Dr. Gerald Pardoen for his impact test data, as well as Mr. Rulon Fronk, Dr. Anshel Schiff, and Mr. Chris Stearns for their individual contributions to the research task.

TABLE OF CONTENTS

LIST OF FIGURES

LIST OF TABLES

ABSTRACT

High voltage transformer bushings have shown vulnerability to damage during past seismic events. One acknowledged explanation for this vulnerability is that the influence of the transformer and the local flexibility around the bushing actually amplifies the stresses experienced by the bushing during ground motion shaking. Guidelines for the seismic qualification of electrical equipment implicitly consider this amplification through a constant amplification factor of 2.0 between the amplitude of the ground motion and the amplitude of the motion at the base of the bushing. This research task investigates the factors that most greatly influence the dynamic response of high voltage bushings as well as attempts to quantify the ground motion amplification for various high voltage transformers. Numerical models of four different high voltage transformers were developed and used for modal and dynamic time-history analyses. In addition, system identification and seismic shake table tests were performed on a full-scale 525 kV transformer-mock bushing system. A numerical model of the test configuration was created to predict the seismic test results through dynamic time-history analyses.

The local flexibility of the transformer near the base of the bushing proved to greatly influence the dynamic characteristics and seismic response of the transformer-bushing assembly. It was concluded from the numerical studies that the assumed amplification factor of 2.0 is not necessarily conservative for all high voltage transformer-bushing systems. However, specific retrofits could be implemented on existing transformers to reduce the dynamic response of high voltage transformer bushings.

1. INTRODUCTION

1.1. Background on Seismic Vulnerability of Electrical Substation Equipment

Electrical Substations are critical components in the electrical network that supplies power for industrial, business and residential use. Several large structural systems exist within these substations, each contributing to the overall functionality of the substation. Figure 1.1 shows a high voltage electrical substation in San Diego, California. Recent seismic events, such as the 1989 Loma Prieta and 1994 Northridge earthquakes, again demonstrated the vulnerability of particular electrical components to moderate and high shaking. Failure commonly occurred in support structures of conductors, anchorage of high voltage equipment and in bushings mounted to transformers and circuit breakers. The damage inflicted upon electrical substation equipment by the Loma Prieta and Northridge earthquakes resulted in roughly $283 million worth of losses [1].

Figure 1.1 - Typical Electrical Substation.

Although disruption of electrical service was minimized by the redundancy within the system, the significant damage incurred from these events as well as prior

earthquakes have motivated a number of organizations to investigate the seismic vulnerability of substation electrical equipment. Several research tasks funded by Pacific Gas and Electric (PG&E), Pacific Earthquake Engineering Research Center (PEER) and the California Energy Commission (CEC) have been initiated with the purpose of gaining knowledge on the seismic response of various substation equipment, establishing better methods of seismically qualifying equipment, and ultimately reducing the seismic vulnerability of substation equipment such that damage can be greatly reduced in future seismic events. This research task investigates the factors that most greatly influence the dynamic response of high voltage bushings and attempts to quantify the amplification for various high voltage transformers

1.2. Background on High Voltage Transformers and Transformer Bushings

High voltage transformers are essential pieces of equipment in any electrical substation. The function of these transformers is to step up or step down the voltage within the transmission lines. Bushings are cantilever like components that protrude vertically, or at a slight angle from the top of the transformer. Porcelain bushings are often composed of a number of annular rings stacked upon one another and post-tensioned together by the internal conductor. During service, the bushing is filled with oil to provide insulation. Bushings are used to connect the electrical coils within the transformer to the external power lines. The structural integrity of bushings is provided by the external insulating material, typically made up of porcelain. Figure 1.2 shows a three phase 230 kV transformer along with bushings. Note that the bushings are the six innermost cantilevers shown protruding from the top of the transformer.

Figure 1.2 - 230 kV Transformer.

Due to the nature of their design, bushings are prone to seismic damage and have proven to be one of the most vulnerable pieces of substation equipment during earthquakes. As a general rule, the higher the voltage rating of a bushing, the heavier and taller it is and therefore the more susceptible it is to damage during seismic loading. A typical 230 kV transformer bushing is shown in Fig. 1.3.

Figure 1.3 – Typical 230 kV Transformer Bushing

Porcelain bushing failure typically occurs through the fracturing or slipping of the porcelain at the connection point between the transformer and the bushing also known as the flange location. The most common failure mode for bushings is oil

leakage due to slipping of the porcelain at the flange location. Due to the size and complexity of the transformer-bushing system, replacement of failed bushings can prove to be a timely and expensive task. For this reason, the IEEE-693 1997 standard [2], which provides seismic design recommendations for substation equipment, has adopted specific design criteria for high voltage bushings in order to ensure adequate seismic performance.

1.3. IEEE-693 Seismic Qualification Guidelines for Electrical Substation Equipment

Like any structural system located in an earthquake prone region, seismic vulnerability of electrical substation equipment must be addressed during the design process. For this reason, specific methods of seismically qualifying substation equipment have been established. These methods and associated criteria are defined within the Institute of Electrical and Electronics Engineers (IEEE) 693-1997 Standard [2]. The IEEE-693 document was written as a guideline for the seismic design of substations. Although substation designers are not required to follow the guidelines within this document, the IEEE seismic design recommendations have generally been adopted for new design by most utilities in seismically active areas. Substation equipment can be qualified by doing static analysis, dynamic analysis, or shake table testing depending upon the type of equipment and voltage rating. The IEEE-693 standard required response spectra (RRS) shown in Fig. 1.4 are used for the analysis and testing of equipment. There are three levels of qualification, high, moderate and low. The infinite frequency or zero period acceleration (ZPA) of the high and moderate RRS is .5g and .25g respectively. The level at which equipment must be qualified is dependant upon the seismicity of the region where it will be in service.

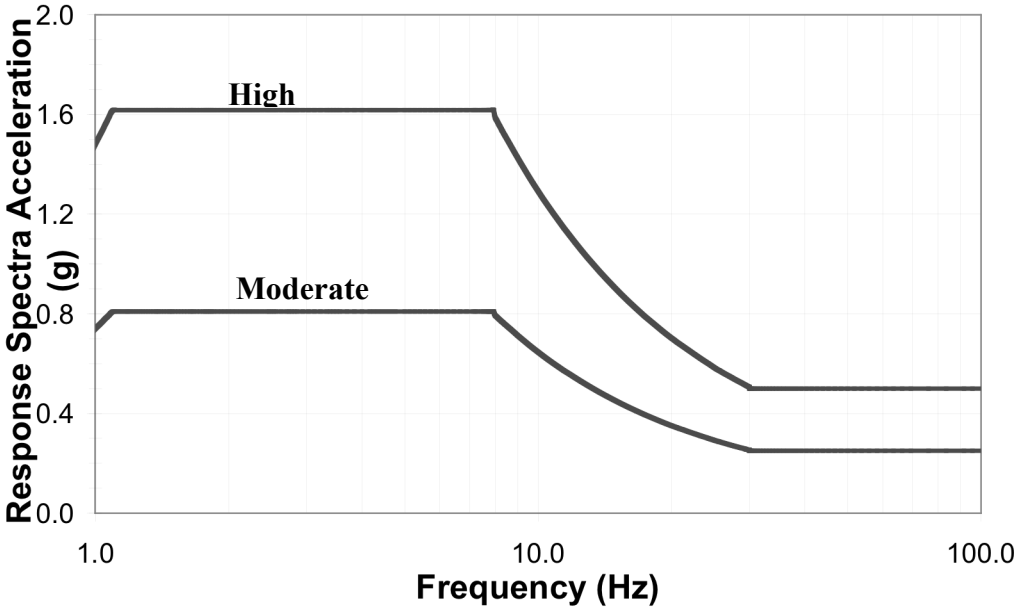

Figure 1.4 - 2% Damped High (.5 ZPA) and Moderate (.25 ZPA) Required Response Spectra defined within the IEEE-693 Standard [2]

The qualification of transformer bushings is specifically addressed within the IEEE 693 standard. The majority of research interests and seismic concerns are focused on bushings rated at voltages exceeding 161kV due to their higher susceptibility to earthquake damage. The IEEE-693 standard states that bushings with voltage ratings exceeding 161kV must be qualified by time-history shake table tests. Since placing a full-scale transformer-bushing system upon a shake table is not economically feasible on a routine basis, bushing qualification tests are performed by placing bushings upon a rigid frame in lieu of the transformer body itself.

Although the transformer body is assumed to be fairly rigid, it is acknowledged that the supporting structure of the bushing, consisting of the turret and transformer frame, amplifies the ground acceleration. Therefore, the IEEE 693

standard assumes that the motion at the base of the bushing is equal to the ground motion multiplied by a factor of 2. Therefore, during bushing qualification through shake table testing, the rigid frame is subjected to ground motions that match the required response spectrum scaled such that it accounts for this amplification. Figure 1.5 shows a 230 kV bushing qualification shake table test setup [3]. Note that a rigid frame supports the bushing and that the input motion shall match 2 times the IEEE-693 high required response spectrum shown in Fig. 1.4.

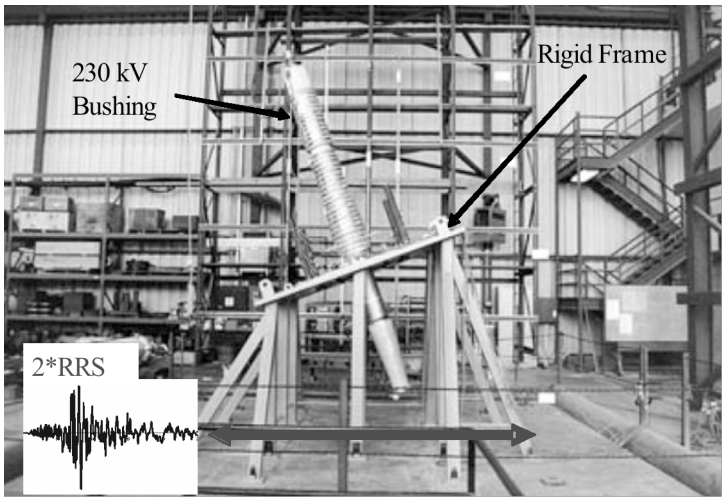

Figure 1.5 - Shake Table Seismic Qualification Test of 230 kV Bushing [3].

1.4. Scope of Research

Previous shake table tests performed as part of PEER projects [3,4,5], as well as the large number of bushing failures that occurred during recent seismic events, have raised doubts about the appropriateness of the bushing qualification tests and more specifically whether the amplification factor of two is indeed valid. Knowledge of exactly how much amplification occurs, and what key parameters of the supporting structure affect this amplification is limited.

There are three specific objectives of this Task 406 of the PEER Lifeline Program. The first objective is to identify the critical parameters of supporting structures that affect the seismic response of a bushing. The second objective of this research is to quantify a range of values for these critical parameters for which the shake table requirements remain valid. The final objective is to define any necessary changes to the requirements for bushing shake table qualification tests that are consistent with the critical parameters identified and possibly recommend design requirements for transformer manufacturers.

The research is broken into two main parts. The first is a series numerical finite element study of various transformer structures and the second is an experimental study during which shake table tests were performed upon a full-scale transformer-bushing system.

The numerical studies were completed after developing three-dimensional finite element models of four different transformers of various manufacturers, sizes and voltages. Using these finite element models, three numerical studies were performed. The first study was conducted to compute the amount of motion amplification that occurs between the ground and top of the transformer tank. This was done by performing linear dynamic time-history analyses on the models and then computing a "spectral amplification", which determines the amount of horizontal acceleration amplification that occurs between the base of the bushing and the ground as a function of frequency. The spectral amplification at the frequency of the bushing was then compared with the dynamic amplification factor of 2.0 defined within the IEEE-693 standard.

The second numerical study was performed in an attempt to reduce the seismic response of transformer-bushing systems. Various retrofit schemes were analyzed with two of the transformer models. The main objective was to find ways to retrofit the top of transformers near the bushing such that the spectral amplification between the ground and base of the bushing could be reduced to below 2.0.

The final numerical study was done to compare the dynamic response of bushings attached to a rigid frame, as is the case for seismic qualification tests, and that of bushings mounted on a transformer tank. The study consisted of dynamic time-history analyses of various bushings using a time-history that matches the IEEE-693 high required response spectrum. The main objective of this study was to determine the amplification in bending stresses experienced by the bushing rather than in spectral response.

The final phase of this research task was to conduct full-scale shake table tests of a 525 kV transformer-mock bushing system. The transformer specimen tested consisted of the steel tank shell without its internal components (i.e. the core, coil and oil). The tank was also stripped of all extraneous appendages such as its radiators, bushings, surge arrestors and control cabinet. Due to their high costs and inherently brittle material, obtaining a real porcelain transformer bushing for testing purposes proved to be impractical. In addition, there was a risk of failing the bushing if a real transformer bushing was used during seismic tests. Therefore, a mock bushing was used in leau of a real transformer bushing during the seismic tests. This mock bushing possessed the same dynamic characteristics of a true transformer bushing.

Frequency evaluation and damping tests were performed to determine the dynamic properties such as predominant natural frequencies and modal viscous

damping values of the transformer and mock bushing. In addition, shake table time-history tests were performed using five different input time-histories at various input amplitude. During the seismic tests, instrumentation recorded the accelerations, displacements and strains at key locations along the transformer and bushing. The shake table tests were used to determine the true dynamic amplification that occurs between the base of the transformer and the base of the bushing. A numerical model of the test configuration was created to predict the modal properties of the system as well as the seismic test results through modal and dynamic time history analysis, thereby validating results from the numerical studies performed.

1.5. Report Layout

The report is organized into six main chapters. This first chapter provided a general overview of the research project. The next three chapters detail the three numerical studies performed upon the developed finite element models. Chapter two describes the numerical study done to evaluate the spectral amplification values of various high voltage transformers. Chapter three deals with potential retrofit schemes that could be utilized to reduce the amount of spectral amplification that occurs between the ground and the base of the bushing. The modified models were analyzed to determine the effectiveness of each retrofit scheme. The fourth chapter of the report details a numerical study that explicitly evaluates the IEEE-693 seismic qualification procedure for high voltage bushings.

The fifth chapter of the report describes the experimental testing of a full-scale 525 kV transformer-mock bushing system. In addition to the testing results for the white noise, damping and time-history tests, a comparison between the

experimental results and the predictions of a numerical model representative of the test configuration is presented. The last chapter summarizes the overall report and provides the final conclusions drawn from the various studies.

2. NUMERICAL STUDY ON THE SPECTRAL AMPLIFICATION ANALYSIS FOR HIGH VOLTAGE TRANSFORMERS

2.1. Scope of Study

The purpose of this study is to quantify the amplification of ground motion that occurs between the transformer foundation and the base of the bushing for various existing transformers. The IEEE-693 standard assumes that the amplification is a constant factor of 2.0, independent of frequency. The appropriateness of this test method has been questioned after significant damage to transformer bushings in service were observed during recent earthquakes, while similar bushings were undamaged in shake table tests. The amplification was quantified by performing linear dynamic time-history analyses on four different finite element models using the structural analysis program SAP 2000 [6]. The analysis consisted of running 20 different historical strong ground motion time-histories scaled to the 2% damped high required level response spectrum shown in Fig. 1.4. From the results of these analyses, the spectral amplification as a function of frequency was computed by taking the ratio of the 2% damped horizontal response spectrum for the acceleration obtained at the base of the bushing to that of the ground acceleration. The spectral amplification at the frequency of the bushing was then compared with the dynamic amplification factor of 2.0 defined within the IEEE-693 standard.

2.2. Description of Transformers Used in Numerical Study

There are many different types of high voltage transformers that vary greatly in weight, size and geometry. Therefore, the dynamic response of transformers, even of the same voltage rating, can widely differ. In an attempt to capture these

variations, four different transformers were modeled using finite elements in order to gain a better understanding of the supporting structure's seismic response for various transformer sizes and manufacturers. The four transformer models were: a 525 kV Transformer A, a 500 kV Transformer B, a 230 kV Transformer C, and a 500 kV Transformer D. Appendix A presents drawings of these four transformers. The 525 kV Transformer A weighs 463 kips and has dimensions of 8.8 ft x 9.9 ft x 22.8 ft. The 500 kV Transformer B weighs 301 kips and has dimensions 5.7 ft x 11.4 m x 15.8 ft. The 230 kV Transformer C weighs 478 kips and has dimensions 10.0 ft x 24.2 ft x 14.4 ft. The 500 kV Transformer D weighs 673 kips and has dimensions of 10.8 ft x 26.0 ft x 16.8 ft. Finite element meshes and photographs of the transformers considered in the study are shown below in Figs. 2.1 through 2.7. Note that Transformers A and B have been stripped of their radiators, bushings, surge arrestors and oil conservator tanks.

Figure 2.1 - 525 kV Transformer A.

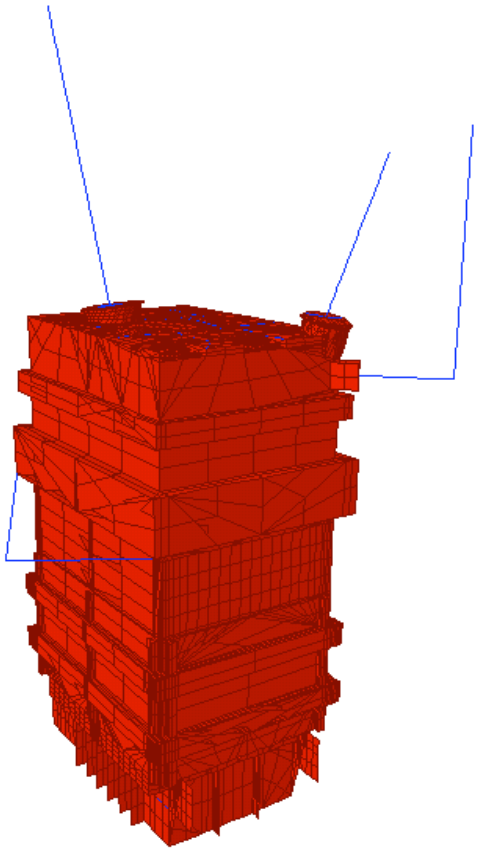

Figure 2.2 - 525 kV Transformer A Finite Element Mesh.

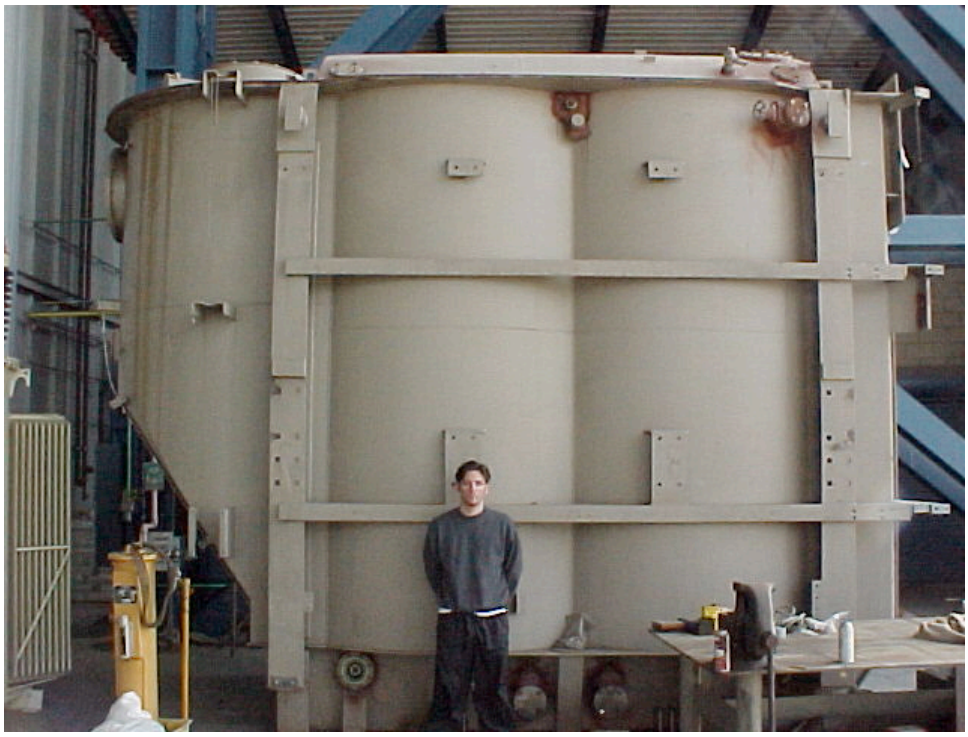

Figure 2.3 - 500 kV Transformer B.

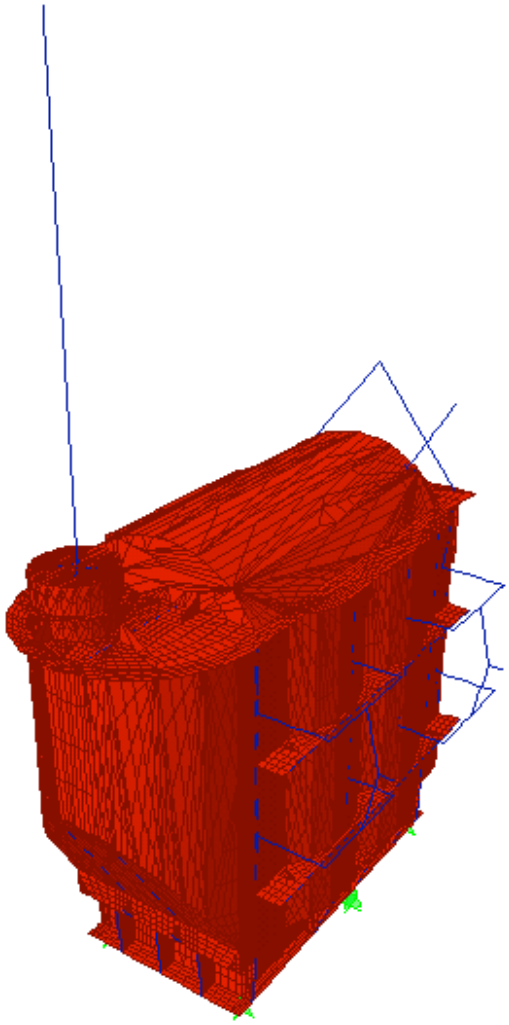

Figure 2.4 - 500 kV Transformer B Finite Element Model.

Figure 2.5 - 230 kV Transformer C and Finite Element Model.

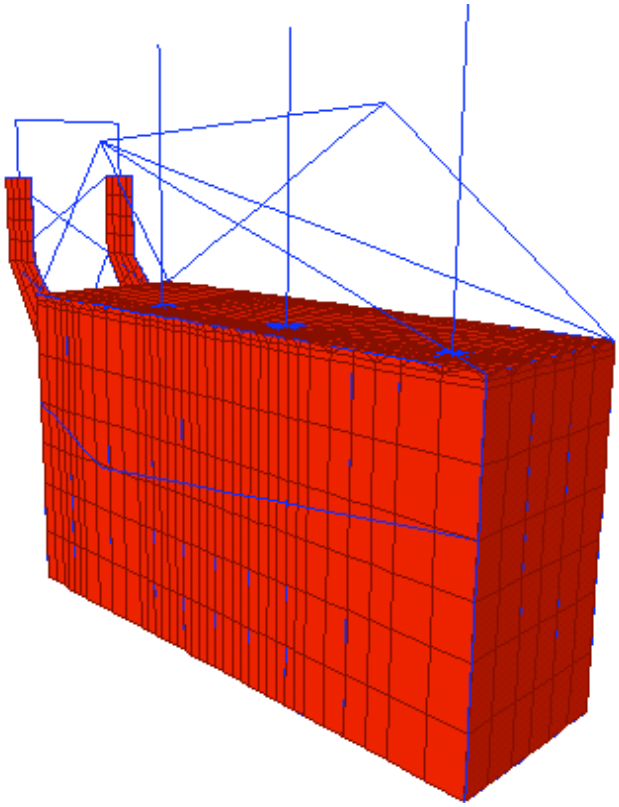

Figure 2.6 - 230 kV Transformer C Finite Element Model.

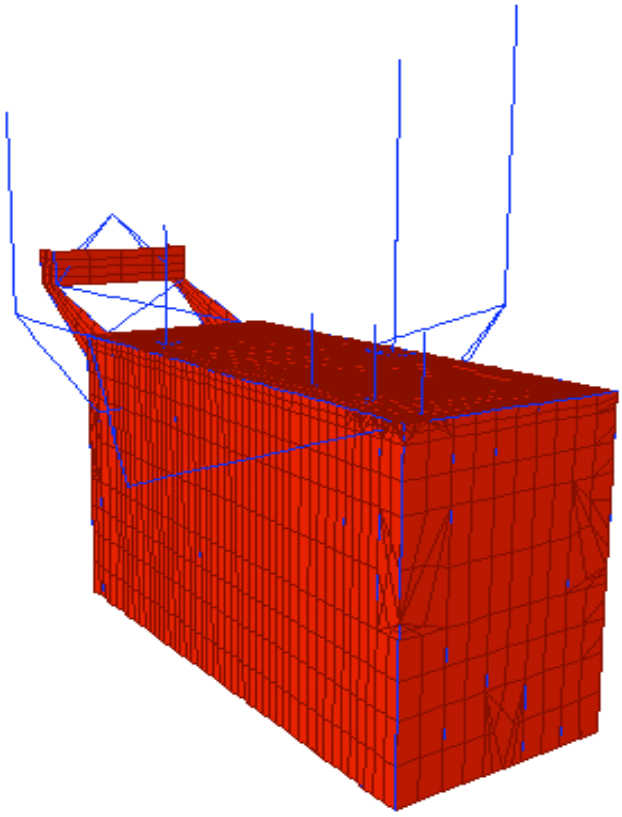

Figure 2.7 - 500 kV Transformer D Finite Element Model.

Although most transformers vary greatly in weight, size, and geometry, they all contain a certain number of key common components: the transformer frame or tank, the core and coil contained within the tank, radiators attached to the outside, bushings mounted on the top of the tank, oil contained within the tank, and often an oil conservator tank also attached to the top of the tank. The majority of a transformer's mass is comprised of the core, copper coils and oil. The tank walls made of steel with a typical thickness of 0.5 in, and stiffeners such as channels, I-beams, or plates welded to the tank walls provide the majority of the lateral stiffness of a transformer tank.

2.3. Description of Transformer Finite Element Models

Each three-dimensional finite element model was built using the structural analysis program SAP2000 [6]. However, before developing the finite element models, certain modeling assumptions had to be made. The first of which was how to model the oil. Oil contained within transformers is generally filled up to the top of the tank. For this condition, oil-sloshing effects become negligible and were not accounted for in modeling. To account for the mass of the oil within the tank, additional mass was symmetrically added to the vertical perimeter of the steel tank walls leading to an appropriate location for the center of gravity of the oil.

Due to the nature of its design, the core and coil can safely be assumed as rigid. However, one significant issue is related to the bracing of the core and coil to the interior walls of the transformer. If it is not braced, then the core and coil provides no stiffness to the tank. The tank and core will act as two separate and independent structures; therefore the mass of the core should not be included in the dynamic analysis. On the other hand, if the core and coil is rigidly braced to the

core and coil, then the whole transformer will be essentially rigid and the mass of the core should be included in the dynamic analysis. Although some cores and coils are lightly braced to the transformer body, most are not. Even the ones that are braced may only be braced at mid-height or braced by wood shims between the core and transformer shell. Therefore it was decided not to include any stiffness from the core and coil as well as neglect this mass in the dynamic modeling. Therefore, the model represents an unbraced core and coil.

Another assumption made was that the radiators and oil conservator tank are rigidly attached to the transformer frame. This allowed for simplification of the model and eliminated some of the non-critical local modes of vibration. To ensure the validity of this assumption, comparison of the transverse and longitudinal frequencies of the transformers were done when allowing for flexibility of these components. It was concluded that making these appendages rigid had no significant effect on the longitudinal and transverse modal properties of both the bushing and transformer body. The appropriate masses of each radiator and oil conservator tank were added at their respective center of gravities.

All bushings were modeled as multiple beam elements with the appropriate geometry, stiffness, and mass. Much of the flexibility of transformer bushings results from gaskets used to prevent oil leaks at the flange connection and at various other locations along the bushing height. Therefore, gasket elements were introduced into the bushing models at the proper locations in order to capture this additional flexibility. Bushing and gasket models were based upon information from available bushing qualification reports and structural drawings included in the transformer manufacturer's reports.

The final assumption dealt with the support conditions of the transformers. Pin supports were used at bolt locations and fully fixed conditions were used at weld locations. Since transformers are typically supported by a concrete pad, roller supports were added under the tank base to prevent out of plane bending of the bottom shell.

Transformer frames were modeled as shell elements with the appropriate thickness and mass. The shell elements allowed for in-plane deformation and out-of-plane bending. Beam elements as well as appropriate shell elements were used for modelling the stiffeners attached to the tank sides. The geometry, thickness and location of all walls, plates and beams were obtained through manufacturer's structural drawings, surveying, and previously provided static models [7, 8, 9].

The weights of various transformer components were determined from the manufacturer's structural drawings. Table 2.1 shows breakdowns of the weights used in each of the finite element models.

Table 2.1 - Component Weights of Transformer Models.

Transformer Component	525 kV Transformer A	500 kV Transformer B
	Weight (kips)	Weight (kips)
Exterior Tank	67.0	30.5
Oil within Tank	77.3	62.0
Oil conservator tank including oil	Not Applicable	11.2
All Radiators including oil	92.8	10.9
All High voltage bushings	3.0	2.9
All Low voltage bushing	1.1	0.7
Tot. weight excluding core and coil	241.2	118.2

Transformer Component	230 kV Transformer C	500 kV Transformer D
	Weight (kips)	Weight (kips)
Exterior Tank	36.6	71.6
Oil within Tank	28.0	82.0
Oil conservator tank including oil	128.0	57.0
All Radiators including oil	21.1	41.9
All High voltage bushings	3.06	3.3
All Low voltage bushing	1.5	1.4
Tot. weight exluding core and coil	218.3	257.2

2.4. Modal Analysis of Transformer Models

Due to the complexity of the finite element models, the number of modes to be considered during analysis had to be greatly reduced. For each model, enough modes were considered such that at least 90% of the total modal mass participation was accounted for in the two principal horizontal directions. The first few modes of vibration were generally associated with the deformation of extraneous elements such as oil conservators, surge arrestors and bushings. The modes that contributed the largest percentage of total modal mass participation were that of transformer frame in the transverse and longitudinal direction. Appendix B shows an illustration of the bushing and transformer modes for each of the transformer models. Tables 2.2 to 2.5 displays the frequencies and modal mass participation for each mode included in the spectral amplification analysis of the four transformers.

For each model, the transverse (narrow) direction had a lower transformer tank natural frequency than in the longitudinal direction. The transformer tank frequencies, summarized in Tables 2.2 to 2.5, are 8.4, 14.2, 10.8 Hz, and 10.5 in the transverse direction and 11.4, 25.3, 25.1, and 20.8 Hz in the longitudinal direction for transformers A, B, C and D, respectively.

The high voltage bushing natural frequencies also shown in Table 2.2 to 2.5 are 2.9, 3.2, 9.1, and 3.4 Hz in the transverse direction and 3.4, 4.9, 10.3, and 8.4 Hz in the longitudinal direction for transformers A, B, C and D respectively. It is worth noting that these frequencies are representative of the modes of vibration of the bushing attached to the transformer supporting structure. Bushings mounted to rigid frames will have much higher frequencies due to the loss of flexibility in the supporting top plate. Typical natural frequencies for 500 kV bushings are around 3-4 Hz when attached to the transformer vs. roughly 8-9 Hz when rigidly attached.

For 230 kV transformer bushings, the natural frequencies are around 6-10 Hz when supported by the transformer vs. 14-20 Hz when rigidly attached. Appendix C presents transformer-bushing frequencies under rigid and transformer mounted conditions.

Table 2.2 - Natural Frequencies, Mode Shape Descriptions, and Modal Mass Participation for Modes Considered in 525 kV Transformer A Analysis.

Mode	Freq. (Hz)	Description	Individual Mode (% Participation)		Cumulative Mode (% Participation Summation)	
			Transverse	Longitudinal	Transverse	Longitudinal
1	2.7	Surger Arrestor (1st Mode)	0.2	0.2	0.2	0.2
2	2.9	H.V. Bushing (1st Mode)	1.0	0.3	1.2	0.4
3	3.0	Surger Arrestor (2nd Mode)	0.1	0.1	1.4	0.5
4	3.4	H.V. Bushing (2nd Mode)	0.4	0.9	1.8	1.4
5	8.4	Transformer Frame (Tran)	67.5	0.0	69.2	1.4
6	11.4	Transformer Frame (Long)	0.0	72.2	69.2	72.8
7	13.2	H.V. Bushing (3rd Mode)	0.0	0.2	69.3	73.0
8	14.6	Surger Arrestor (3rd Mode)	0.3	0.9	69.5	74.0
9	15.3	Surger Arrestor (4th Mode)	0.5	0.4	70.0	74.3
10	20.2	Trans. Frame (Tran 2nd Mode)	13.6	0.0	83.7	74.4
11	24.8	Trans. Shell (Out of Plane Bending)	0.0	0.7	83.7	75.1
12	33.9	Trans. Frame (Long. 2nd Mode)	0.1	13.5	83.8	88.5
13	42.8	Trans. Frame Torsional Mode	2.2	0.1	86.0	88.6
14	50.7	Trans. Shell (Out of Plane Bending)	7.0	0.6	93.0	90.0

Table 2.3 - Natural Frequencies, Mode Shape Descriptions, and Modal Mass Participation for Modes Considered in 500 kV Transformer B Analysis

Mode	Frequency (Hz)	Description	Individual Mode (% Participation)		Cumulative Mode (% Participation Summation)	
			Transverse	Longitudinal	Transverse	Longitudinal
1	3.2	H.V. Bushings (1st Mode)	3.0	0.3	3.0	0.3
2	4.9	H.V. Bushings (2nd Mode)	0.4	2.8	3.4	3.1
3	14.2	Transformer Frame (Tran)	72.4	0.0	75.7	3.1
4	21.9	Tran. Frame & L.V. Bushing (Long)	0.0	26.9	75.7	30.0
5	25.3	Transformer Frame (Long)	0.0	38.8	75.7	68.8
6	34.7	H.V. Bushings (3rd Mode)	0.9	0.0	76.6	68.8
7	41.1	Tran. Shell (Out of Plane Bending)	0.4	0.1	77.0	68.9
8	41.9	Tran. Frame (2nd Mode Tran)	0.0	1.4	77.0	70.3
9	46.2	H.V. Bushings (4th Mode)	0.9	0.7	77.9	71.0
10	46.5	Oil Conservator Tank (Long)	0.1	0.5	77.9	71.5
11	54.9	Tran. Frame (3rd Mode Tran)	1.9	0.2	79.9	71.7
12	58.2	Tran. Shell (Out of Plane Bending)	2.5	0.5	82.4	72.2
13	63.1	Tran. Frame (2nd Mode Long)	0.1	4.4	82.4	76.6
14	68.1	Tran. Shell (Out of Plane Bending)	0.0	0.3	82.5	76.9
15	78.5	Tran. Frame (3rd Mode Tran)	0.0	11.1	82.5	88.0
16	82.2	Tran. Frame (2nd Mode Long)	9.9	0.1	92.3	88.2
17	94.7	Tran. Shell (Out of Plane Bending)	0.1	7.2	92.4	95.3

Table 2.4 - Natural Frequencies, Mode Shape Descriptions, and Modal Mass Participation for Modes Considered in 230 kV Transformer C Analysis.

Mode	Frequency (Hz)	Description	Individual Mode (% Participation)		Cumulative Mode (% Participation Summation)	
			Transverse	Longitudinal	Transverse	Longitudinal
1	9.1	H.V. Bushings (Tran)	17.9	0.0	17.9	0.0
2	10.3	H.V. Bushings (Long)	1.4	0.1	19.3	0.1
3	10.8	Tran. Frame (Tran)	23.8	0.1	43.1	0.2
4	11.6	Tran. Frame & Bushings (Tran)	13.5	0.1	56.6	0.3
5	12.0	Oil Conservator Tank (Long)	0.2	12.5	56.7	12.7
6	13.2	H.V. Bushings (Long)	0.0	0.0	56.8	12.7
7	13.5	H.V. Bushings (Long)	0.0	1.1	56.8	13.8
8	16.9	Tran. Frame (2nd Mode Tran)	13.8	0.0	70.6	13.8
9	19.2	Tran. Shell (Out of Plane Bending)	10.5	0.1	81.1	13.9
10	25.1	Tran. Frame (Long)	0.5	58.2	81.6	72.1
11	26.0	Tran. Frame (3rd Mode Tran)	9.2	2.3	90.8	74.4
12	37.2	Tran. Shell (Out of Plane Bending)	1.9	0.6	92.7	75.1
13	37.9	Tran. Frame (2nd Mode Long)	0.0	14.8	92.7	89.9
14	41.3	Tran. Shell (Out of Plane Bending)	0.3	1.3	92.9	91.2

Table 2.5 - Natural Frequencies, Mode Shape Descriptions, and Modal Mass Participation for Modes Considered in 500 kV Transformer D Analysis.

Mode	Frequency (Hz)	Description	Individual Mode (% Participation)		Cumulative Mode (% Participation Summation)	
			Transverse	Longitudinal	Transverse	Longitudinal
1	2.7	H.V. Arrestor (Mode 1)	0.2	0.0	0.2	0.0
2	2.9	H.V. Arrestor (Mode 2)	0.0	0.1	0.2	0.1
3	3.4	H.V. Bushing (Tran)	0.4	0.0	0.5	0.1
4	6.3	Oil Conservator Tank (Mode 1)	0.0	0.5	0.5	0.7
5	7.0	Oil Conservator Tank (Mode 2)	0.0	6.4	0.5	7.1
6	7.4	L.V. Arrestor (Mode 1)	7.1	0.0	7.7	7.1
7	8.1	L.V. Arrestor (Mode 2)	0.9	0.0	8.5	7.1
8	8.4	H.V. Bushing (Long)	0.0	0.4	8.6	7.5
9	8.4	H.V. Bushing (Mode 3)	4.6	0.0	13.2	7.5
10	9.9	Oil Conservator & L.V. Bushing	2.3	0.0	15.5	7.5
11	10.5	Transformer Frame (Tran)	37.5	0.0	53.0	7.5
12	11.0	H.V. Arrestor (Mode 3)	0.0	0.0	53.0	7.5
13	12.5	L.V. Bushing	0.0	0.0	53.0	7.5
14	14.9	L.V. Arrestor (Mode 3)	0.5	0.3	53.4	7.8
15	15.8	Tran. Frame (Tran 2nd Mode)	29.8	0.0	83.2	7.9
16	17.7	Tran. Shell (Out of Plane Bending)	1.5	0.0	84.6	7.9
17	19.9	H.V. & L.V. Bushings + Arrestors	0.6	0.5	85.2	8.3
18	20.8	Tran. Frame (Long Mode 1)	0.3	30.9	85.5	39.2
19	21.9	Tran. Frame (Long Mode 2)	0.4	37.6	85.9	76.8
20	22.8	Tran. Frame (Long 2nd Mode)	0.4	10.4	86.2	87.2
21	28.7	Tran. Shell (Out of Plane Bending)	0.1	0.0	86.3	87.3
22	37.8	Oil Conservator Tank (Mode 4)	5.6	0.1	91.9	87.3
23	44.9	Tran. Shell (Out of Plane Bending)	0.0	0.2	91.9	87.5
24	47.9	Tran. Shell + Oil Conservator	0.2	5.0	92.1	92.6

2.5. Earthquake Ground Motions Considered

The 20 ground motions chosen for this study are representative of feasible events that could occur within the California region [10]. These strong ground motions were recorded from various recent seismic events with varying fault mechanisms. All ground motions are such that the location of measurement was far enough from the fault rupture to be free of any near-fault directivity pulse conditions. Of the 20 ground motions, three are from the Superstition Hills 1987 earthquake, seven were recorded during the Northridge 1994 earthquake, six are from the Loma Prieta 1989 earthquake, two are from the Landers 1992 earthquake, and the last two are from the Cape Mendocino 1992 earthquake. Table 2.6 presents details of the 20 ground motions selected for the analytical study. Appendix D presents the acceleration time-histories for each earthquake record. The acceleration response spectra for each of these 20 records at 2% damping are presented in Appendix E.

Before the analyses were performed, each of the time histories were scaled to match the IEEE-693, 2% damped, high required response spectrum at the two fundamental frequencies of each transformer tank. The two fundamental transformer tank frequencies correspond to vibration in the transverse and longitudinal directions. The scaled mean response spectrum of all 20 earthquake records for each transformer and direction is shown in Figs. 2.8 through 2.15. The scaled peak ground accelerations for the ground motions in the longitudinal and transverse direction are presented for each transformer in Appendix F.

Table 2.6 - Earthquake Ground Motions Selected for Analysis.

Earthquake Event	Year	Mw	Station	PGA (g)
Superstition Hills	1987	6.7	Brawley	0.116
Superstition Hills	1987	6.7	El Centro Imp. Co. Cent.	0.258
Superstition Hills	1987	6.7	Plaster City	0.186
Northridge	1994	6.7	Beverly Hills 14145 Mulhol	0.416
Northridge	1994	6.7	Canoga Park - Topanga Can	0.356
Northridge	1994	6.7	Glendale - Las Palmas	0.357
Northridge	1994	6.7	LA - Hollywood Stor FF #	0.231
Northridge	1994	6.7	LA - N Faring Rd	0.273
Northridge	1994	6.7	N. Hollywood - Coldwater Can.	0.271
Northridge	1994	6.7	Sunland - Mt Gleason Ave	0.157
Loma Prieta	1989	6.9	Capitola	0.529
Loma Prieta	1989	6.9	Gilroy Array # 3	0.555
Loma Prieta	1989	6.9	Gilroy Array # 4	0.417
Loma Prieta	1989	6.9	Gilroy Array # 7	0.226
Loma Prieta	1989	6.9	Hollister Diff. Array	0.279
Loma Prieta	1989	6.9	Saratoga - W Valley Coll.	0.332
Cape Mendocino	1992	7.1	Fortuna Fortuna Blvd #	0.116
Cape Mendocino	1992	7.1	Rio Dell Overpass - FF #	0.385
Landers	1992	7.3	Desert Hot Springs #	0.154
Landers	1992	7.3	Yermo Fire Station #	0.152

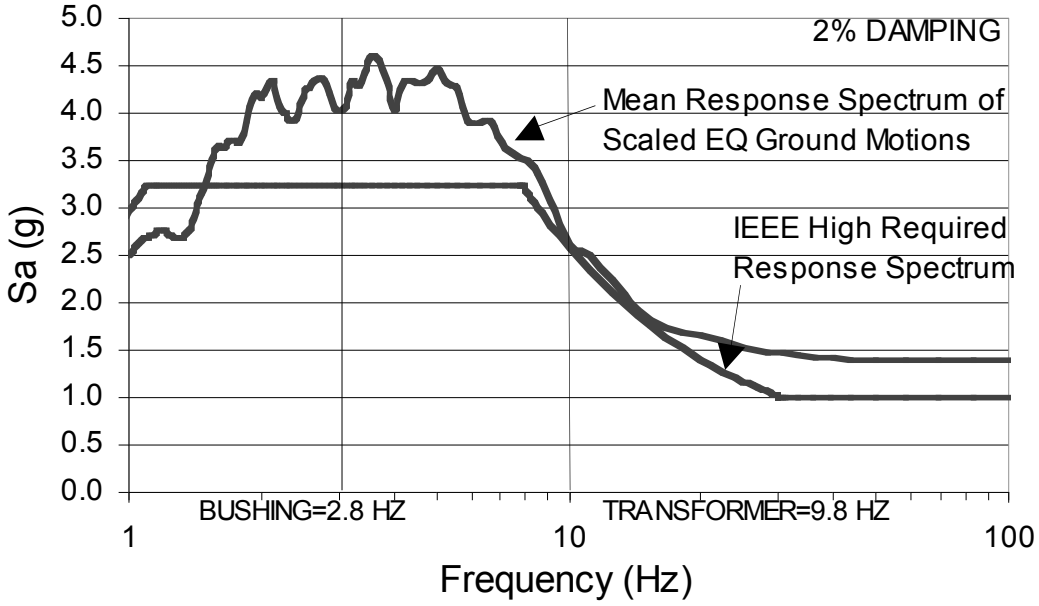

Figure 2.8 - 2% Damped Scaled Acceleration Response Spectra for 525 kV Transformer A in Transverse Direction.

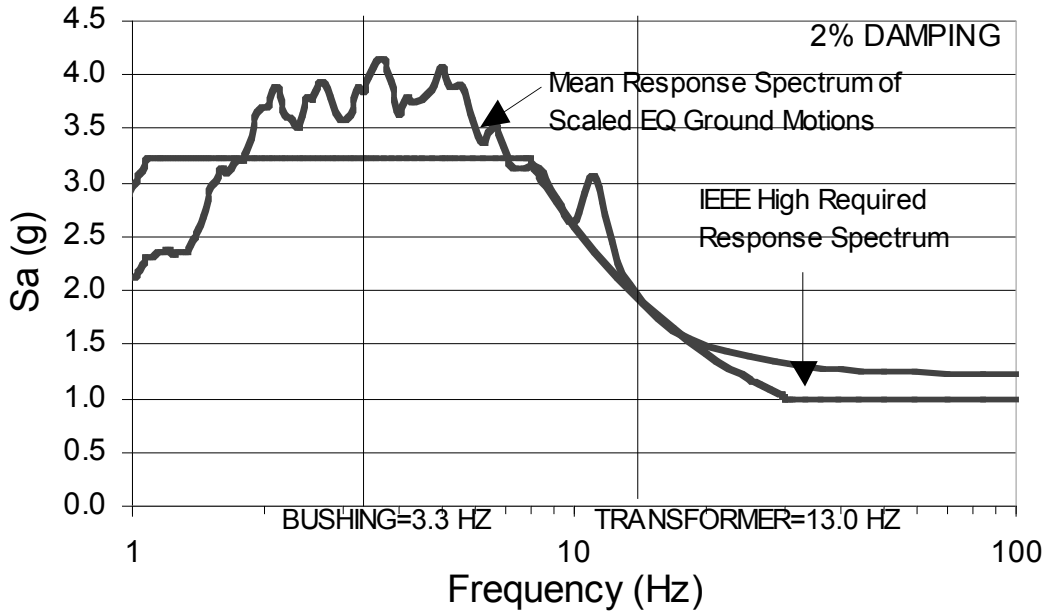

Figure 2.9 - 2% Damped Scaled Acceleration Response Spectra for 525 kV Transformer A in Longitudinal Direction.

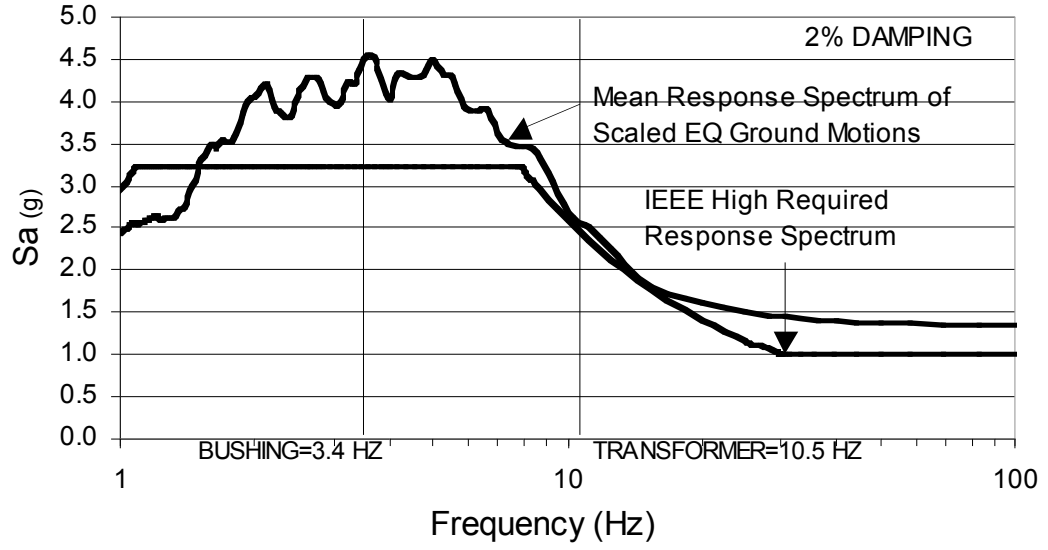

Figure 2.10 - 2% Damped Scaled Acceleration Response Spectra for 500 kV Transformer D in Transverse Direction.

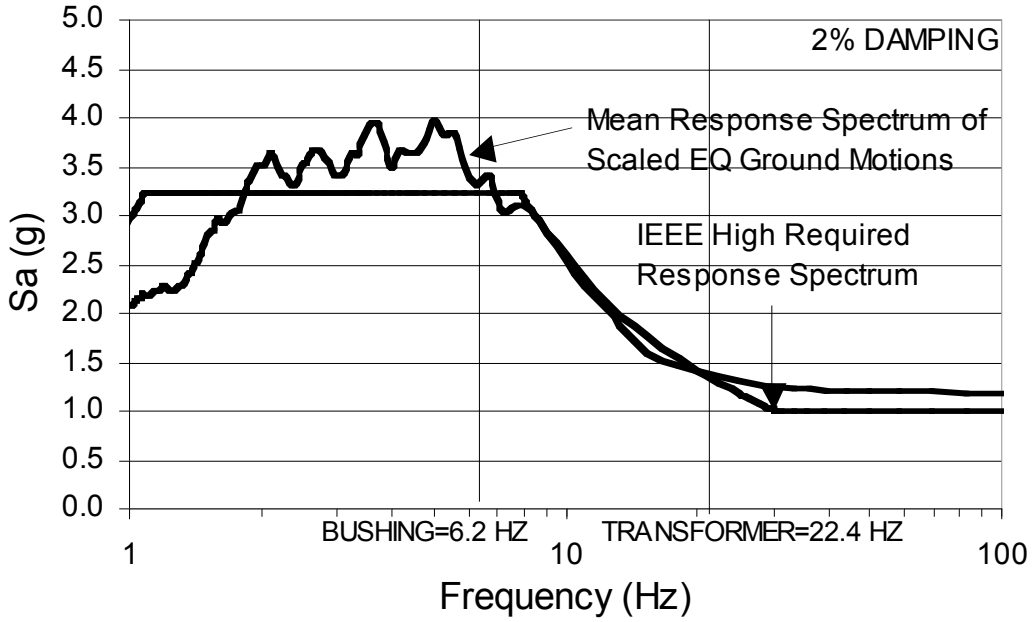

Figure 2.11 - 2% Damped Scaled Acceleration Response Spectra for 500 kV Transformer D in Longitudinal Direction.

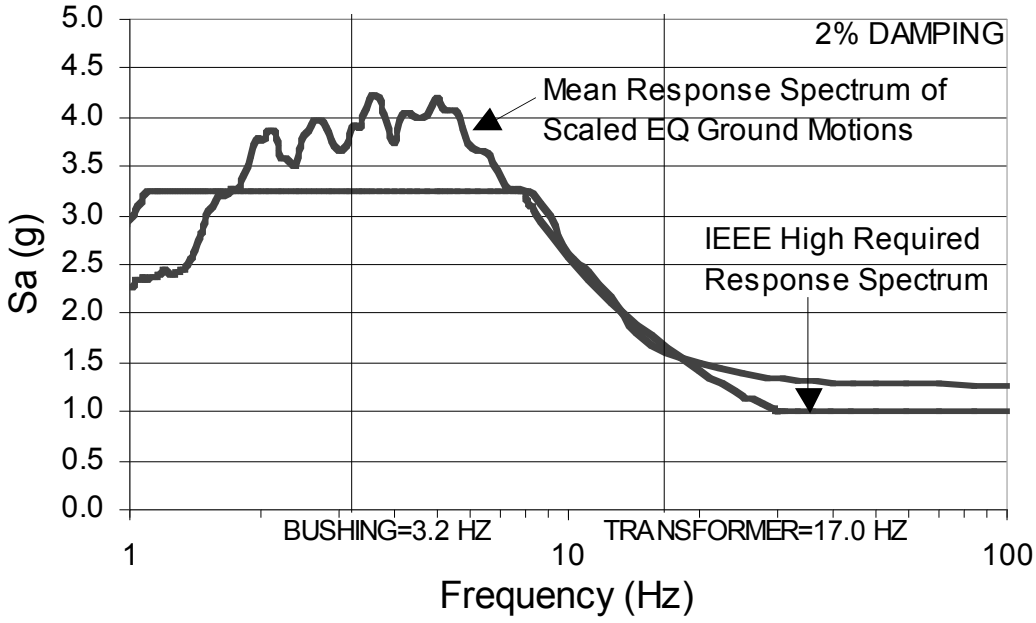

Figure 2.12 - 2% Damped Scaled Acceleration Response Spectra for 500 kV Transformer B in Transverse Direction.

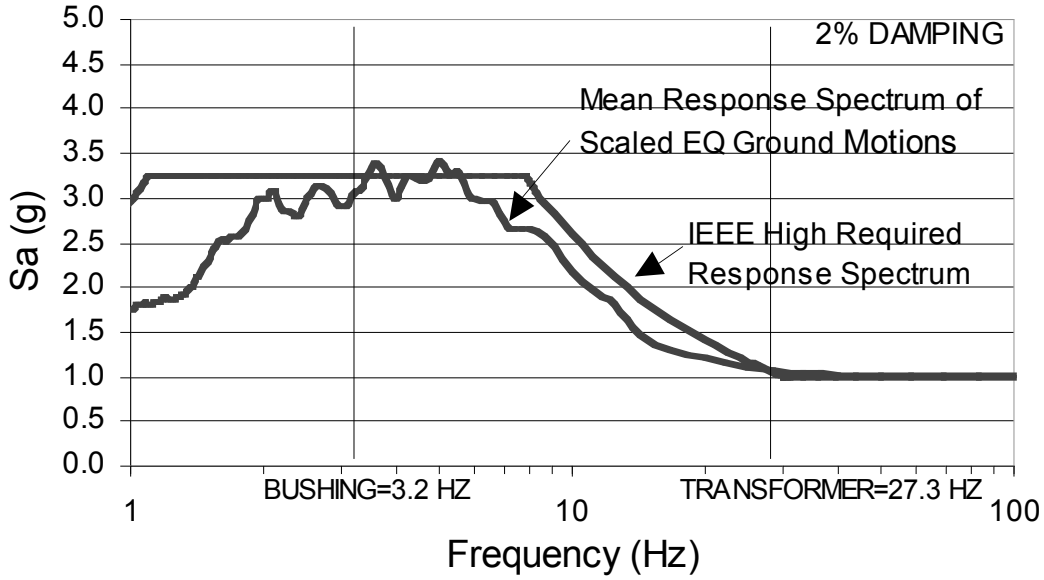

Figure 2.13 - 2% Damped Scaled Acceleration Response Spectra for 500 kV Transformer B in Longitudinal Direction.

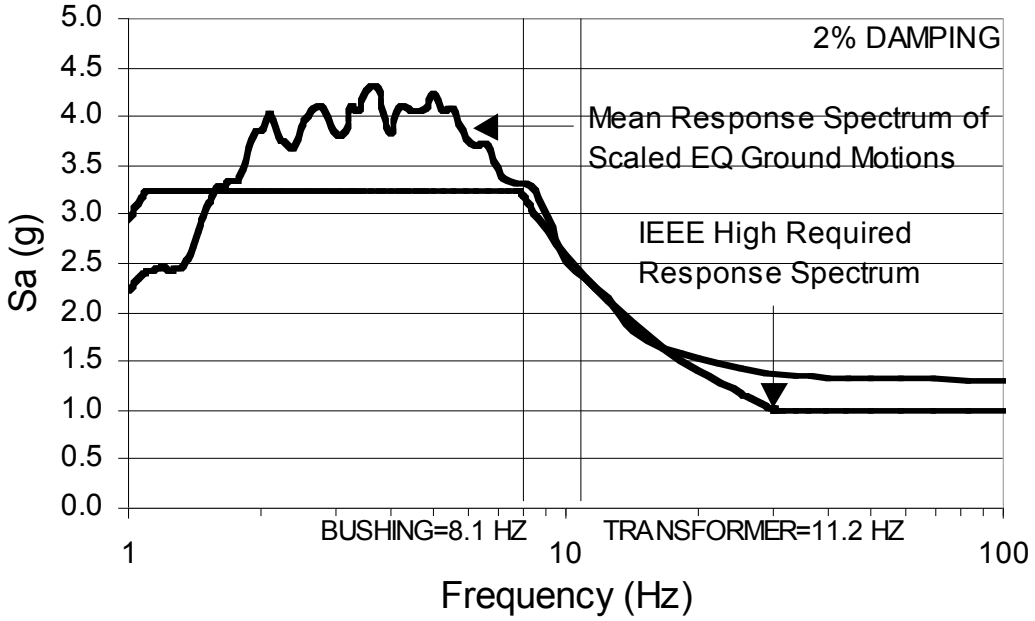

Figure 2.14 - 2% Damped Scaled Acceleration Response Spectra for 230 kV Transformer C in Transverse Direction.

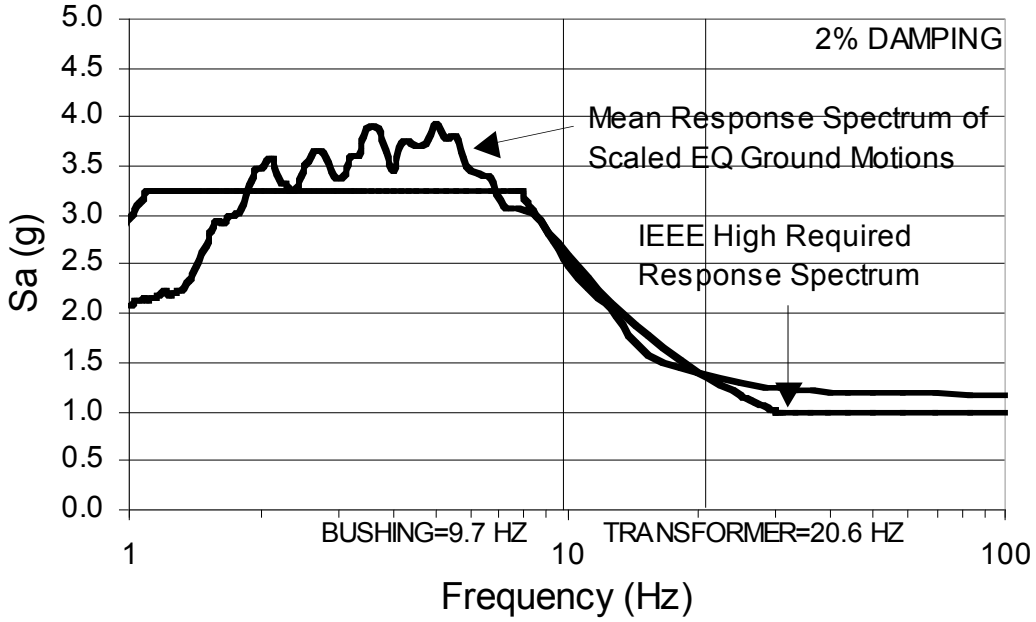

Figure 2.15 - 2% Damped Scaled Acceleration Response Spectra for 230 kV Transformer C in Longitudinal Direction.

2.6. Analysis Procedure

For each of the four transformers used in this study, a three-dimensional finite element model was developed using the structural analysis program SAP 2000 [6]. Dynamic time-history analyses were then performed on these finite element models using the 20 scaled strong ground motions. For the dynamic time-history analysis, the method of modal superposition was utilized such that the dynamic response is determined by the contribution of a specified number of modes.

For a particular transformer, the 20 earthquake records were separately run in both the longitudinal and transverse directions; after which, the dynamic amplification that occurs between the base of the bushing and the input ground motion was computed as a function of frequency. For a given record, the amplification was quantified by taking the ratio of the 2% damped response spectrum computed at the base of the high voltage bushing (i.e. top of the

transformer) to the corresponding 2% damped response spectrum of the ground motion being considered. This spectral ratio is defined as a "spectral amplification", which explicitly gives the dynamic amplification as a function of frequency through:

$$Spectral\ Amplification = \frac{Response\ Spectrum\ at\ Base\ of\ Bushing}{Response\ Spectrum\ of\ Ground\ Motion} \quad (1)$$

The mean, mean plus one standard deviation and mean minus one standard deviation values of the spectral amplification of the 20 earthquake records analyzed were computed for each of the four transformers in both the longitudinal and transverse direction and then compared with the IEEE-693 assumed frequency independent amplification value of 2.0.

It must be noted that the definition of spectral amplification given by equation (1) does not directly consider the rotational acceleration at the base of the bushing, which will also affect its dynamic response.

2.7. Spectral Amplification Results

The spectral amplification results for each of the transformers exhibited three common trends. First, for a given transformer in a given direction, there are generally two major peaks in the spectral amplification. These two peaks occur at the natural frequency of the transformer tank and the natural frequency of the bushing in the given direction. In addition, the magnitude of the amplification at the transformer frequency was consistently higher than the magnitude at the frequency of the bushing. Finally, the amplification that occurred in the transverse direction for each transformer was larger than that of the longitudinal direction.

These trends can be observed in the spectral amplification results shown in Figs. 2.16 and 2.17. These figures show the mean, mean plus one standard deviation and mean minus one standard deviation values of the spectral amplification for the 500 kV Transformer D in the transverse and longitudinal direction respectively.

It can be seen in Figs. 2.16 and 2.17 that the mean amplification at the transformer frequency is larger than the IEEE assumed value of 2.0 in both directions. However, the mean spectral amplification at the bushing frequency is slightly larger than 2.0 in the transverse direction and slightly smaller than 2.0 in the longitudinal direction.

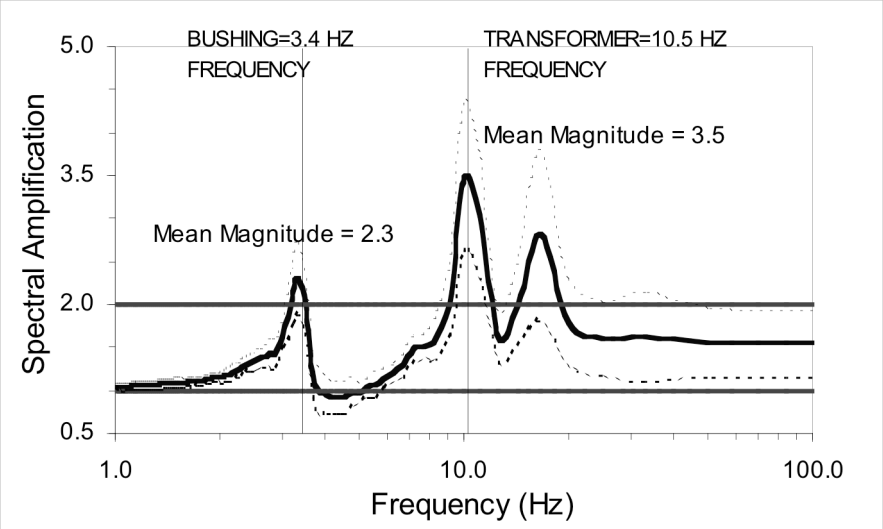

Figure 2.16 - Spectral Amplification Results for 500 kV Transformer D in the Transverse Direction.

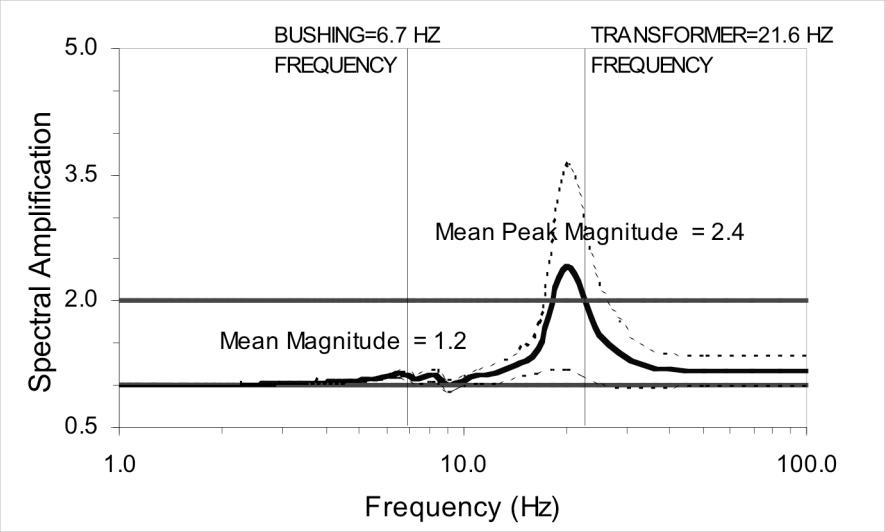

Figure 2.17 - Spectral Amplification Results for 500 kV Transformer D in the Longitudinal Direction.

Graphs of the mean response spectrum results as well as mean plus one standard deviation and mean minus one standard deviation of the spectral amplification results for each transformer are presented in Figs. 2.18 to 2.23. Figures 2.24 to 2.31 present the mean response spectra obtained at the base of the transformer and at the base of the bushing for the same cases.

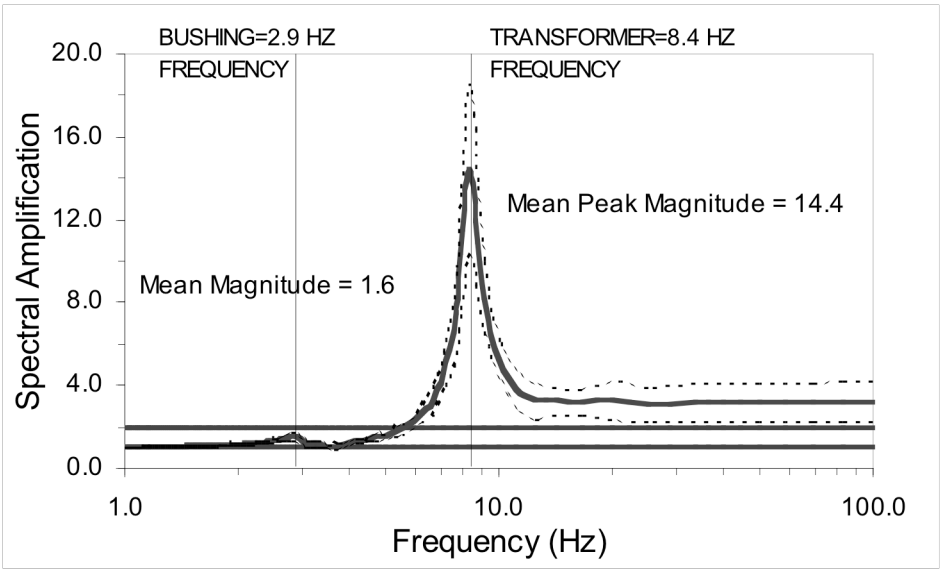

Figure 2.18 - Spectral Amplification Results for 525 kV Transformer A in the Transverse Direction.

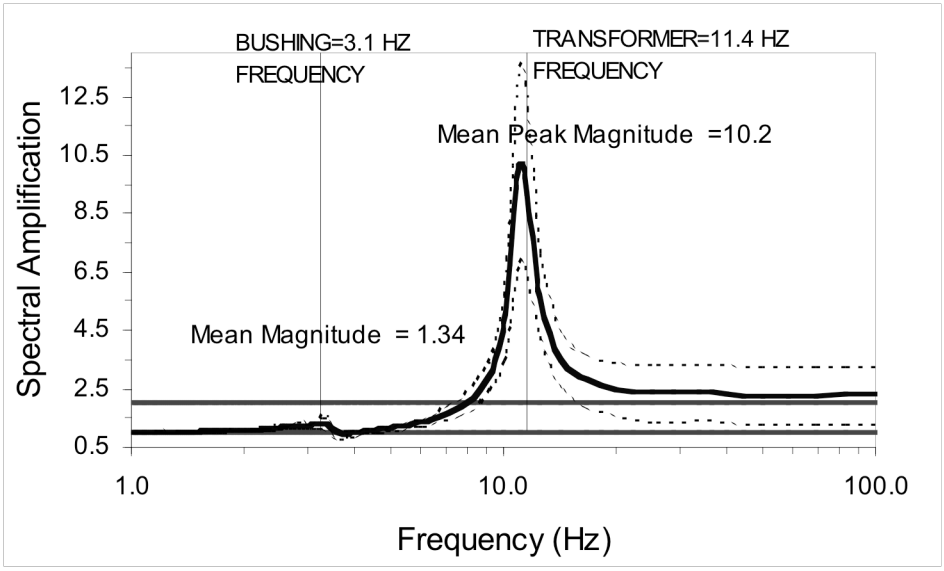

Figure 2.19 - Spectral Amplification Results for 525 kV Transformer A in the Longitudinal Direction.

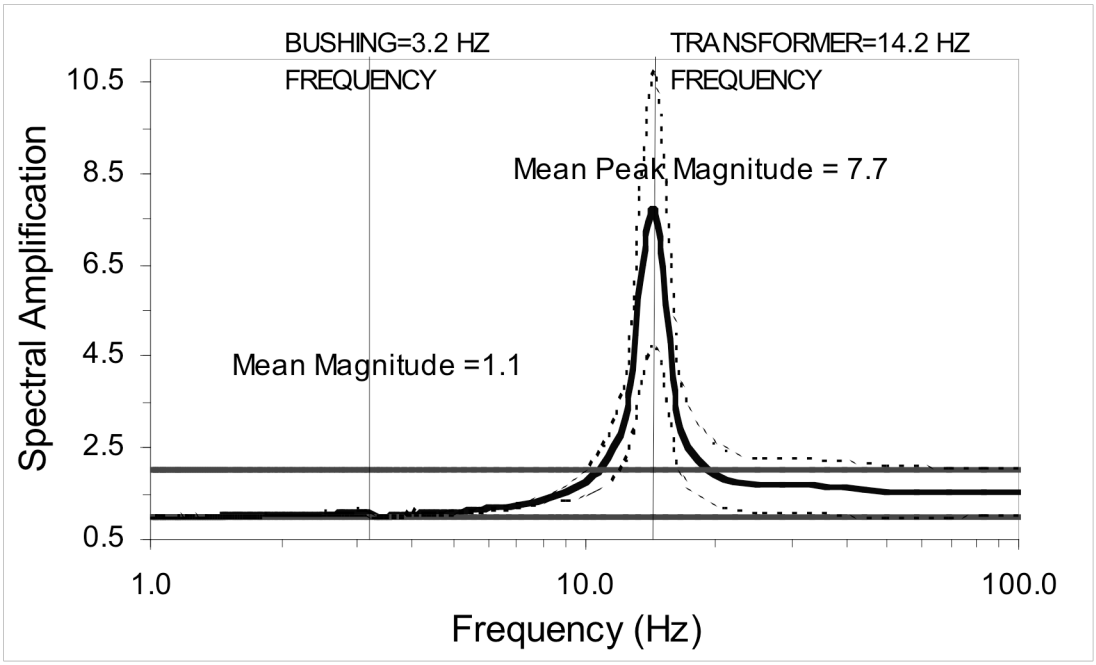

Figure 2.20 - Spectral Amplification Results for 500 kV Transformer B in the Transverse Direction.

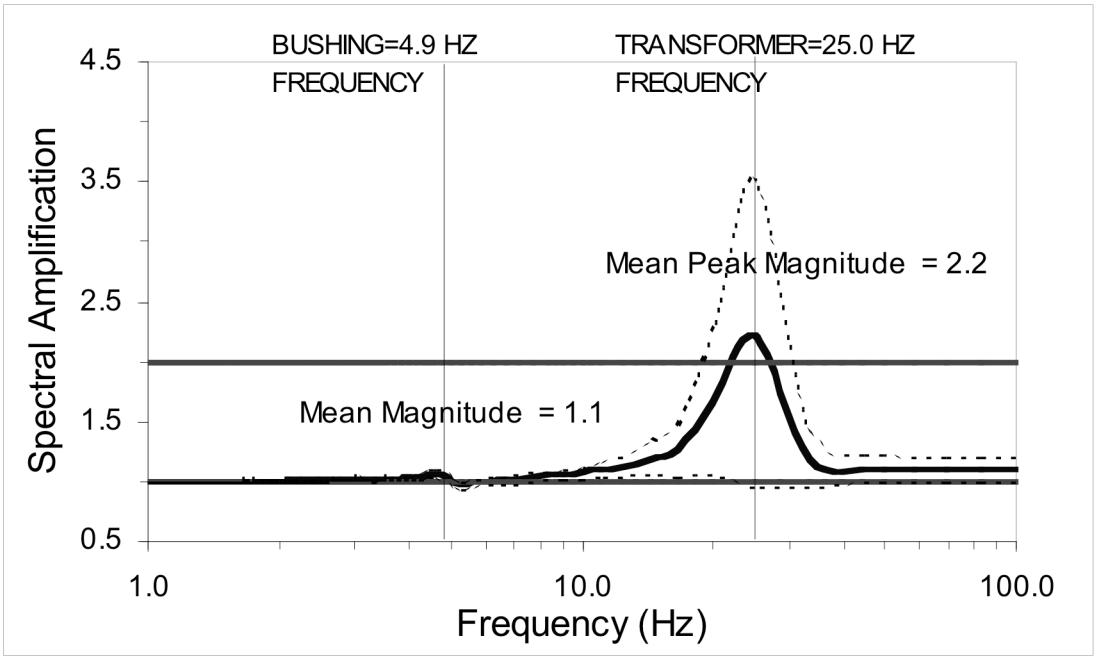

Figure 2.21 - Spectral Amplification Results for 500 kV Transformer B in the Longitudinal Direction.

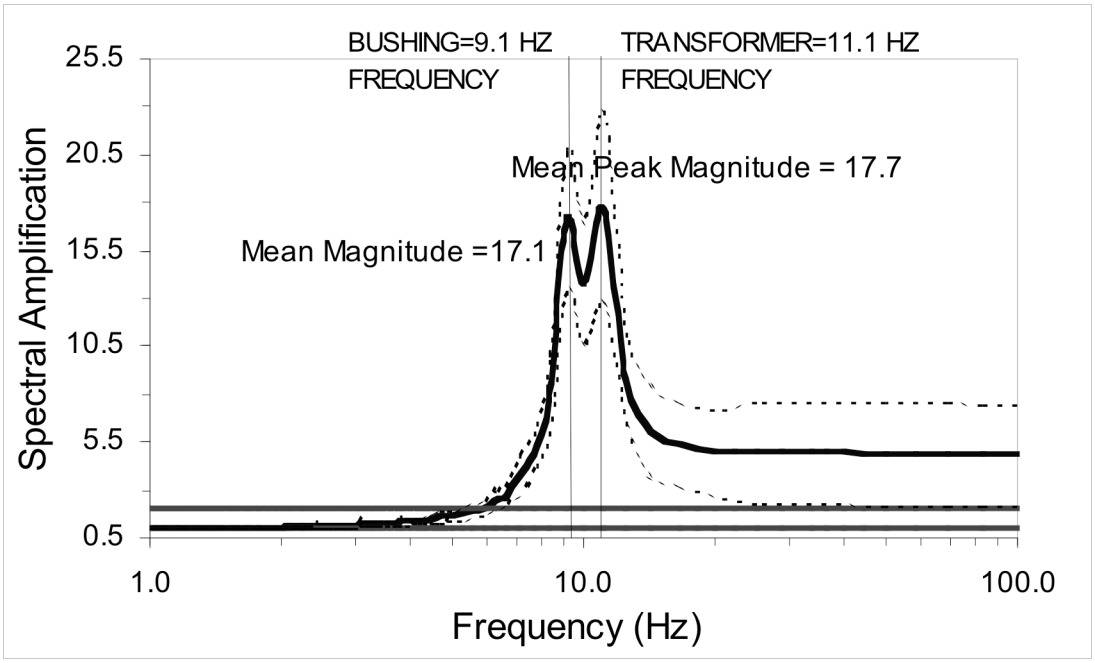

Figure 2.22 - Spectral Amplification Results for 230 kV Transformer C in the Transverse Direction.

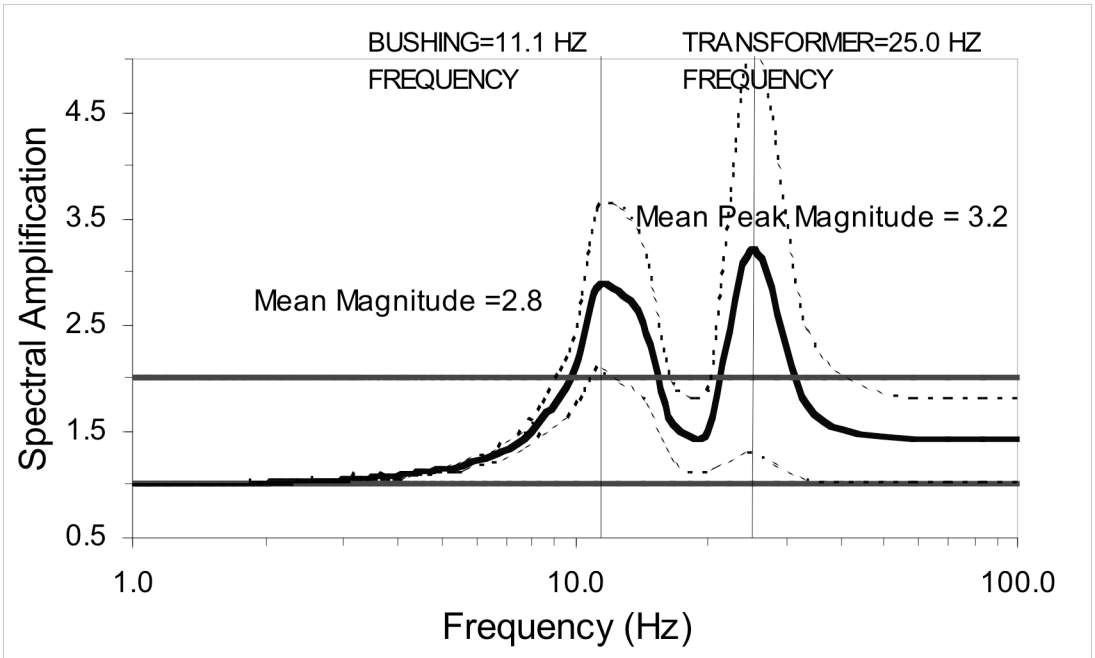

Figure 2.23 - Spectral Amplification Results for 230 kV Transformer C in the Longitudinal Direction.

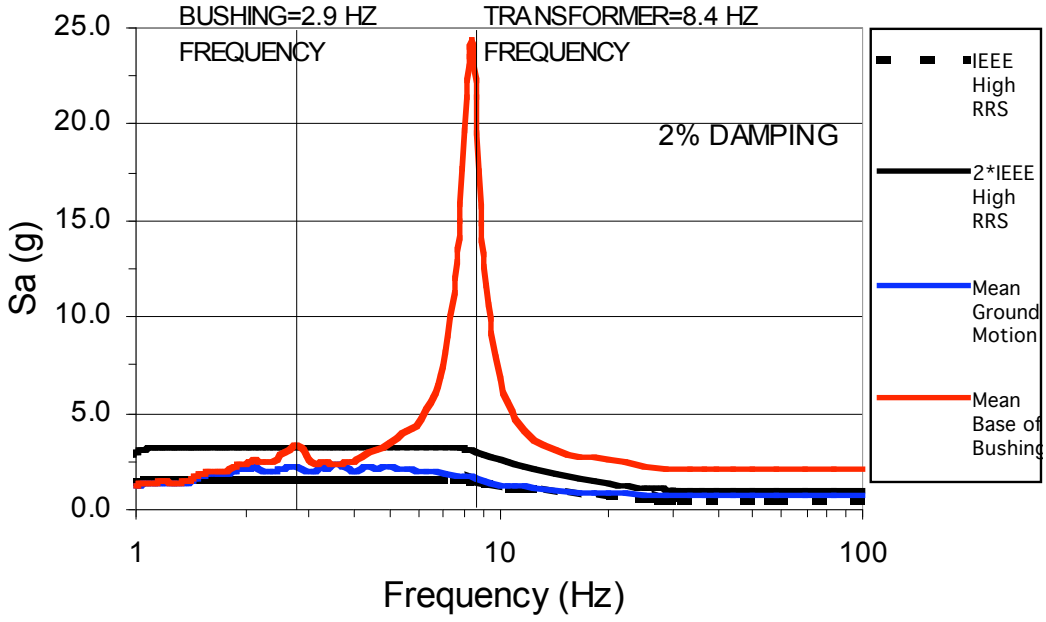

Figure 2.24 - Mean Response Spectrum Results for 525 kV Transformer A in the Transverse Direction.

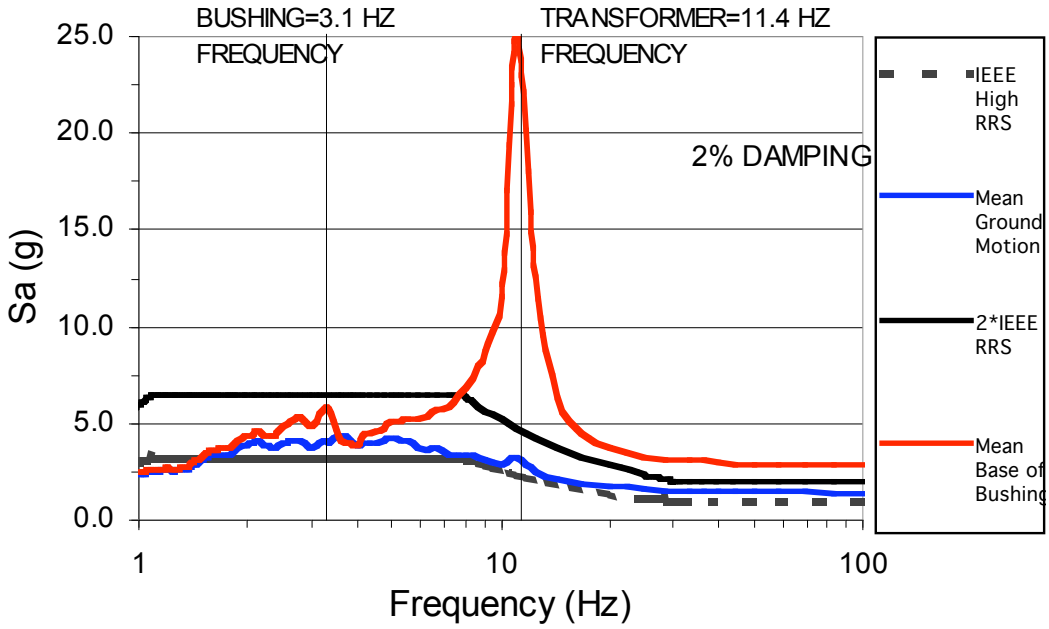

Figure 2.25 - Mean Response Spectrum Results for 525 kV Transformer A in the Longitudinal Direction.

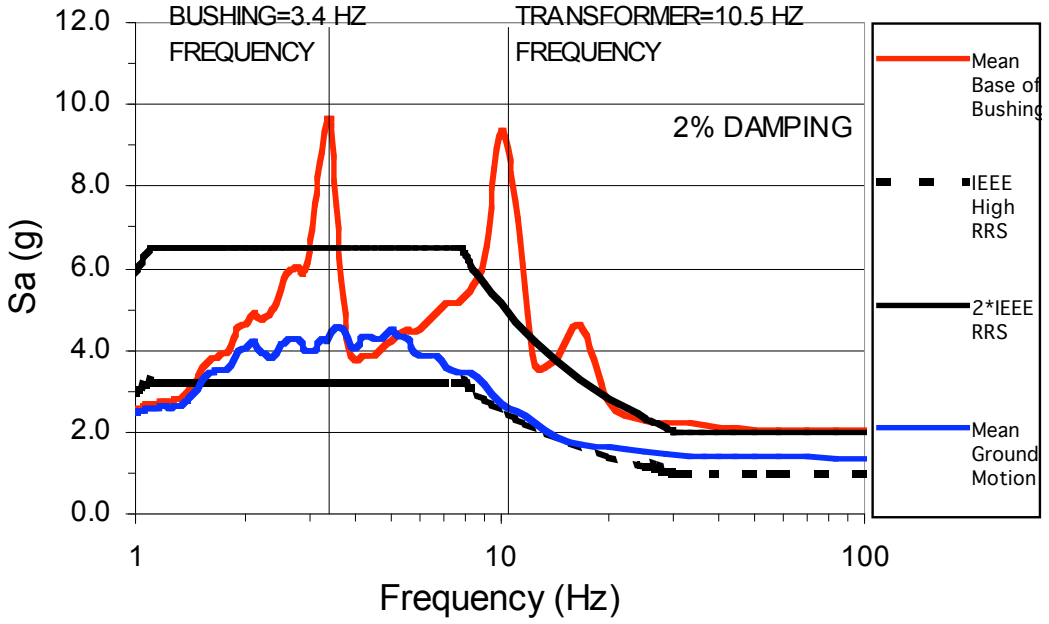

Figure 2.26 - Mean Response Spectrum Results for 500 kV Transformer D in the Transverse Direction.

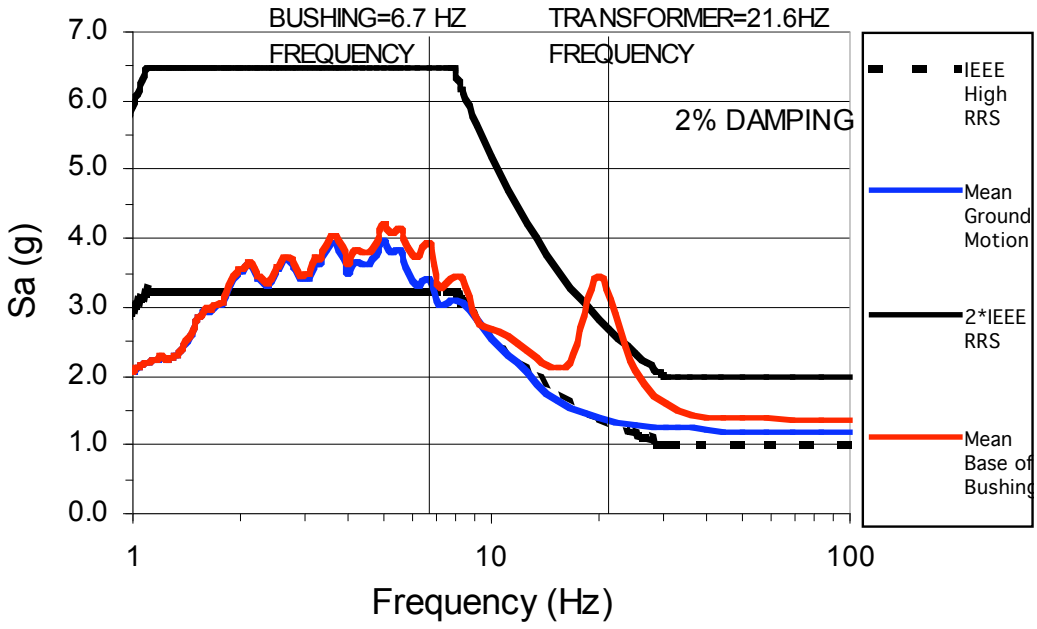

Figure 2.27 - Mean Response Spectrum Results for 500 kV Transformer D in the Longitudinal Direction.

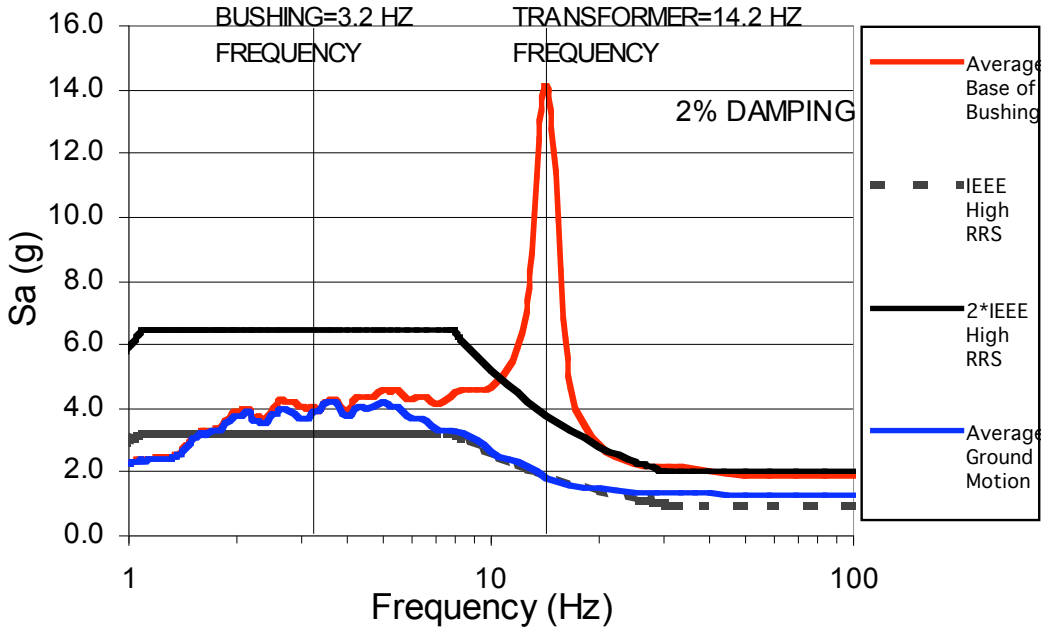

Figure 2.28 - Mean Response Spectrum Results for 500 kV Transformer B in the Transverse Direction.

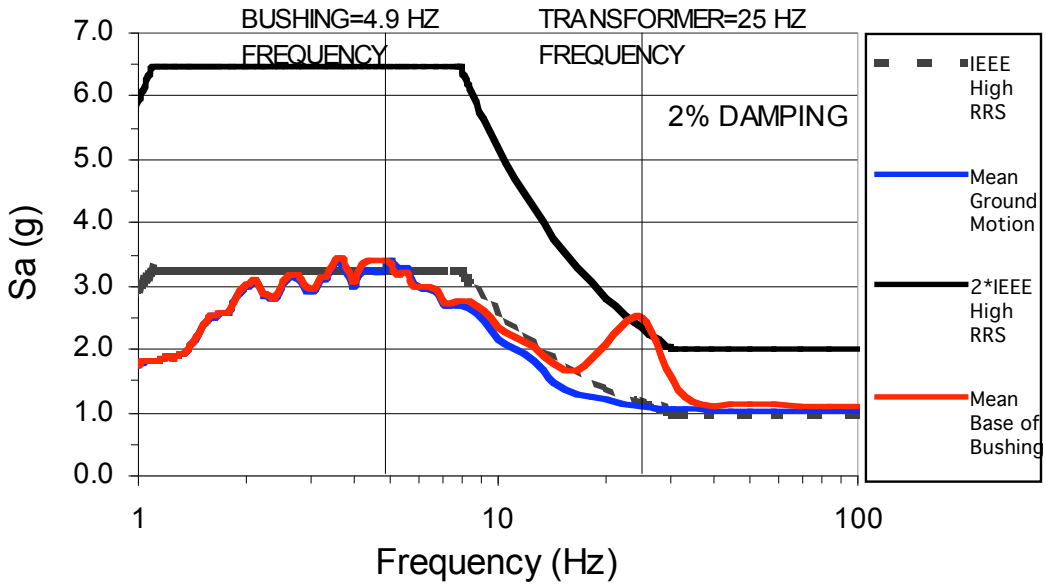

Figure 2.29 - Mean Response Spectrum Results for 500 kV Transformer B in the Longitudinal Direction.

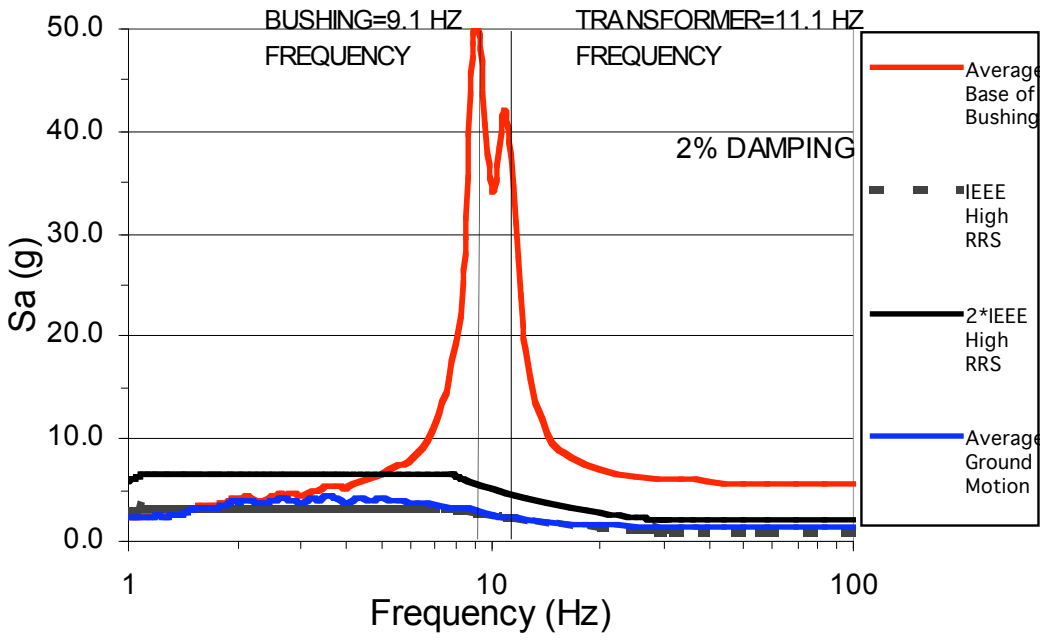

Figure 2.30 - Mean Response Spectrum Results for 230 kV Transformer C in the Transverse Direction.

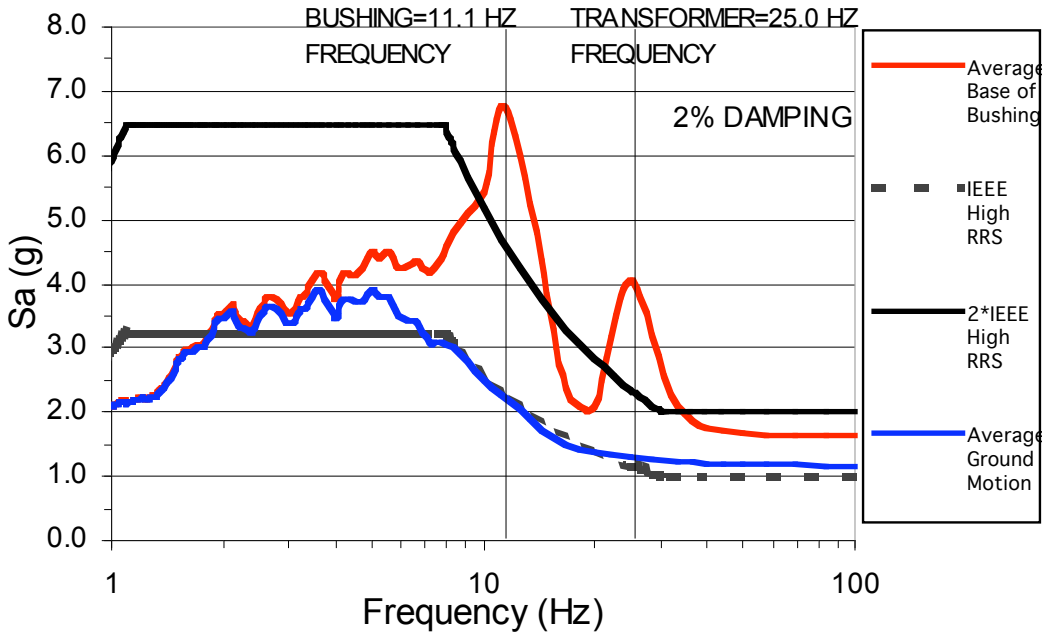

Figure 2.31 - Mean Response Spectrum Results for 230 kV Transformer C in the Longitudinal Direction.

Although the amplification at various frequencies is of interest, ultimately the main concern for this study is the amplification that occurs at the frequency of the bushing since this will govern the behavior of the bushing under seismic excitation. The mean spectral amplification at the bushing frequency in the transverse direction was found to be 1.6, 1.1, 17.1, and 2.3 Hz for Transformers A, B, C, and D respectively. The mean spectral amplification at the bushing frequency in the longitudinal direction was found to be 1.3, 1.1, 2.8, and 1.2 Hz for Transformers A, D, B, and C respectively. Table 2.7 summarizes these results and also shows the spectral amplification that occurred at the transformer tank frequencies.

Table 2.7 - Mean Spectral Amplification Results at Transformer Tank and Bushing Frequency.

Transformer	Component	Transverse Direction	
		Frequency (Hz)	Spectral Amplification
A	*Tank*	8.4	14.4
	Bushing	2.9	1.6
B	*Tank*	14.2	7.7
	Bushing	3.2	1.1
C	*Tank*	11.1	17.7
	Bushing	9.1	17.1
D	*Tank*	10.5	3.5
	Bushing	3.4	2.3

Transformer	Component	Longitudinal Direction	
		Frequency (Hz)	Spectral Amplification
A	*Tank*	11.4	10.2
	Bushing	15.0	2.2
B	*Tank*	25.0	2.2
	Bushing	4.9	1.1
C	*Tank*	25.0	3.2
	Bushing	11.1	2.8
D	*Tank*	21.6	2.4
	Bushing	6.7	1.2

2.8. Summary

The presumption about transformer tanks is that they are essentially rigid. However, the results of the finite element analyses obtained herein show that transformer structures are much more flexible than currently assumed. The majority of the flexibility occurs on the transformer top plate upon which bushings are attached. This local flexibility significantly reduces the natural frequency of the bushings, thereby changing the response of the bushing during seismic loading. Current bushing qualification tests performed according to the IEEE-693 standard do not take into account this reduced natural frequency during shake table testing. As a result, the bushing response from qualification testing is not necessarily representative of the response that will occur in the field. Table 2.8 shows the natural frequencies for various bushings under these two mounting conditions.

Table 2.8 - Bushing Natural Frequencies for Different Support Conditions.

Transformer	Bushing Voltage Rating (kV)	Support	1st Mode (Hz)
A	525	Rigid	8.9
A	525	Transformer	2.9
B	500	Rigid	8.7
B	500	Transformer	3.2
C	230	Rigid	18.9
C	230	Transformer	9.1
D	500	Rigid	8.9
D	500	Transformer	3.5

An example of the effect of not accounting for in-field mounting conditions may be observed by considering a 230 kV porcelain bushing. Its fixed condition natural frequency is roughly 19 Hz, but is reduced to about 9 Hz when attached to the top of the transformer. When looking at the IEEE-693 acceleration response spectrum shown in Fig. 1.4, it can be seen that the difference in spectral acceleration at these two frequencies is quite large. At the frequency associated with the bushing attached to the transformer (9Hz), the spectral acceleration is more than two times that of the bushing frequency associated with a rigid attachment (19Hz). Therefore, this reduced bushing natural frequency should be accounted for during seismic qualification tests.

Regarding spectral amplification, the largest amplifications occur at two predominant frequencies: the natural frequency of the transformer frame and the natural frequency of the bushing. In addition, the transverse (lower frequency) direction consistently resulted in larger amplifications than in the longitudinal (higher frequency) direction. Although the amplifications were generally significantly larger than 2.0 at the frequency of the transformers, only the 500 kV Transformer Dand 230 kV Transformer Cs had mean amplifications larger than 2.0 at the bushing frequencies. In fact, the 230 kV Transformer C appears to cause a

very large amplification in the ground motion directed in its transverse direction. This result can be explained when comparing the bushing and transformer natural frequencies. As shown in Table 2.7, these two natural frequencies for the 230 kV Transformer C were much closer to each other than for the other transformers considered. The fact that the highest amplifications occurred when these two natural frequencies were relatively close to each other seems rather intuitive; however, no clause in the IEEE-693 standard currently accounts for such a situation. Figure 2.32 shows plot that relates the mean spectral amplification as a function of the transformer frequency and bushing frequency ratio. As the ratio of the transformer and bushing frequencies become closer to one, a larger amplification occurs at the bushing frequency. In fact, the results shown seem to follow an exponential pattern. The difference in amplification between frequency ratios of 1.0 and 2.0 is much larger than between the frequency ratios of 2.0 and 3.0.

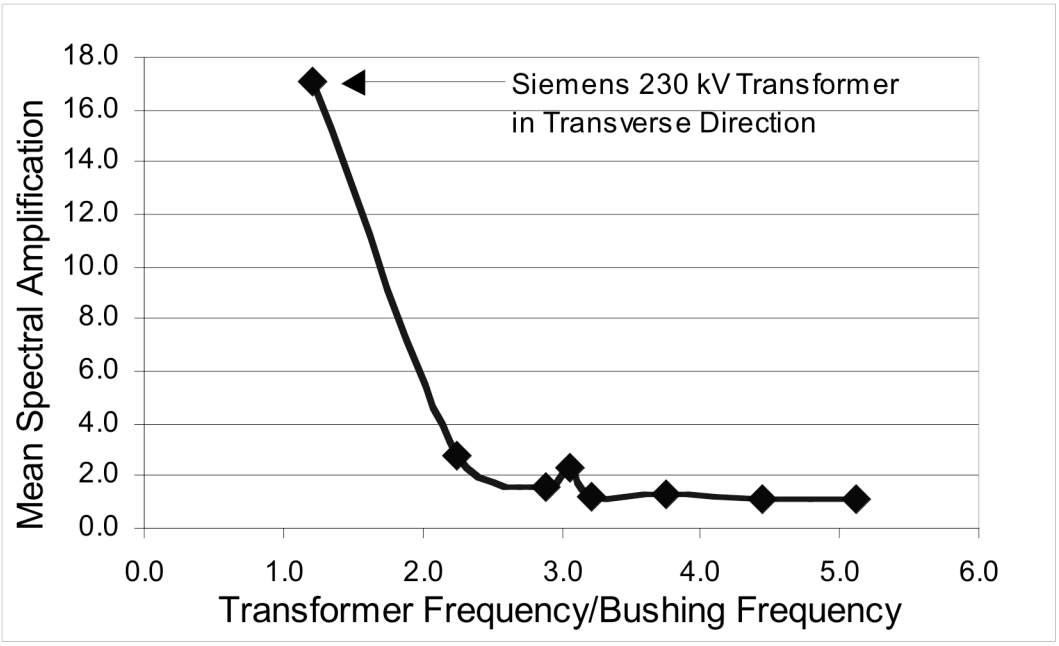

Figure 2.32 - Relationship between Mean Spectral Amplification and Transformer/Bushing Frequency Ratios.

Clearly, the response of the transformer equipment tends to be filtered at the frequency of transformer. In other words, once the accelerations reach the base of the bushings, much of the energy will be concentrated at the transformer tank frequency. Therefore, bushings that have fundamental frequencies close to the fundamental frequency of the transformer will cause significant interaction and result in large ground motion amplifications.

The spectral amplification values computed in this study show that the assumed amplification value of 2.0 appears to be conservative for some, but not all transformers considered. Due to difference in overall weight, geometry, and size between transformers of different voltage or manufacturer, it is difficult to generalize the results of this study. However, it can be stated safely that seismic qualification test procedure for bushings as defined in the IEEE-693 standard does not completely represent the true structural dynamics of the bushing transformer

system. It is highly appropriate that seismic qualification tests consider such cases as the 230 kV Transformer C where the bushing and tank frequencies are close enough to significantly increase the amplification that occurs between the ground and bushing base. In addition, the fundamental frequencies of the bushing attached to the qualification test support should more accurately represent the fundamental frequencies of the bushing when attached to a transformer top.

3. NUMERICAL STUDY OF RETROFITTED 230 KV TRANSFORMER C

3.1. Scope of Study

The objective of this chapter is to investigate feasible retrofit schemes that could be implemented on existing transformers in order to reduce the amplification that occurs between the ground and the bushing attachment point. From the numerical study conducted in the previous chapter, the 230 kV Transformer C resulted in the largest spectral amplification among the four transformers considered, and appears to be the most critical. For this reason, the numerical retrofit study conducted in this chapter was limited to Transformer C only.

With the retrofitted model, the analysis consisted of running the 20 different strong ground motion time-histories defined in the previous chapter in the two principal horizontal directions of the transformer. Each time-history was scaled to the 2% damped high required level response spectrum at the frequency of the transformer. From the analysis, the spectral amplification was then computed using the procedure described in the previous chapter. The spectral amplification value at the frequency of the bushing was then compared with the spectral amplification obtained from the un-retrofitted case.

3.2. Retrofit Configurations Considered

There are several different methods that could be effective in reducing the amount of amplification that occurs and thereby reduce the overall dynamic response of the transformer bushing. Results from the first numerical study show that the amplification tends to increase as the natural frequency of bushing becomes closer to

that of the transformer. Therefore, one logical way of reducing the bushing response is to separate the natural frequencies of the transformer and bushing. The natural frequency of a body is a function of its mass and stiffness. Therefore the separation of the frequencies can be achieved by one of two ways; adding lumped mass or increasing the stiffness of either system.

By adding lumped mass to either the bushing or the transformer, some undesirable consequences occur. The increased mass will reduce the natural frequency of whichever component it is attached to. In the case of earthquakes, much of the energy is commonly in the lower frequency range of 1-10Hz. Therefore, by reducing the natural frequency, it can potentially increase the energy that is inputted from the earthquake. In addition to this, larger mass will increase the seismic inertia forces exerted on the transformer-bushing system. These added inertia forces might overstress the structural components or anchorage of the transformer. Finally, if lumped mass were added to the bushing, its displacement response is likely to increase during earthquake loading. This is generally undesirable considering that bushings are interconnected via conducting cables to other electrical equipment within the substation.

Increasing the stiffness near the bushing is much more advantageous. Generally speaking, stiffer electrical equipment tends to result in less damage during earthquake events than the more flexible types of equipment. The easiest way to increase the stiffness of either the transformer or the bushing is to use bracing. There are several types of braces, and several ways of bracing a structure. In order to increase the stiffness of the bushing, braces can be attached to the bushing turret or the top plate of

the transformer can be stiffened. Either method will result in an increased natural frequency of the bushing, which ultimately should reduce the amplification between the ground and bushing mounting point. In addition to bracing the bushing, the transformer may be braced by using bracing elements attached to the interior core. The interior core can essentially be considered as rigid block; therefore, the introduction of interior bracing members would greatly stiffen the transformer tank. Interior bracing could only be considered for new construction of transformers however. For existing transformers, tank stiffening could be achieved by adding bracing elements that are attached to the tank on down to the foundation.

Although there are several ways for which the transformer tank or the bushing may be stiffened, only two different bracing configurations were considered in this numerical study. The first is the addition of double angle braces that are attached to the top of the turret and top of the transformer tank. Double angle braces provide good stiffness and allow for easy attachment. Since the bushing naturally vibrates in the two horizontal principal directions of the transformer, two braces were attached on each of the high voltage (230kV) bushings in these two directions. A conceptual drawing of the bracing attachment is shown in Fig. 3.1. For the analysis, L6”x6”x3/4” angles were used as bracing members.

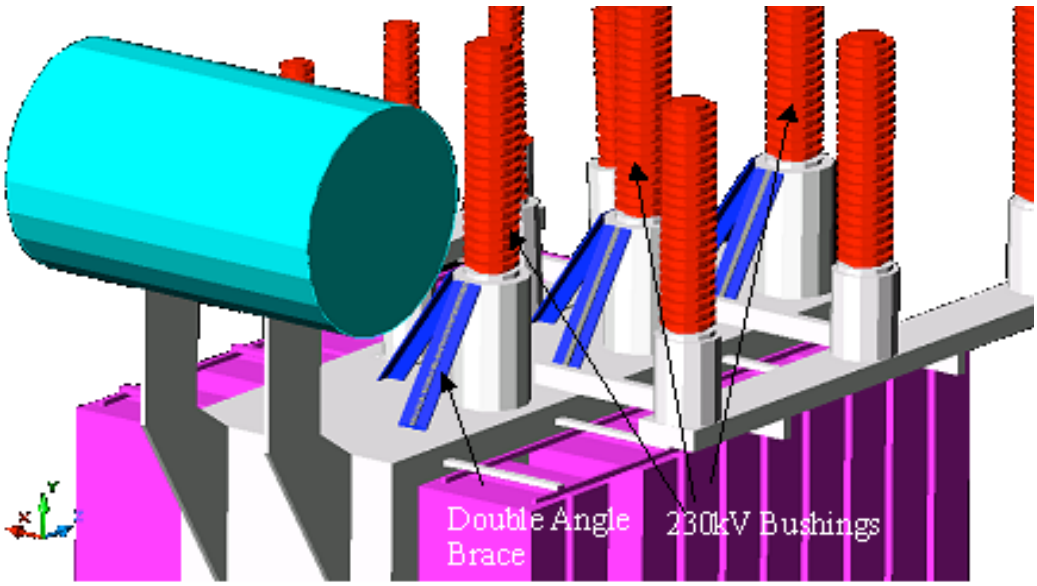

Figure 3.1 - First Bracing Configuration for 230kV Transformer C.

The second bracing configuration that was analyzed was four bracing elements attached to the top of transformer tank on down to the foundation in addition to the double angle braces attached to the bushings as described above. From the numerical study conducted in the previous chapter, it was found that the vibration in the transverse direction of the transformer resulted in a much larger spectral amplification. Therefore, the four bracing members were attached to the transformer in such a manner that it increased the stiffness of the tank in the transverse direction. The bracing members used for analysis were four W18x143 I-beams. Figure 3.2 shows a conceptual drawing of the second bracing scheme analyzed.

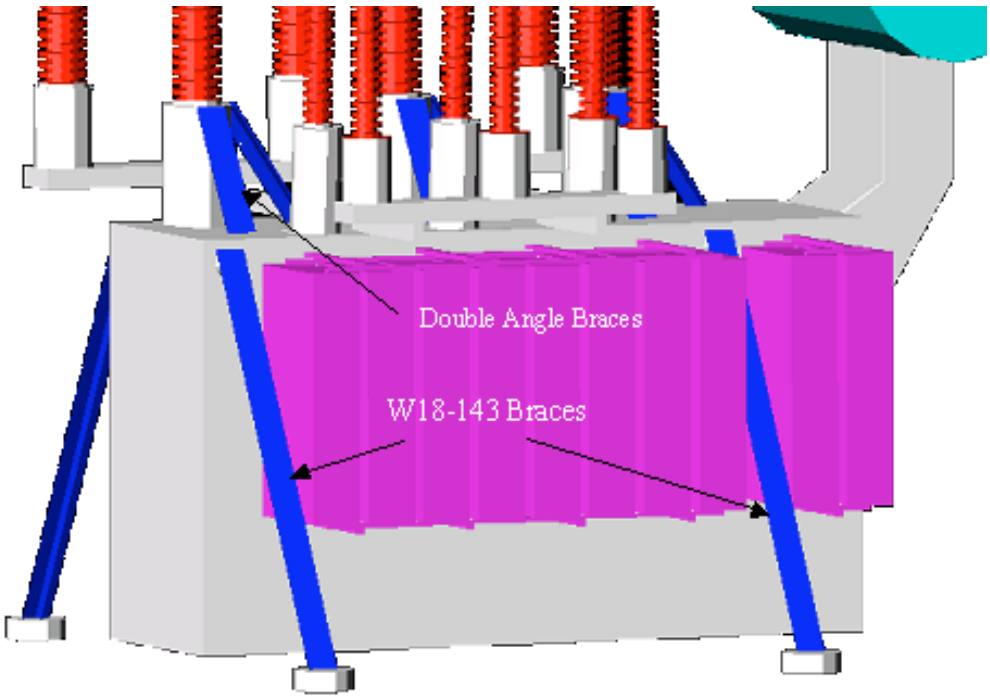

Figure 3.2 - Second Bracing Configuration for 230kV Transformer C.

3.3. Analysis Procedure

Bracing elements were added to the 230kV Transformer C finite element model in the two configurations as described above. Dynamic time-history analyses were then performed using the same 20 scaled strong ground motions described in the previous chapter. For the dynamic time-history analysis, the method of modal superposition was utilized such that the dynamic response is determined by the contribution of a specified number of modes.

The 20 earthquake records were separately run in both the longitudinal and transverse directions; after which, the dynamic amplification that occurs between the base of the bushing and the input ground motion was calculated. For a given record,

the spectral amplification was quantified by taking the ratio of the 2% damped response spectrum computed at the base of the high voltage bushing to the corresponding 2% damped response spectrum of the ground motion being considered, as described in the previous chapter.

The mean, mean plus one standard deviation and mean minus one standard deviation values of the spectral amplification of the 20 earthquake records analyzed were computed for the 230kV Transformer C in both the longitudinal and transverse direction and then compared with the spectral amplification results obtained in the un-retrofitted case.

3.4. Spectral Amplification Results

In the first retrofit configuration, the double angle braces effectively increased the stiffness of the three high voltage bushings. The natural frequency of the bushings in the transverse direction without any bracing was 9.1Hz (see Table 2.7). After adding the braces, the transverse frequency increased to 12.7 Hz. Appendix G presents the modal properties of the two retrofitted finite element models.

The calculated mean spectral amplification values in the transverse direction at the transformer frequency and bushing frequency were 11.2 and 5.0 respectively. In the longitudinal direction, the mean spectral amplification values were 2.8 at the transformer frequency and 1.6 at the bushing frequency. Graphs of the mean, mean plus one standard deviation and mean minus one standard deviation of the spectral amplification results for the first retrofit configuration are presented in Figs. 3.3 and

3.4. The mean response spectrum results for both retrofit configurations are shown in Appendix H.

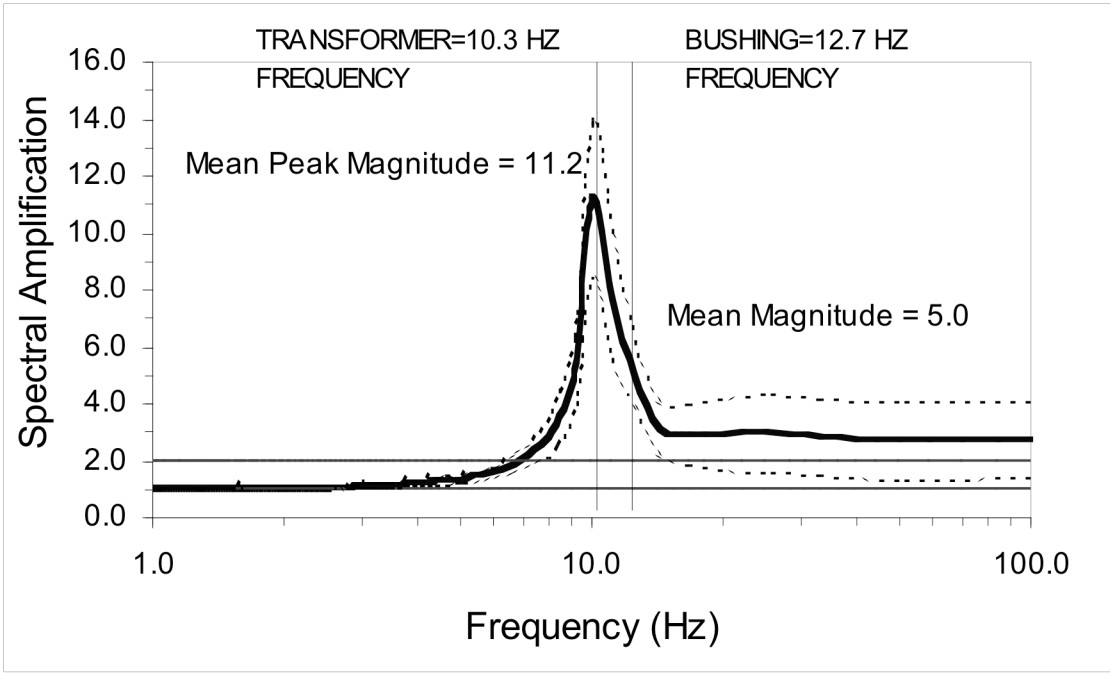

Figure 3.3 - Spectral Amplification Results for 230 kV Transformer C in the Transverse Direction (Retrofit Configuration 1).

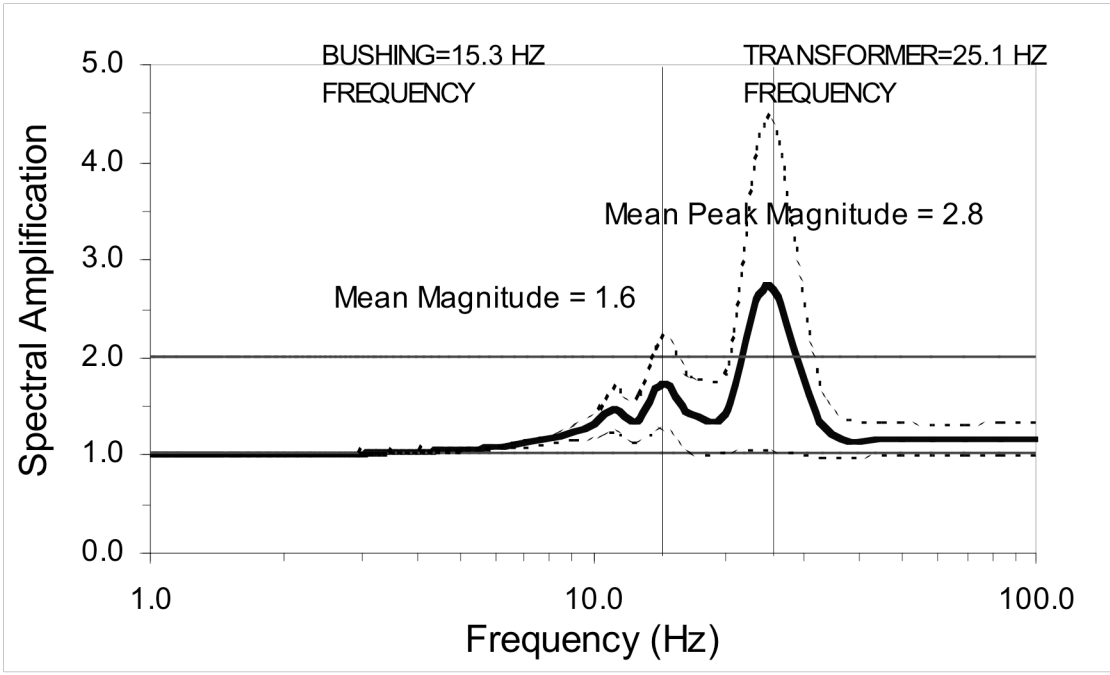

Figure 3.4 - Spectral Amplification Results for 230 kV Transformer C in the Longitudinal Direction (Retrofit Configuration 1).

For the second retrofit configuration, braces were attached to the transformer tank in addition to the braces attached to each high-voltage bushing turret. The tank braces added significant lateral stiffness to the tank, which increased its natural frequency in the transverse direction from 11.1Hz to 21.5Hz. Refer to appendix H for the modal results for the second retrofit configuration.

The calculated mean spectral amplification values in the transverse direction at the transformer frequency and bushing frequency were 1.7 and 4.2 respectively. In the longitudinal direction, the mean spectral amplification values were 2.8 at the transformer frequency and 1.5 at the bushing frequency. Graphs of the mean, mean plus one standard deviation and mean minus one standard deviation of the spectral amplification results for the first retrofit configuration are presented in Figs. 3.5 and 3.6. The mean response spectra results are shown in Appendix H.

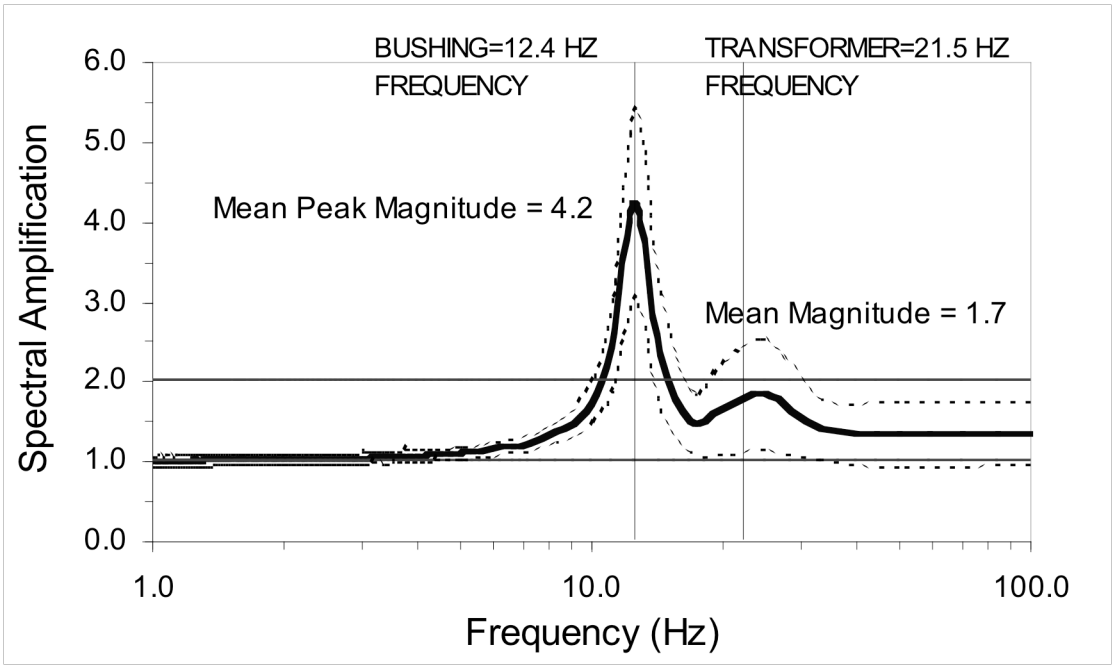

Figure 3.5 - Spectral amplification results for 230 kV Transformer C in the Transverse direction (Retrofit Configuration 2).

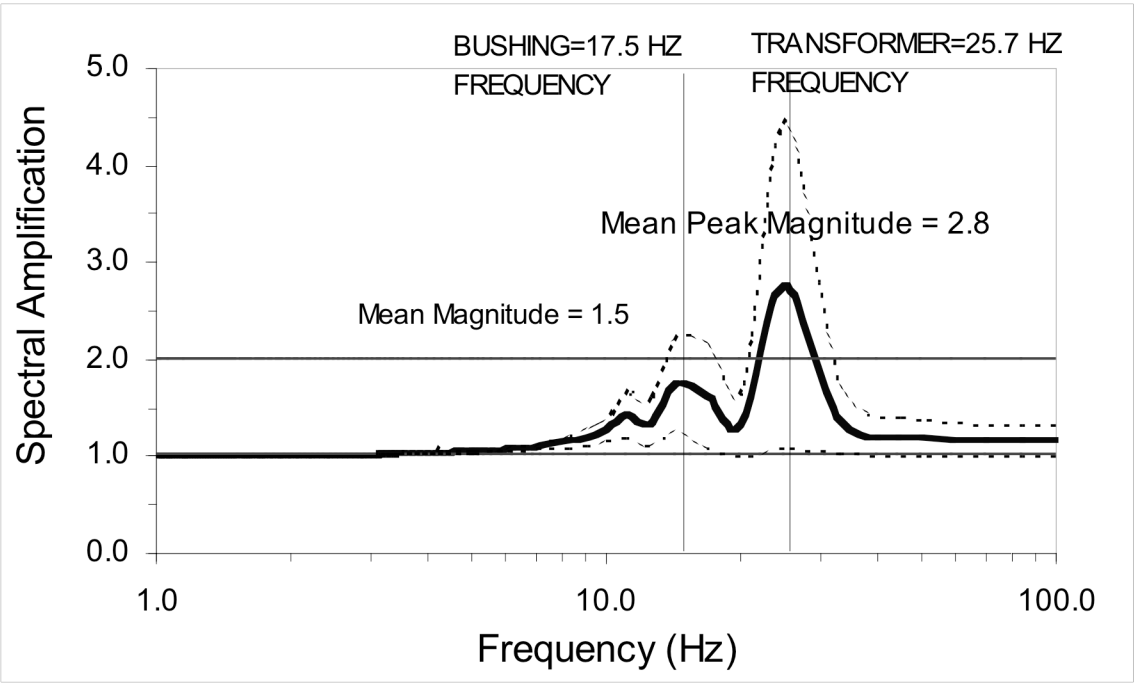

Figure 3.6 - Spectral Amplification Results for 230 kV Transformer C in the Longitudinal Direction (Retrofit Configuration 2).

3.5. Summary

From the results of the numerical study on the spectral amplification of the four transformers described in Chapter 2, it became apparent that the largest spectral amplification occurred in the 230 kV Transformer C. From this study, the spectral amplification was found to be 17.1 and 2.8 at the bushing frequency in the transverse and longitudinal direction respectively. It is quite clear that the assumed amplification value of 2.0 defined within the IEEE-693 does not apply to all transformers. The large transverse amplification occurred in the 230kV Transformer C due to several factors that have yet to be considered within the IEEE-693 standard. Among them, the most influential factors were the local flexibility around the bushing mounting point and the

fact that the natural frequency of the tank was relatively close to the natural frequency of the bushings.

In an attempt to reduce the large amplification that may occur to some transformers such as the 230 kV Transformer C, certain retrofit configurations were considered and analyzed. While several retrofits could potentially resolve the two influential factors described above, only two retrofits were chosen based upon their overall feasibility.

The first retrofit configuration effectively increased the stiffness around the bushing mounting point by attaching braces to the bushing turret. Although it provided stiffness, this retrofit did not resolve the concern regarding the close match between the transformer tank and bushing predominant frequencies. Despite this, the spectral amplification was significantly reduced when the turret bracing was introduced. The spectral amplification in the transverse direction reduced to 5.0 at the frequency of the bushing. This is a large reduction from the non-retrofitted case where the spectral amplification value in the transverse direction was 17.7. The spectral amplification in the longitudinal direction dropped below the IEEE-693 standard defined value of 2.0. Table 3.1 summarizes the spectral amplification results that occurred at the bushing and transformer frequencies for the retrofitted and non-retrofitted 230kV Transformer C.

The second retrofit configuration was designed to partially resolve both of the influential factors that appear to significantly increase the amplification of the ground motion. The bracing on the bushing turrets added stiffness to the bushing support conditions while the bracing on the transformer tank effectively separated the

transformer tank and bushing transverse frequencies. As expected, the spectral amplification in the transverse direction was reduced relative to the first retrofit configuration. However, the reduction in amplification from 5.0 to 4.2 was not as large as was anticipated. The addition of the braces mounted to the transformer tank didn't have much positive effect, which leads one to believe that flexibility of the transformer top has a larger influence on the amplification between the ground and the base of the bushing.

Table 3.1 - Mean Spectral Amplification Results at Transformer Tank and Bushing Frequencies for Retrofitted and Non-retrofitted 230 kV Transformer C.

Transformer	Component	Transverse Direction	
		Frequency (Hz)	Spectral Amplification
Non-Retrofitted	*Tank*	11.1	17.7
	Bushing	9.1	17.1
Retrofit 1	*Tank*	10.3	11.2
	Bushing	12.7	5.0
Retrofit 2	*Tank*	21.5	1.7
	Bushing	12.4	4.2

Transformer	Component	Longitudinal Direction	
		Frequency (Hz)	Spectral Amplification
Non-Retrofitted	*Tank*	25.0	3.2
	Bushing	11.1	2.8
Retrofit 1	*Tank*	25.1	2.8
	Bushing	15.3	1.6
Retrofit 2	*Tank*	25.7	2.8
	Bushing	17.5	1.5

From the results obtained in this study, it is concluded that the addition of bracing attached to the bushing turret is an effective and fairly simple manner of stiffening the mounting conditions and ultimately reducing the dynamic response of the bushing. Although only one bracing design that stiffened the bushing mounting conditions was analyzed, several additional or alternative stiffening designs could be implemented

depending upon the transformer details and the desired stiffness. For transformers that have relatively flexible top plates and relatively tall turrets upon which the bushings are supported such as the 230 kV Transformer C, the implementation of stiffening members should be considered in order to reduce the chance of bushing failures during future seismic events.

4. EVALUATION OF IEEE-693 SEISMIC QUALIFICATION TESTING GUIDELINES

4.1. IEEE-693 Seismic Qualification Testing Guidelines for High Voltage Bushings

In order to seismically qualify particular types of equipment located in regions of moderate to high seismicity, the IEEE-693 standard require shake-table tests to be performed. Shake table tests are primarily conducted on tri-axial shake tables such that the equipment can be subjected to accelerations in the two perpendicular horizontal directions, and in the vertical direction simultaneously. The IEEE-693 standard has defined a required response spectrum to be used for testing and design purposes of electrical equipment. The required response spectrum is a broadband response spectrum that envelopes the effects of earthquakes in different regions with various magnitude/distance combinations as well as site conditions ranging from rock to soft soil. Figures 4.1 and 4.2 show the IEEE-693 required high response spectrum and moderate response spectrum for various levels of damping.

The required response spectrum to be used for qualification depends upon the seismicity of the region and the amount of damping inherent in the equipment to be tested. For most equipment, the 2% damped required response spectrum is typically used, unless otherwise justified. When conducting shake table tests, the two horizontal input motions on the shake table are required to envelope the required response spectrum at the predominant natural frequency of the equipment, while the vertical component must meet or exceed 80% of the required response spectrum [2].

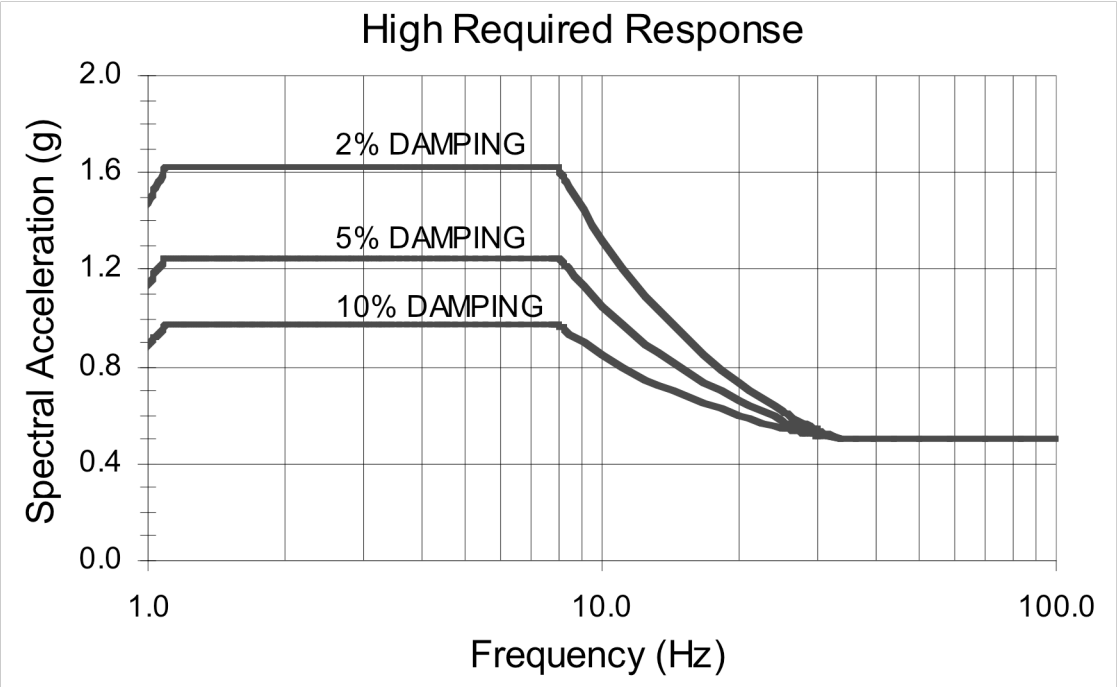

Figure 4.1 - IEEE-693 High Required Response Spectra [2]

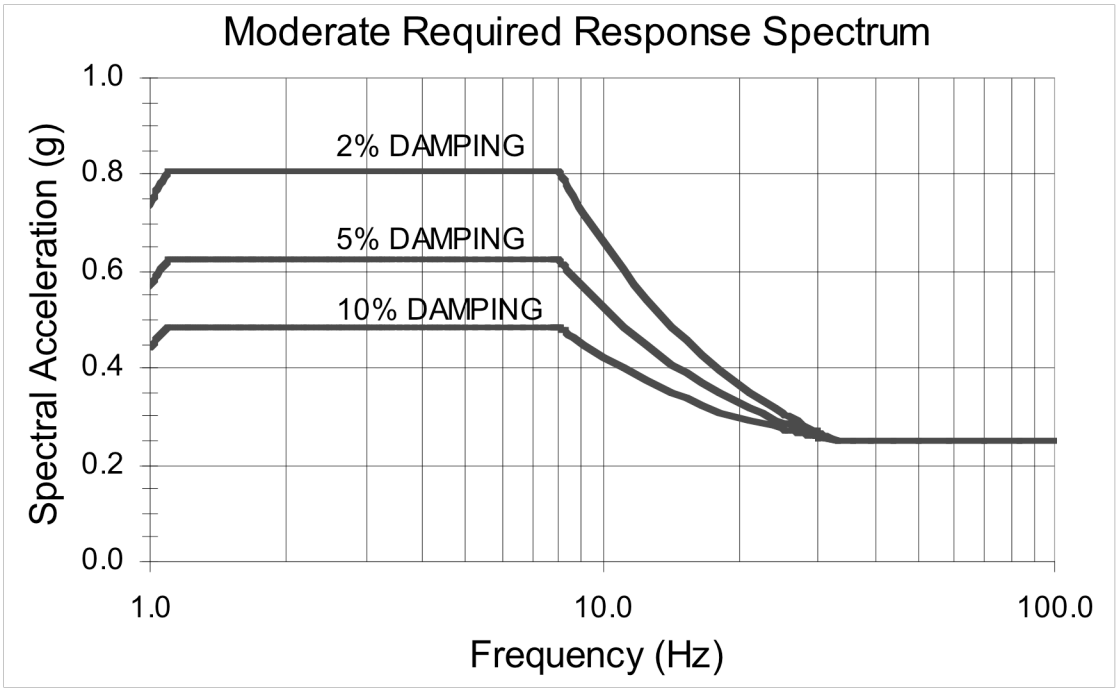

Figure 4.2 - IEEE-693 Moderate Required Response Spectra [2].

During the shake table tests, the stresses within the equipment material are monitored. In order for the equipment to be accepted, the stresses developed in the equipment shall not exceed the allowable stress for that particular material. In addition, the equipment should be fully functional and must not have developed any oil or gas leaks.

To meet the requirements of the IEEE-693 standard, bushings with voltage ratings of 161 kV and above which are operating in regions of moderate to high seismicity, must be seismically qualified by time-history shake table tests. Generally, it is recommended that electrical equipment be tested with mounting conditions that are similar to its in-service configuration. Bushings are typically mounted on the top of transformers, and therefore due to the size and weight of high voltage transformers, the testing of a bushing mounted on top of a transformer is not practical on a routine basis. During qualification tests, bushings are mounted upon a rigid frame that is supported on the shake table in luau of the transformer. The rigid frame must not have any modes of vibration with frequencies less than 33Hz in order to be acceptable. It is recognized within the IEEE-693 qualification standard that the transformer tank will influence the response of the bushing. The stresses that develop within the bushing as a result of the ground motion are amplified by the transformer body as well as the local flexibility of the top plate. To account for this amplification, the bushing is tested at twice the required response spectrum. Therefore, the horizontal test response spectra, calculated from the two perpendicular horizontal acceleration time histories of the shake table, must envelope two times the required response spectrum at the predominant natural frequencies of the bushing, while the vertical component must

meet or exceed 80% the required response spectrum multiplied by two. Figure 4.3 below shows a photograph of qualification test on a 230kV bushing performed at the University of California, Berkeley [3].

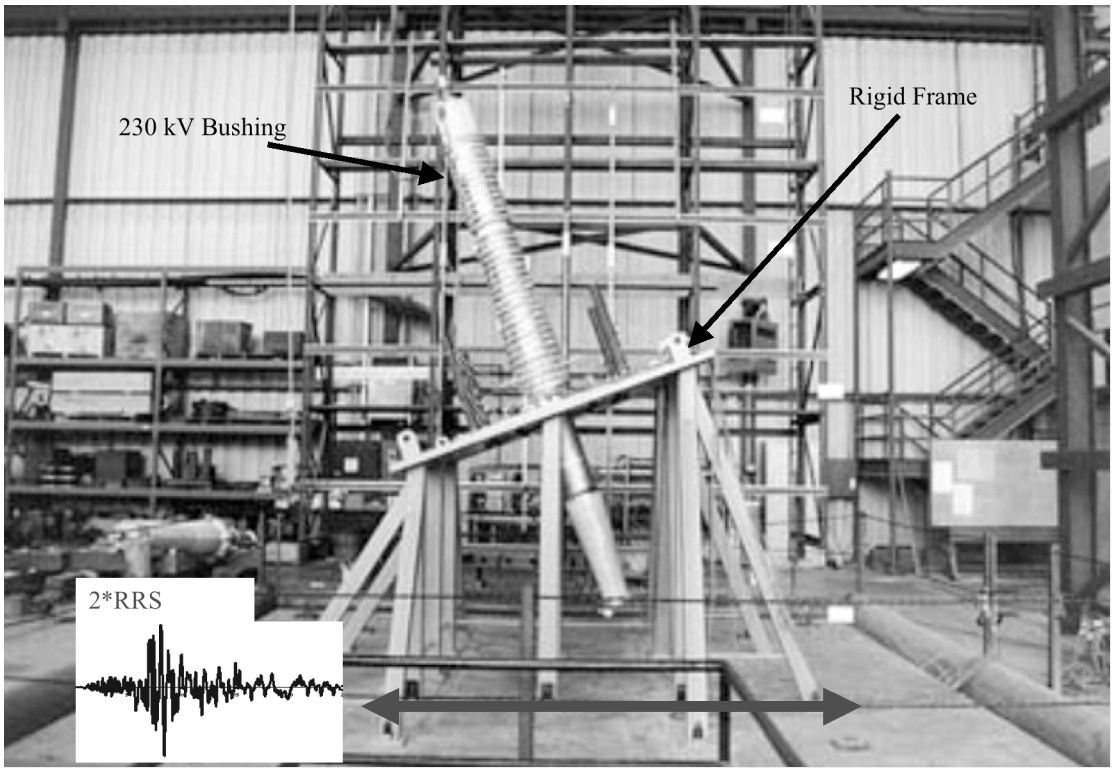

Figure 4.3 - Bushing Qualification Test of a 230kV Bushing [3].

4.2 Scope of Study

In the first two numerical studies described in chapters 2 and 3, the amplification was defined by finding the spectral amplification in a given direction for a particular transformer. The spectral amplification was computed by using the horizontal acceleration time histories at the base of the bushing and the base of the transformer to compute the response spectrum ratio. Although the spectral amplification gives good insight into the influence of the transformer on the bushing response, it does not

necessarily reflect the amplification in stress within the bushing between rigid and transformer tank mounting conditions. One reason for this is the fact that the spectral amplification fails to capture the rotational component of the bushing response, which can be significant given the relatively high flexibility of the mounting conditions. This rotation induces bending stress within the bushing that may not be accounted for in the spectral amplification analysis.

Ultimately, the increase in stress that occurs in a bushing under the two different mounting conditions is the desired quantity for design purposes. By knowing this stress amplification, seismic tests could be performed with an amplified ground motion that corresponds to the expected increase in stress in the bushing when mounted on a transformer. Therefore, this numerical study was performed in an attempt to better define the amplification in stresses experienced by a bushing mounted on a transformer tank.

The majority of the bushing stress during seismic loading occurs due to bending. Because of this, the peak bending moment at the base of the bushing was selected as the evaluation parameter for this study. Through time-history dynamic analysis, the peak bending moment at the base of the bushing was computed for a given transformer. Then, the rigid IEEE-693 seismic qualification testing conditions for bushings was replicated. With this rigid condition, the same time-history dynamic analysis was performed and the peak bending moment of the bushing was found. The amplification was defined by taking the ratio of the peak bending moment of the bushing mounted on the transformer and the peak bending moment of the bushing rigidly mounted.

4.3 Analysis Procedure

For this numerical study, three different bushings were considered, the 500kV bushing from Transformer D, the 230 kV bushing from Transformer C and the 525kV bushing from Transformer A. These three bushings were chosen because their corresponding transformers resulted in the largest spectral amplifications from the first numerical study conducted in Chapter 2.

For each of these bushings, a dynamic time-history dynamic analysis was performed under two mounting conditions. The first mounting condition was representative of in-field conditions. Therefore, the bushing was analyzed as being mounted on the transformer. The second mounting condition represented the IEEE-693 bushing shake table qualification test. Therefore, the bushing was rigidly mounted.

Time-history dynamic analyses were performed using a time-history that matches the IEEE-693, 2% damped, high required response spectrum. This time-history, developed by Gregory L. Fenves and Shakhzod M. Takhirov from UC-Berkeley, is an acceleration record recorded from the 1992 Landers earthquake that has been filtered and matched to the IEEE required response spectrum. Figures 4.4 and 4.5 show the time-history and its 2% damped response spectrum respectively.

For each bushing, the record was run in each of the three orthogonal directions of the bushing for a given mounting condition. The two horizontal acceleration inputs matched the 2% damped response spectrum while the vertical acceleration input matched 80% of the response spectrum.

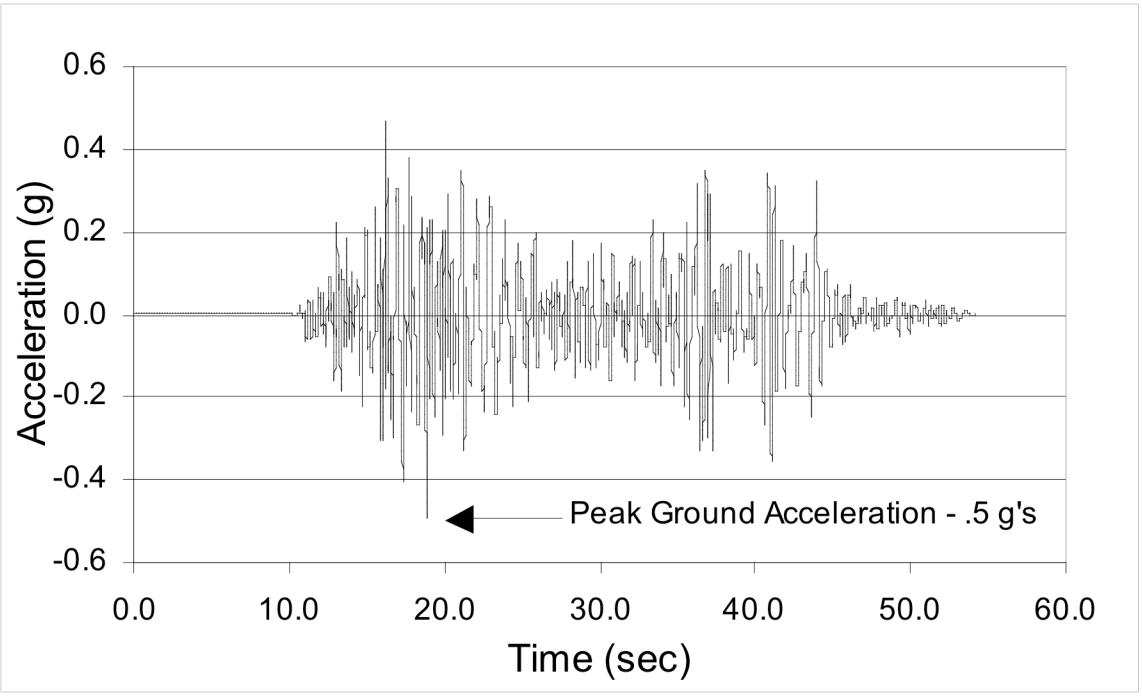

Figure 4.4 - Landers Record Filtered and Matched to the IEEE Required Response Spectrum (Fenves G.L., and Takhirov S., Personal Communications).

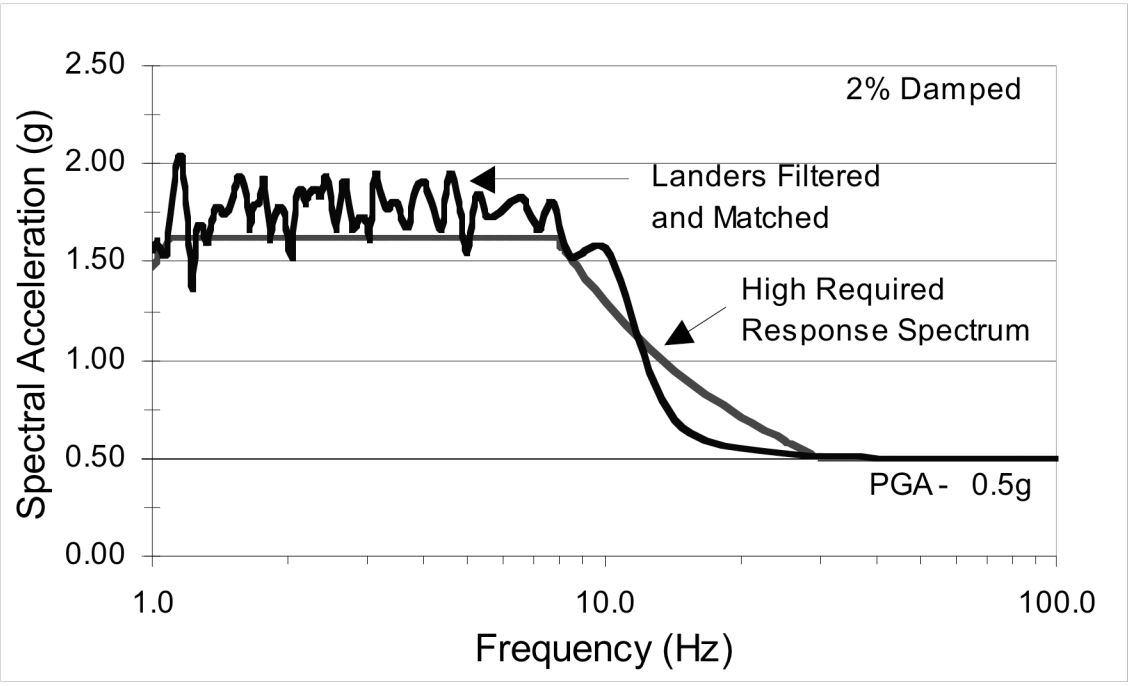

Figure 4.5 - Response Spectrum of Landers Filtered and Matched Record Compared with the IEEE-693 High Required Response Spectrum.

From each analysis, the bending moment at the base of the bushing was obtained in its two horizontal axes as a function of time. The maximum bending moment at a given time was computed by:

$$Mmax = \sqrt{M_{22}^2 + M_{33}^2} \qquad \textbf{(4.1)}$$

where M_{22} and M_{33} correspond to the bending moment about the bushing's x and y axes, respectively.

For a given bushing, the moment amplification was computed by taking the ratio of the maximum bending moment obtained with transformer-mounted boundary conditions over the maximum bending moment obtained attached to a fixed base.

This peak bending moment amplification was then compared with the amplification value of 2.0 defined within the IEEE-693 standard as well as the spectral amplification values found in the first numerical study described in Chapter 2.

4.4 Results of Study

The influence of the transformer tank and flexibility of the top plate increased the peak bending moment of the bushing. For the 525kV Transformer A bushing, the 500kV Transformer D bushing, and the 230kV Transformer C bushing, the peak moment amplification was 1.1, 1.7 and 7.9 respectively. In other words, for the Transformer C bushing, the peak bending moment of the bushing was 7.9 times greater when mounted upon the transformer than when it is rigidly mounted, as is the case during seismic qualification tests.

Using the same time-history that matched the IEEE-693, 2% damped, high required response spectrum, spectral amplifications were computed for the same three

transformers in order to compare the different amplification definitions. It was found that the peak bending moment amplification is significantly less than the spectral amplification, as shown in Fig. 4.6. Naturally, the two values differ for each transformer due to their respective definition. The moment amplification is a representation of the amplification in stress that is to be expected when a bushing is mounted on top of a particular transformer vs. a bushing mounted on a rigid stand. The spectral amplification at the bushing frequency represents the amplification of the horizontal spectral acceleration of the bushing vibrating at its fundamental frequency between the two different mounting conditions described above. Nonetheless, it is interesting to compare the variation in these two amplification values. For the 230kV Transformer C, the amplification of the peak bending moment was less than half of the spectral amplification at the bushing frequency. Both transformers A and D experienced spectral and bending moment amplifications less than 2.0 at their corresponding bushing frequency. Also, both transformers A and D experienced an amplification of their peak bending moment of about 70% of the spectral amplification at their respective bushing frequency.

When comparing the peak bending moment within a particular bushing between the two mounting conditions, only the 230kV Transformer C bushing had an amplification larger than the assumed amplification value of 2.0 defined within the IEEE-693.

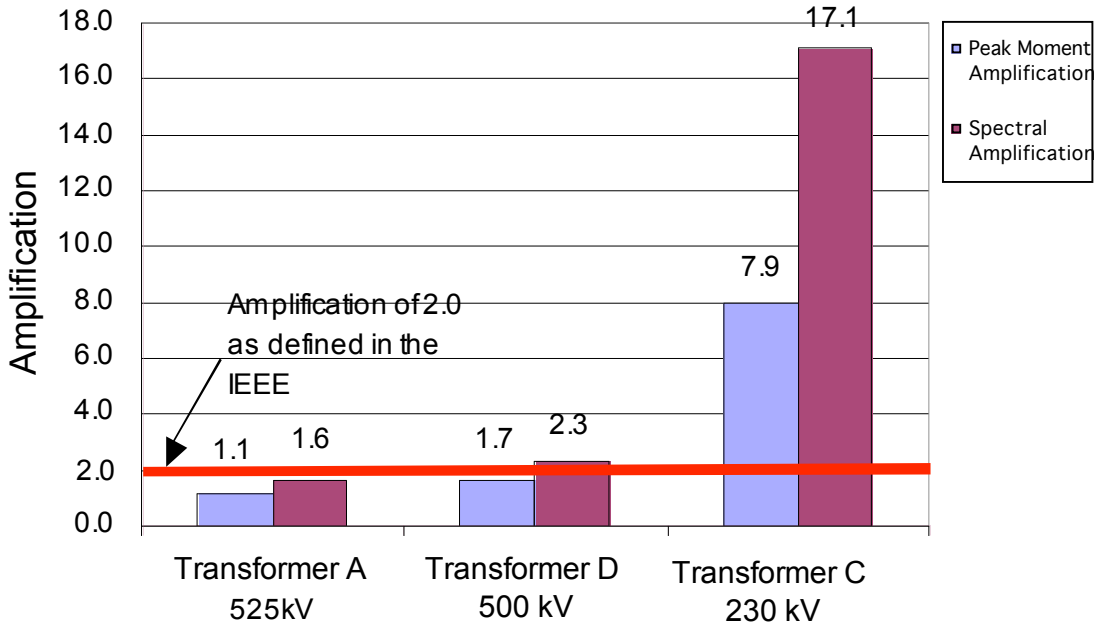

Figure 4.6 - Peak Bending Moment and Spectral Amplifications for Various Transformers.

4.5 Summary

This study was performed as another way of checking the validity of the amplification value of 2.0 given in the IEEE-693 standard. The spectral amplification is an effective way to determine the influence of the transformer tank and local flexibility on the response of a bushing; however, it does not directly determine the expected increase in stress that should be considered during bushing qualification tests. Instead of comparing the difference in the bushing horizontal spectral acceleration between the two mounting conditions, this study directly compares the peak bending moment and thereby the peak bending stress for a particular bushing during qualification tests vs. this same bushing in its in field mounting conditions subjected to the same seismic loading.

The results of this study show that the amplification value of 2.0 defined within the IEEE-693 standard is not a conservative assumption for all cases. For the 230kV Transformer C bushing mounted upon the transformer, the peak bending moment was 7.9 times larger than if it were rigidly mounted. In other words, for this particular bushing mounted on its respective transformer, the stresses that are induced in the bushing during seismic loading will be much larger than if it were rigidly mounted. It should be noted that these peak moment amplification values were determined for only one ground motion time-history. This amplification may vary for different time-histories; however, the objective of this study was to directly compare between what is done for bushing shake table tests used to qualify the equipment and what may occur for a bushing realistically mounted that undergoes the same level of shaking.

For the case of the 230kV Transformer C bushing, the IEEE-693 qualification method would greatly underestimate the amplification of stress that occurs due to the transformer tank and local flexibility around the bushing. By looking at the peak bending moment amplifications for the 500kV Transformer D and 525kV Transformer A bushings, it can be concluded that the IEEE-693 bushing qualification procedure is in fact conservative. The bending stress experienced by these bushings during the design earthquake will not likely exceed the stress induced during the qualification test.

The same trends exist between these results and the results obtained from the first numerical study. In both cases, the 230kV Transformer C resulted in the largest amplification, while the 500kV Transformer D resulted in the second largest amplification. Just as well, the 500kV Transformer D and the 525kV Transformer A

had amplification values close to what is assumed within the IEEE-693 qualification document. However, for both studies, the 230kV Transformer C had amplification values much larger than the amplification value of 2.0 used during qualification tests. Although, the two studies measure different parameters, they are both influenced by the dynamic properties of the bushing-transformer system. Therefore, the large peak moment amplification that occurred with the 230kV Transformer C bushing is partially a result of the relatively close predominant natural frequencies of the bushing when mounted on the transformer and the transformer tank.

It is concluded that the influence of the transformer tank and the local flexibility of its top plate tends to increase the bending stresses that a bushing is subjected to during seismic loading. This is acknowledged within the IEEE-693 seismic qualification document. However, to account for this, the IEEE-693 standard merely requires shake table tests be performed by using twice the required response spectrum. Provided the bending stress within the bushing increases linearly within increasing ground acceleration, this means that the qualification method qualifies bushings to twice the bending stress to account for the transformer tank influence. Although this method appears to be conservative in some cases, in other cases the increase in bending stress within the bushing due to the transformer influence may be much larger than 2.0.

Practically, qualification tests that match the peak moment amplification values obtained in this study for the 230kV Transformer C bushing are not feasible. Surely, testing to such a level would exceed the table limitations as well as fail the bushing specimen. Instead of changing the testing requirements, it makes better sense to

change the dynamic properties of the transformer-bushing system (i.e. stiffen certain components). As mentioned in the second numerical study described in Chapter 3, there are several methods of retrofitting a transformer such that the bushing responds differently during seismic loading. Regardless, a method needs to be adopted in order to predict or recognize situations such as the 230kV Transformer C, where the bushing bending stresses experienced during the design earthquake will be much larger than the peak stresses that occurred during the qualification testing. Once a transformer's hazard is identified, proper measures or retrofits can be implemented to prevent future failure of the bushings during the design earthquake.

5. SHAKE TABLE TESTS OF A FULL SCALE HIGH VOLTAGE TRANSFORMER - MOCK BUSHING SYSTEM

5.1 Scope of Experimental Testing

This chapter describes the shake table testing of a 525kV transformer-bushing system. The opportunity to test on a shake table a full-scale high voltage transformer is significant. Never before has a high voltage electrical transformer been shake table tested in the United States. The shake table tests performed allowed for the unique opportunity to identify the dynamic properties of the system as well as better understand the performance of a transformer during seismic loading. There were three main objectives of the experimental portion of this research.

The first objective was to determine the fundamental natural frequencies, corresponding mode shapes and damping values of the transformer-bushing system. Natural frequencies and mode shapes were obtained by performing white noise tests, during which the transformer was subjected to a random base excitation. By knowing the fundamental frequencies of the system, the shake table was then used to excite specific modes of the structure. Once excited, the table was abruptly halted, and the exponential decay of vibration was measured in order to determine the damping characteristics of that particular mode.

The second objective of the testing was to experimentally quantify the amplification between the ground motion and the motion at the base of the bushing. Using the several ground motion time-histories, the spectral amplification was calculated as defined in the first two numerical studies.

Finally, the third objective of the experimental testing was to validate the results obtained from the numerical studies. For this purpose, a modified finite element model of the 525kV Transformer A that represents the transformer test specimen was developed and calibrated according to the experimental results. The finite element model was developed in an attempt to replicate as accurately as possible the experimental conditions. By doing this, the results of the numerical studies previously discussed are better validated.

5.2 Description of UC-San Diego Earthquake Simulation Facility

The seismic tests were performed on a uniaxial shake table at the University of California, San Diego. The plan dimensions of the shake table are 10ft x 16ft. The shake table can support a maximum payload of 40 tons and was designed for an overturning moment of 8000 kip-inches. A 90-kip dynamic-rated actuator propels the shake table with a peak-to-peak stroke of 12 inches. The shake table frame is supported on two eight 5 in. diameter Garlock DU cylinders sliding on two stationary shafts roughly 8” in diameter. The peak sinusoidal velocity of the table is 40 in/s. The achievable peak accelerations that can be achieved are 9.0 g’s and 1.0 g’s for the bare table and fully loaded table respectively. The frequency range of the table is 0 to 50Hz [11]. The advanced control system of the shake table allows for the simulation of earthquake ground motions with high fidelity. A photograph of the shake table is shown in Fig. 5.1. The I-beam frame on top of the shake table is part of the mounting frame used to support the transformer specimen.

Figure 5.1 - Uniaxial Shake Table at UC-San Diego.

5.3 Description of Test Setup

To support the transformer test specimen, a steel frame was constructed and mounted on top of the shake table. The frame, composed of W12x26 I-beams, was constructed with an existing frame used for a previous shake table test, and additional beam members that outlined the footprint of the test specimen. All W12x26 beam members were welded to one another, and the lower flanges were bolted to the shake table. The shake table frame provided a mounting surface, upon which the transformer specimen could be welded to. Figure 5.2 shows a drawing of the complete shake table frame. The yellow W12x26 beams were welded together to the prior existing frame (red members).

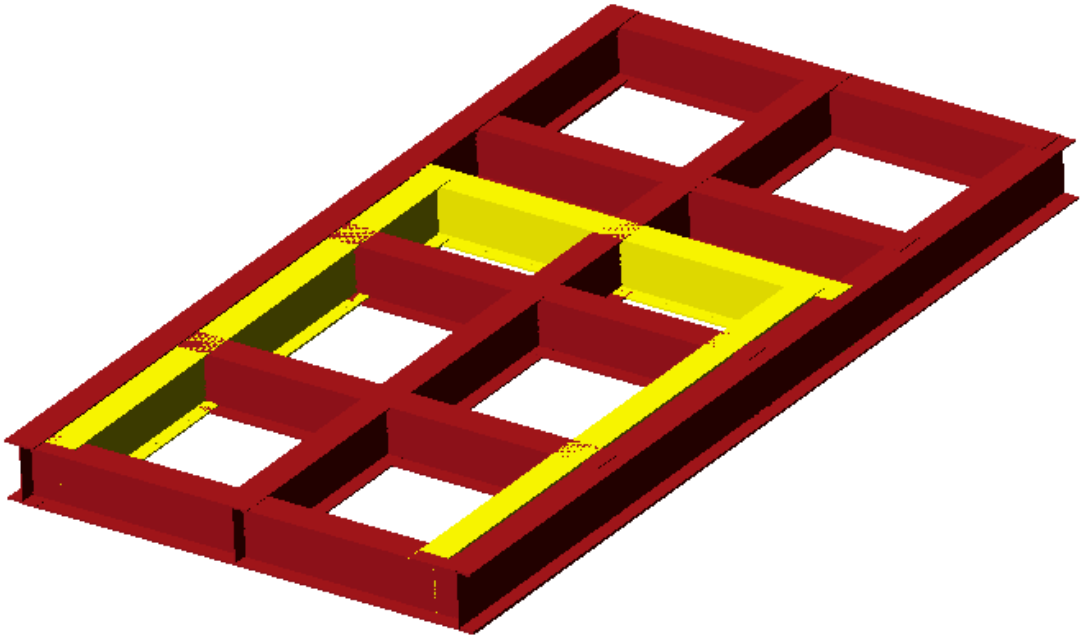

Figure 5.2 - Shake Table Mounting Frame.

5.4 Description of Transformer and Mock Bushing

The transformer specimen that was chosen for the shake table testing was a 525kV Transformer A. The transformer, graciously donated by PG&E, was taken out of service at the Midway substation in Bakersfield, California. The transformer consisted of just the steel tank that houses the core, coil and oil. The tank was stripped of all extraneous appendages such as its radiators, bushings, surge arrestors and control cabinet. Figure 5.3 shows the transformer at Midway substation after being taken out of service and stripped.

Figure 5.3 - 525kV Transformer A Test Specimen.

The dimensions of the transformer are 8.8 ft x 9.9 ft x 22.8 ft in height. The total weight of the tank is 67 kips. The test specimen was not completely representative of a true transformer due to missing components. Provided the interior core does not stiffen the tank, as assumed in the modeling, the majority of the transformer stiffness is a result of the steel tank structure itself. Regardless, the flexible mounting conditions of the bushing are of greater importance to the bushing response. The transformer tank included all stiffening elements on top of the transformer; therefore, the realistic bushing boundary conditions were captured during testing.

The steel tank sides and top plate are ½ inch thick while the bottom plate of the transformer is roughly 1-¼ inches thick. Several stiffening elements were welded to

the interior of the top plate. These stiffening elements were composed of thin plates and channels. These stiffening elements can be seen in Fig. 5.4. This photograph was taken within the upper half of the transformer looking toward the top plate. In addition to the stiffening elements attached to the top plate, several compounded steel lamina were tack welded to the interior of tank. These acted as a buffer between the steel tank and the core and coils mounted within the tank.

Figure 5.4 - Interior of Upper Half of Transformer Tank.

Due to the size and weight of the transformer tank, transportation of the tank was achieved by separating the transformer into two halves. The lower half of the

transformer was welded to the steel frame mounted on the shake table. The upper half of the tank was then loaded upon the bottom half and welded together on the perimeter of the flange. Figure 5.5 shows photograph of the upper half of the transformer tank being lowered onto the bottom portion of the tank. It was desired to mount the transformer such that the axis of shaking was parallel with the transverse axis of the transformer; however, this was not feasible due to spatial limitations. Therefore, the transformer was mounted such that shake table motion acted in the longitudinal direction of the tank.

Figure 5.5 - Transformer Test Specimen Being Assembled on Shake Table.

Porcelain transformer bushings are expensive and inherently brittle. Obtaining a real transformer bushing for testing purposes proved to be impractical. In addition,

there was a risk of failing the bushing if a real one was used during seismic tests. However to improve the validity of the shake table tests, it was necessary to capture the same dynamic characteristics of the transformer bushing system. Therefore, a mock bushing was used in lieu of a real transformer bushing during the seismic tests.

The mock bushing was designed such that it exhibited similar dynamic properties as a 525kV bushing. The mock bushing closely matched the total mass, stiffness and center of gravity of a real 525 kV porcelain bushing. In addition, the mock bushing was designed to exhibit roughly the same inertial forces and overturning moment induced during the shake table tests.

The particular typical 525kV bushing considered for testing is made of porcelain and has a total weight of 3.1 kips. The total height of the bushing above the flange was 4.1m. Using the structural analysis program SAP2000, the natural frequency of this typical 525kV bushing was estimated to be 3.1Hz when supported upon the 525kV Transformer A. The center of gravity of the 525kV bushing is located at 111.8 inches above its base.

The mock bushing was comprised of a three annular steel sections used as mounting plates, two steel tubular sections, and a steel plate upon which a concrete block was attached. The diameter of the main tube was 14 inches with a wall thickness of 3/8 in. The concrete block dimensions are 3 ft x 5 ft x 1 ft. A steel plate with ½ in thickness connected the concrete block to the steel tube. The total height of the mock bushing including the concrete block and attachment plates is 10'-1/2". Figures 5.6 and 5.7 show the dimensions and various components of the mock bushing as well as the mock bushing as it was attached to the transformer tank. As seen in Fig. 5.7, the

turret attachment plate was bolted to the turret upon the transformer top plate. The turret and mock bushing were tilted 7.8 degrees from the vertical axis. The bushing was rotated along a plane oriented 45 degrees from either main axis of the transformer.

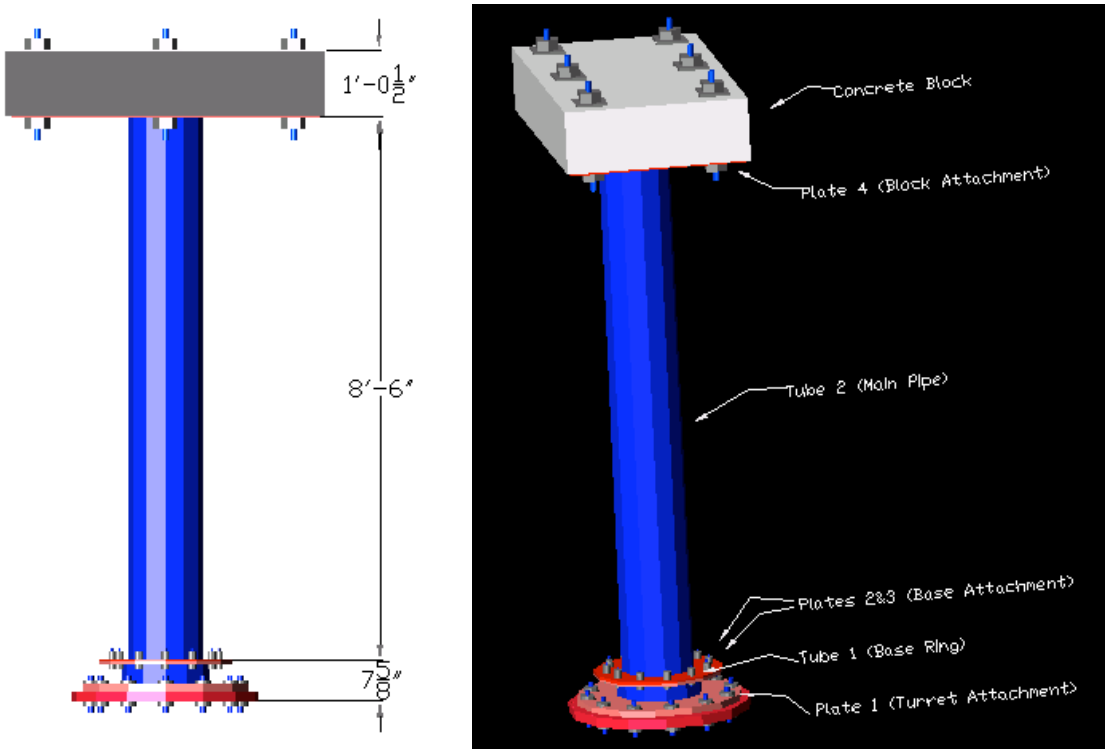

Figure 5.6 - Dimensions and Components of Mock Bushing.

Figure 5.7 - Mock Bushing Assembly Attached to Top of Transformer Tank.

The total weight of the mock bushing assembly is 3.1 kips. The center of gravity of the mock bushing is located at 112.1 in above its base. The fundamental frequency of the mock bushing is 2.9 Hz when attached to the transformer tank. Table 5.1 summarizes the physical and dynamic properties of the mock bushing and 525kV bushing. The mock bushing design proved to closely match the true bushing properties.

Table 5.1 - Dynamic and Physical Properties of Mock Bushing and 525kV Bushing.

Property	Mock Bushing	Actual Bushing
Total Height (in.)	120.5	161.8
Total Weight (lbs.)	3116	3090
Center of Gravity (in.)	112.1	111.8
Fixed Base Natural Frequency (Hz)	8.8	8.9
Transformer Mounted Natural Frequency (Hz)	2.9	3.1
Stiffness (kips/in.)	23.0	25.1
Yield Moment (kip-in.)	3195	1100
Yield Force (kips)	28	9.8

5.5 Instrumentation Setup

The transformer and mock bushing were outfitted with over fifty sensors to measure the acceleration, displacement and strain at various locations of interest. Before installing the instrumentation for the shake table tests, it was necessary to identify the specific parameters of interest as well as locations from which they could optimally be measured.

The first sequence of testing to be conducted is the system identification test. The objective of this test series is to capture the dynamic properties of the transformer bushing system such as natural frequencies, mode shapes and damping values. In order to identify these properties, several accelerometers were strategically placed to measure the acceleration along the height of the transformer and mock bushing. From the finite element models, it was recognized that the transformer had two fundamental modes of vibration corresponding to the complete tank vibrating along its transverse and longitudinal axis. Therefore the accelerometers placed on the transformer tank measured the acceleration in each of these principal directions. Figure 5.8 shows the East face of the transformer where 6 accelerometers were mounted to measure the

transverse accelerations experienced during testing. Four accelerometers were also placed along the length the mock bushing in order to characterize its dynamic properties as well as to measure the accelerations during testing.

The flexibility of the top plate was of particular interest due to the effect it has on the ground amplification. Therefore a number of displacement transducers were placed on the top plate in an effort to capture this local flexibility. The 525 kV Transformer A finite element model developed in the first numerical study was modified to represent the test specimen, and then used as a predictive tool. Utilizing this model, an array of transducers as shown in Fig. 5.9 was strategically arranged upon the top plate to capture the top plate largest out of plane deformations. Four displacement transducers were also attached to the top of the turret. These instruments measured the vertical displacement of the turret relative to the top plate. In other words, these were attached in order to determine the amount of rocking motion in the turret.

Figure 5.8 – Accelerometers Locations on East Face of Transformer Tank

Another objective of the shake table testing was to quantify the ground motion amplification. For this reason, bending stress values at the base of the mock bushing and accelerations on the turret were of particular importance. Therefore, eight accelerometers were attached to the top of the turret. These accelerometers measured the vertical and horizontal accelerations around the top of the turret. In addition, six uniaxial strain gauges were attached at the base of the steel tube. From these gauges,

the bending stress and thereby the peak bending moments at the base of the mock bushing could be calculated. Figure 5.10 shows a clear display of several instruments attached on or near the turret.

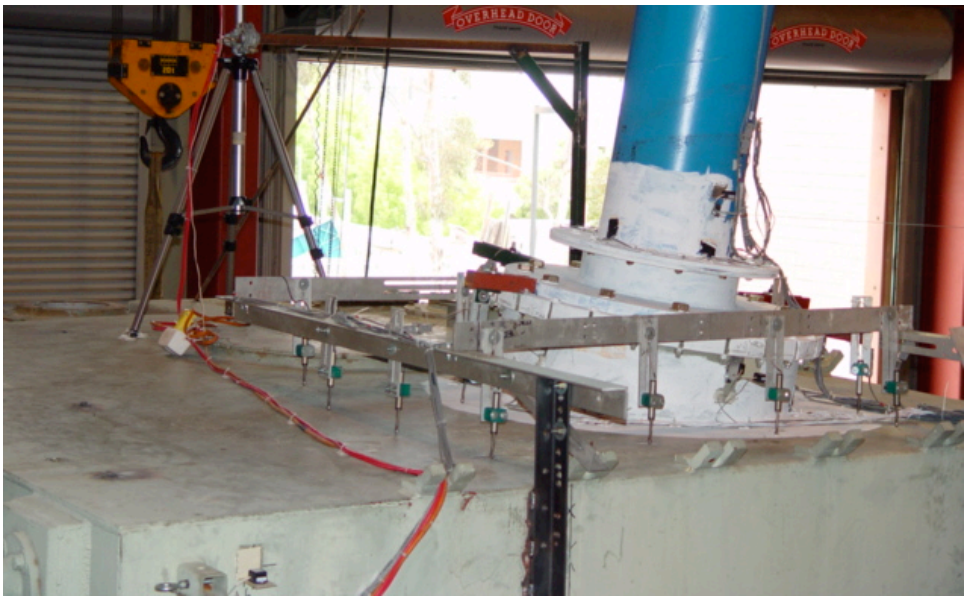

Figure 5.9 - Displacement Transducers Measuring the Out of Plane Displacement of the Top Plate.

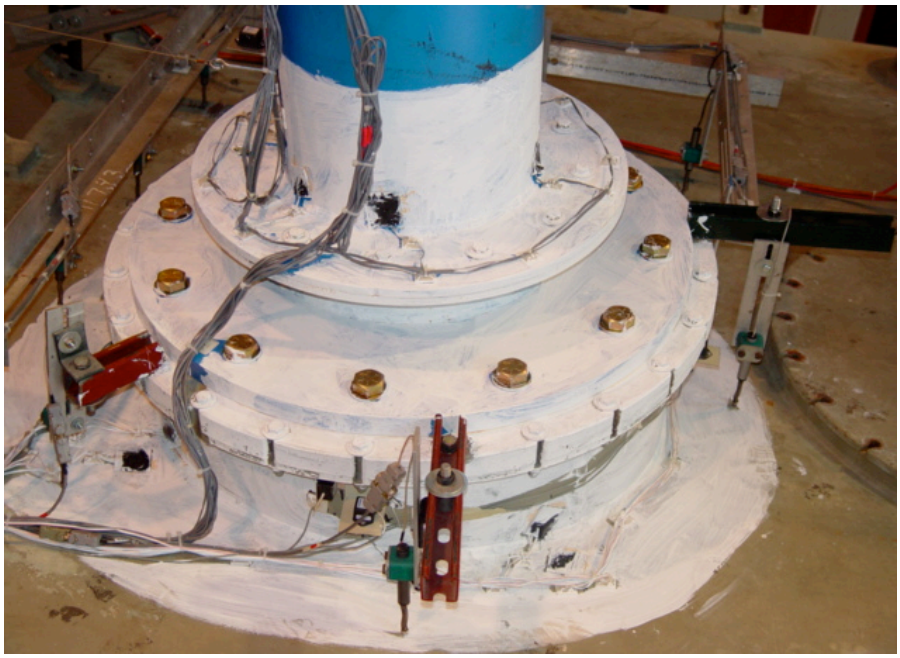

Figure 5.10 - Close up View of Instrumentation Attached to Turret.

For finite element model calibration purposes, displacement transducers and strain gauges were added to specific locations to measure the relative horizontal displacements of the structure and to capture regions of large stress concentrations. A total of ten string potentiometers were used to measure the relative horizontal displacement of the transformer and mock bushing along the axis of shaking. A concrete strong wall adjacent to the shake table was used as the fixed attachment point for these instruments. Figure 5.11 shows the string potentiometers attached between the strong wall and the South face of the transformer.

Figure 5.11 - Strong Wall and Horizontal String Potentiometers.

To gain an understanding of the stress distribution on the transformer tank during earthquake excitation, the finite element model was used to predict the locations of maximum stress concentrations. Results showed that the attachment region of the turret and transformer top plate produces the largest stresses; therefore eight strain gauge rosettes were attached at the base of the turret to capture the local strain values. The strain gauge rosettes measure the strain in three different directions along a plane. Given these three strain readings, the stress along any axis within that plane can be deduced at the strain gauge location. In addition to these strain gauges, a brittle latex paint (white wash) was brushed onto this particular area as seen in Fig. 5.10. This white wash paint, which flakes off during yielding, is used for the visual inspection of yielded steel. Although yielding wasn't expected, this paint was added for quick visual evaluation of the peak stresses around this area.

Figure 5.12 shows the location of all the instruments used during the shake table testing. The instruments are labelled according their function and number. An "A" prefix indicates an accelerometer, a "D" prefix denotes a horizontal displacement transducer, a "P" prefix indicates a vertical displacement transducer, and an "S" prefix indicates a strain gauge. Appendix I provides specific details of the instruments used during testing such as physical locations, directions of measurement, and type of instrument.

5.6 Earthquake Ground Motions and Shake Table Fidelity

A total of five earthquake acceleration time histories were selected for use during the shake table tests. Three of the records were actual ground motions recorded during

seismic events in the California region, while the other two records were synthetically produced to match the IEEE-693 response. Figures 5.13 through 5.17 shows each of these unscaled acceleration time-histories. Their corresponding 2% damped absolute acceleration response spectra are given in Appendix J.

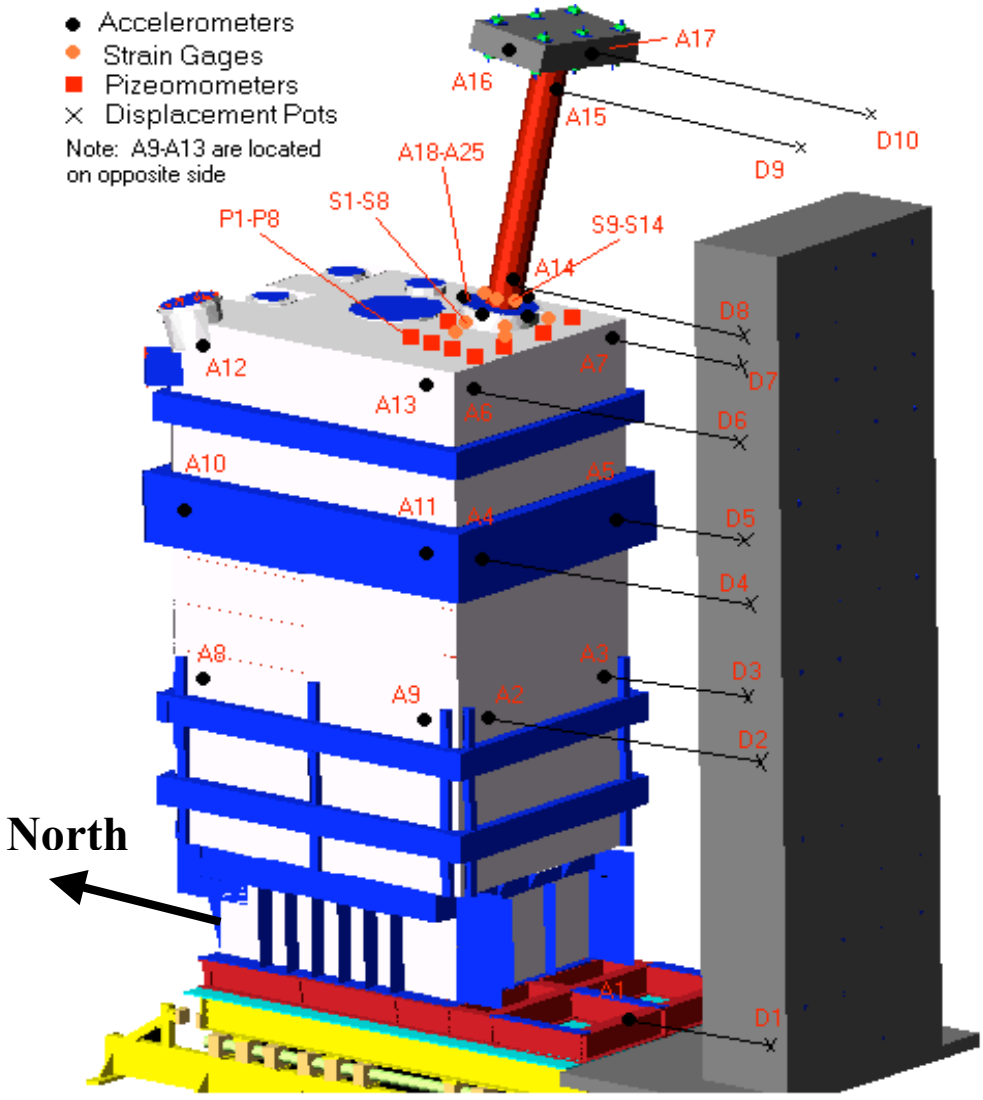

Figure 5.12 - Instrumentation Layout.

Before selecting the three recorded ground motions, a spectral amplification analysis was performed on the 525kV Transformer A test specimen model just as was

done in the first numerical study (see Chapter 2). Once again, the same twenty time histories shown in Appendix D were used in the analysis. Each of the time- histories was scaled such that its response spectrum matched the IEEE-693 high required response spectrum at the longitudinal frequency of the transformer model. From the analysis, the acceleration time-history at the base of the mock bushing was used to compute a 2% damped response spectrum for each record. After which, the mean, mean +1 standard deviation, and mean –1 standard deviation of all twenty response spectra were calculated. The three records that most closely matched the mean, mean +1 standard deviation, and mean –1 standard deviation spectra were selected for the shake table tests.

The Cape Mendocino (Mw 7.1) earthquake record was recorded at the Fortuna Blvd. Station in 1992. The peak ground acceleration (PGA) for this record is 0.116 g. This record was selected to match the mean –1 standard deviation of the twenty response spectra calculated at the base of the mock bushing on the test model [10].

Two records were selected from the 1997 Northridge earthquake (Mw 6.7). The first record was recorded at the Beverly Hills 14145 Mulhol station. This record has a PGA of 0.415 g and was selected to match the mean + 1 standard deviation. The other acceleration time-history was recorded at the Canoga Park station. It has a PGA of 0.356 g and was selected to match the mean of the twenty response spectra [10].

The IEEE-693 time-history, provided by Anshel Schiff, is a synthetic record that was used for seismic qualification of electrical equipment according to the IEEE-693 standard. The other synthetic record was originally recorded from the Landers

earthquake event (M_w =7.2) in 1992. It was then filtered and modified to match the IEEE-693 2% damped required response spectrum.

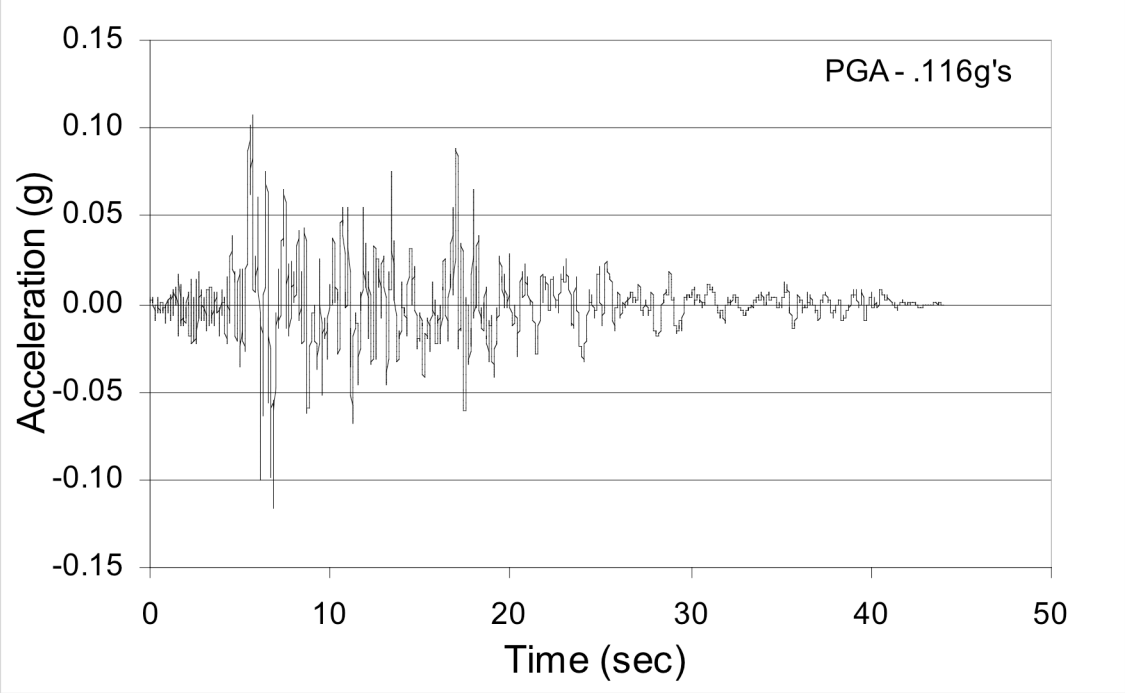

Figure 5.13 - Cape Mendocino (Fortuna Blvd.) Shake Table Time-History.

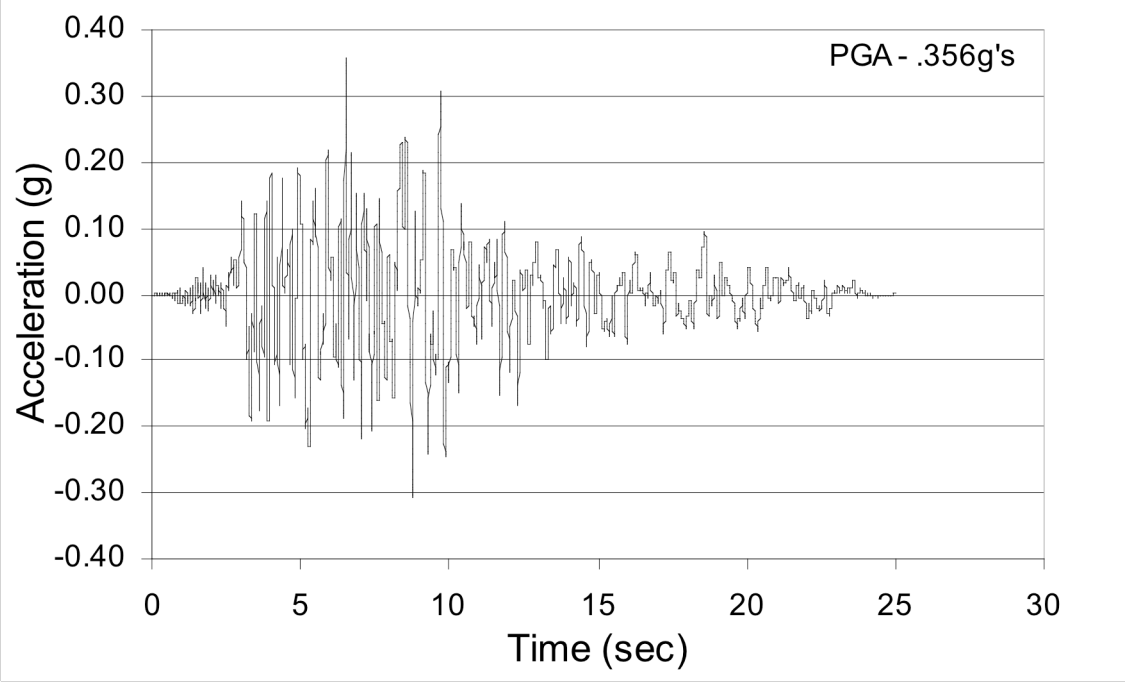

Figure 5.14 - Northridge (Canoga Park) Shake Table Time-History.

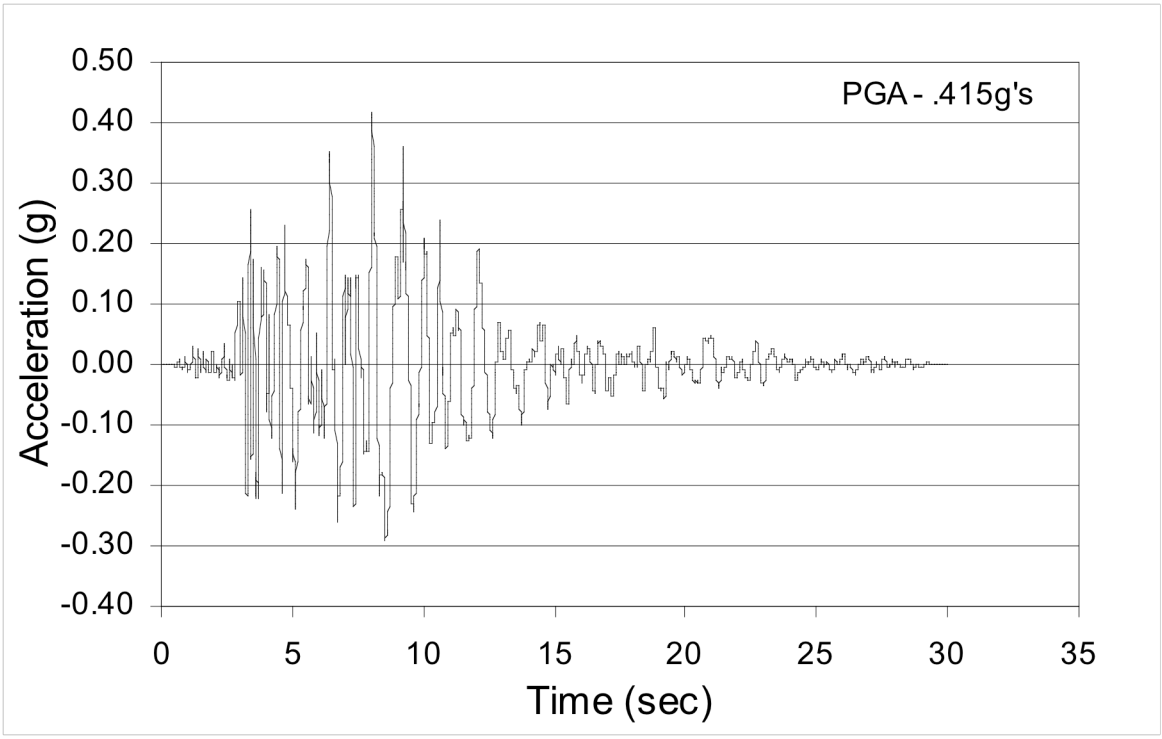

Figure 5.15 - Northridge (Mulhol) Shake Table Time-History.

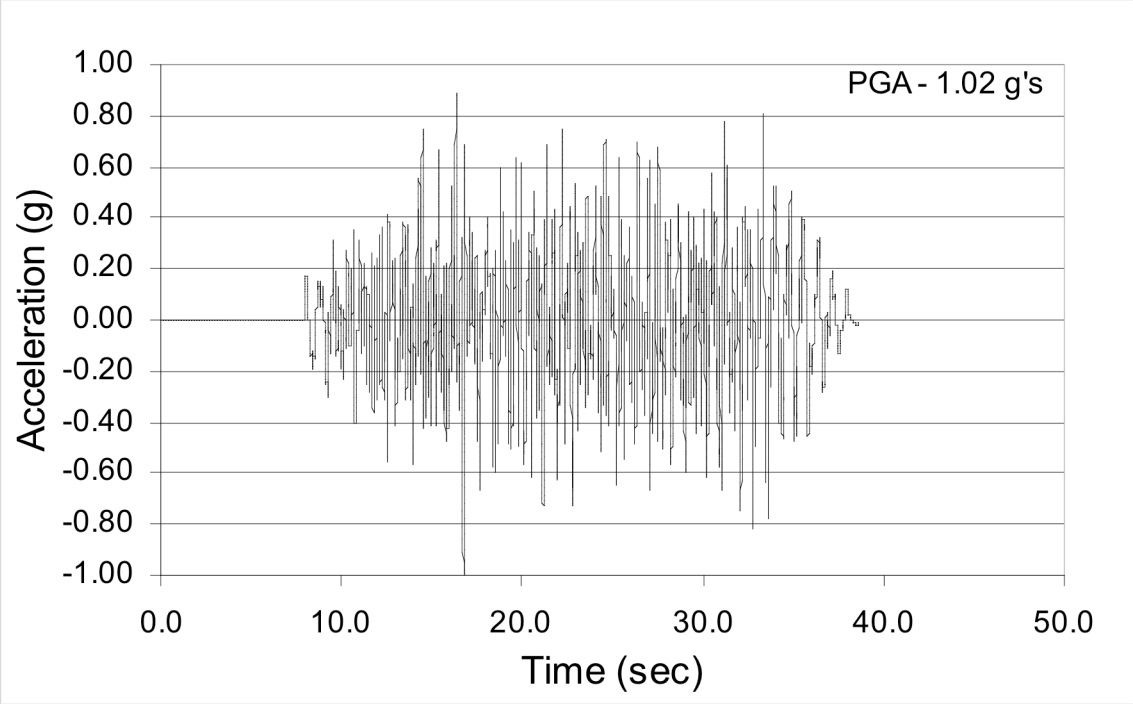

Figure 5.16 - IEEE Shake Table Time-History.

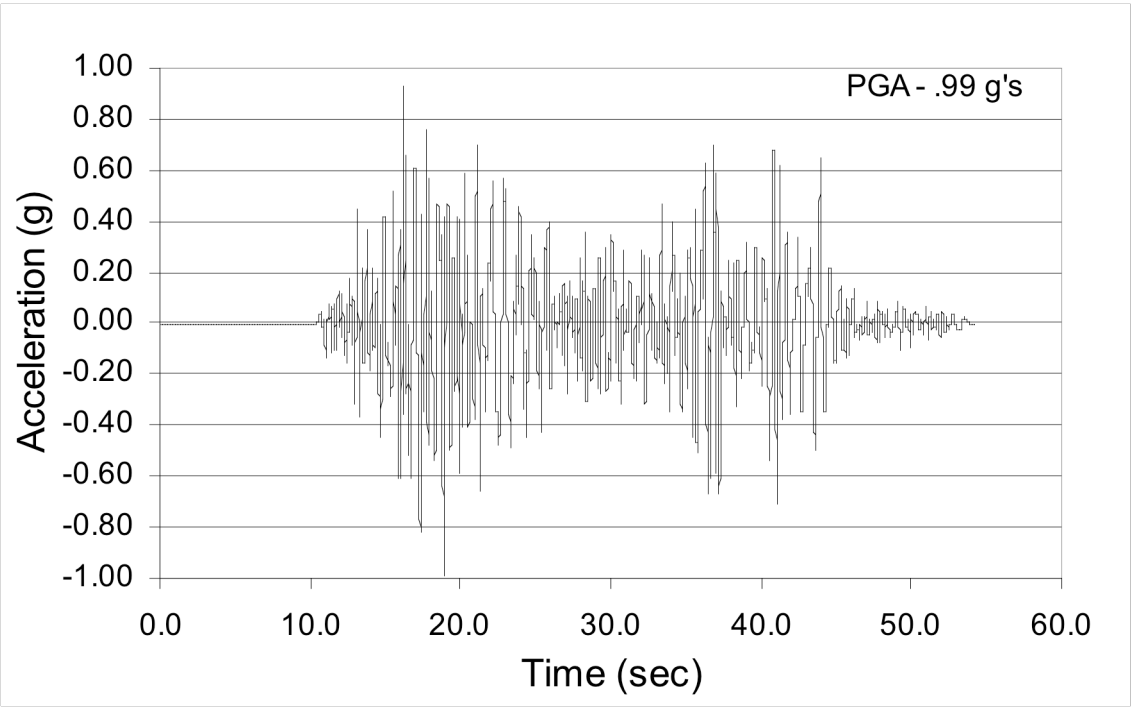

Figure 5.17 - Landers (Filtered and Matched) Shake Table Time-History.

Due to the height and large mass of the transformer, the limiting factor for ground motion intensities was the overturning moment capacity of the shake table. The overturning moment capacity of the table is 8000 kip-inches. Therefore, it was determined from the transformer test model that the peak ground acceleration that could be safely implemented on the table without exceeding the table overturning capacity was 0.4 g. Knowing this, the performance of the shake table was optimized at two different intensity levels, .1g PGA and .25g PGA.

The tuning of the shake table was performed with a white noise input with only the bottom half of the transformer attached to the table. In order to avoid damage to the complete transformer or shake table, no further tuning was attempted with the complete transformer-mock bushing system upon the table. Differences between the

recorded shake table acceleration (feedback signal) and the input acceleration (desired signal) were apparent. However, this distortion is not significant for these exploratory tests since the actual table acceleration was used for modal validation and the system remains essentially linear. Appendix K compares the 2% damped acceleration response spectra for the acceleration time histories of the feedback signals and desired signals for each of the five records considered in the shake table study.

5.7 Shake Table Test Program

Three different shake table test series were performed on the transformer-mock bushing system. The first series consisted of frequency evaluation tests to determine the fundamental vibration frequencies and their corresponding mode shapes of the system. The second test series performed involved damping evaluation tests from which the percentage of critical damping for each mode of vibration could be determined. The final test sequence was a series of seismic tests using the acceleration records described in Section 5.6.

The frequency evaluation tests were performed using a flat white noise excitation. The excitation frequency range was between 0 and 50 Hz. During the 11-minute white noise excitation, acceleration time-histories were recorded from each of the accelerometers. The modal analysis software U2 was utilized to determine the natural frequencies from power spectral density plots of the absolute acceleration time histories of various accelerometers [12]. The corresponding mode shapes were found by comparing the relative amplitudes of the spectral density plots and phase difference

between different accelerometer measurements. Table 5.2 is a summary of the test protocol adhered to during the frequency evaluation tests.

Table 5.2 Frequency Evaluation Test Protocol

Nyquist Frequency	50 Hz
Sampling Rate	100 Hz
Number of Points Per Sampling Window	4096
Duration of Each Sampling Window	41 sec
Frequency Resolution	.0244 Hz
Number of Sampling Windows	16
Total Duration	655.2 sec

The damping evaluation tests were performed by introducing a low-amplitude sinusoidal excitation at specific frequencies corresponding to the natural frequencies of the system determined during the frequency evaluation tests. Once a steady-state resonance had occurred, the shake table excitation was abruptly stopped causing a logarithmic decay in the vibration amplitude of the test structure. Acceleration time-histories recorded during the damping tests were then used to evaluate the percentage of critical damping for that particular mode through the use of the logarithmic decrement method [13].

The seismic tests were conducted using the five ground acceleration records described earlier at seven different intensities. The peak input acceleration of the records ranged from 0.05 g to a maximum of 0.35 g by increment of 0.05g. The shake table seismic testing sequence is shown in Table 5.3. Note that only the Northridge (Mulhol) record was tested at an intensity of 0.35 g due to larger overturning moments produced by the other four records. Data was acquired during the seismic tests at a sampling rate of 100 Hz and filtered with a 50 Hz low-pass filter.

Table 5.3 Seismic Testing Sequence

Record	Sequence 1 (Intensity %	Sequence 2 (Intensity % g)	Sequence 3 (Intensity % g)	Sequence 4 (Intensity %
Cape Mendocino	5	10	15	20
Northridge (Mulhol)	5	10	15	20
Northridge (Canoga Park)	5	10	15	20
IEEE	5	10	15	20
Landers	5	10	15	20

Record	Sequence 5 (Intensity %	Sequence 6 (Intensity % g)	Sequence 7 (Intensity % g)
Cape Mendocino	25	---	---
Northridge (Mulhol)	25	30	35
Northridge (Canoga Park)	25	---	---
IEEE	25	---	---
Landers	25	---	---

5.8 Results of Frequency Evaluation Tests

Prior to conducting the frequency evaluation tests, it was anticipated that four predominant modes of the transformer-bushing system could be identified. The mock bushing was expected to have two modes of vibration below 4 Hz. The transformer tank was expected to have its lowest two natural frequencies correspond with the tank vibrating in the transverse (perpendicular to shake table motion) and longitudinal (parallel to shake table motion) directions with frequencies of around 13 Hz and 20 Hz respectively.

From the data collected during the white noise tests, spectral densities were plotted for each of the accelerometers. This spectral density was computed by averaging several Fast Fourier Transform (FFT) spectra calculated over several intervals of the recorded data. From the plots, only three predominant modes of vibration could be identified. Two modes were associated with the bushing, and the third mode was the tank vibrating in the longitudinal (North-South) direction. The

natural frequency of the tank vibrating in the transverse direction could not be clearly identified during the white noise testing, due to the lack of excitation in that direction.

In order to verify and complement the results of the frequency evaluation tests, data was borrowed from several impact tests conducted prior to the white noise test. Dr. Gerald Pardoen from the University of California, Irvine conducted some impact hammer tests in the East-West direction of the transformer. An accelerometer placed near the top of the tank recorded the transverse acceleration after an impact was made. The frequency response function (FRF) was computed using the absolute acceleration time-history by first converting the signal into to the frequency domain using the Fast Fourier Transform (FFT). Examination of the FRF from the impact test was successful in identifying a tank natural frequency in the transverse direction (East-West).

The first two measured natural frequencies of the system are related to the vibration of the mock bushing. These two frequencies are 2.61 Hz and 3.30 Hz. The transverse frequency of the transformer tank is 14.6 Hz and the longitudinal frequency was found to be 6.74 Hz, much lower than anticipated. Reasons for why the longitudinal frequency of the tank was much lower than expected will be discussed later in Section 5.11.

Spectral density plots for various accelerometers are shown in Figs. 5.18 and 5.19. The FRF plot computed with the accelerometer data obtained during an impact test is also displayed. Figure 5.18 is the spectral density plot using the recorded north-south and east-west absolute acceleration time-histories of the mock bushing concrete block.

A spectral density plot and FRF clearly showing the two predominant natural frequencies of the tank are presented in Fig. 5.19.

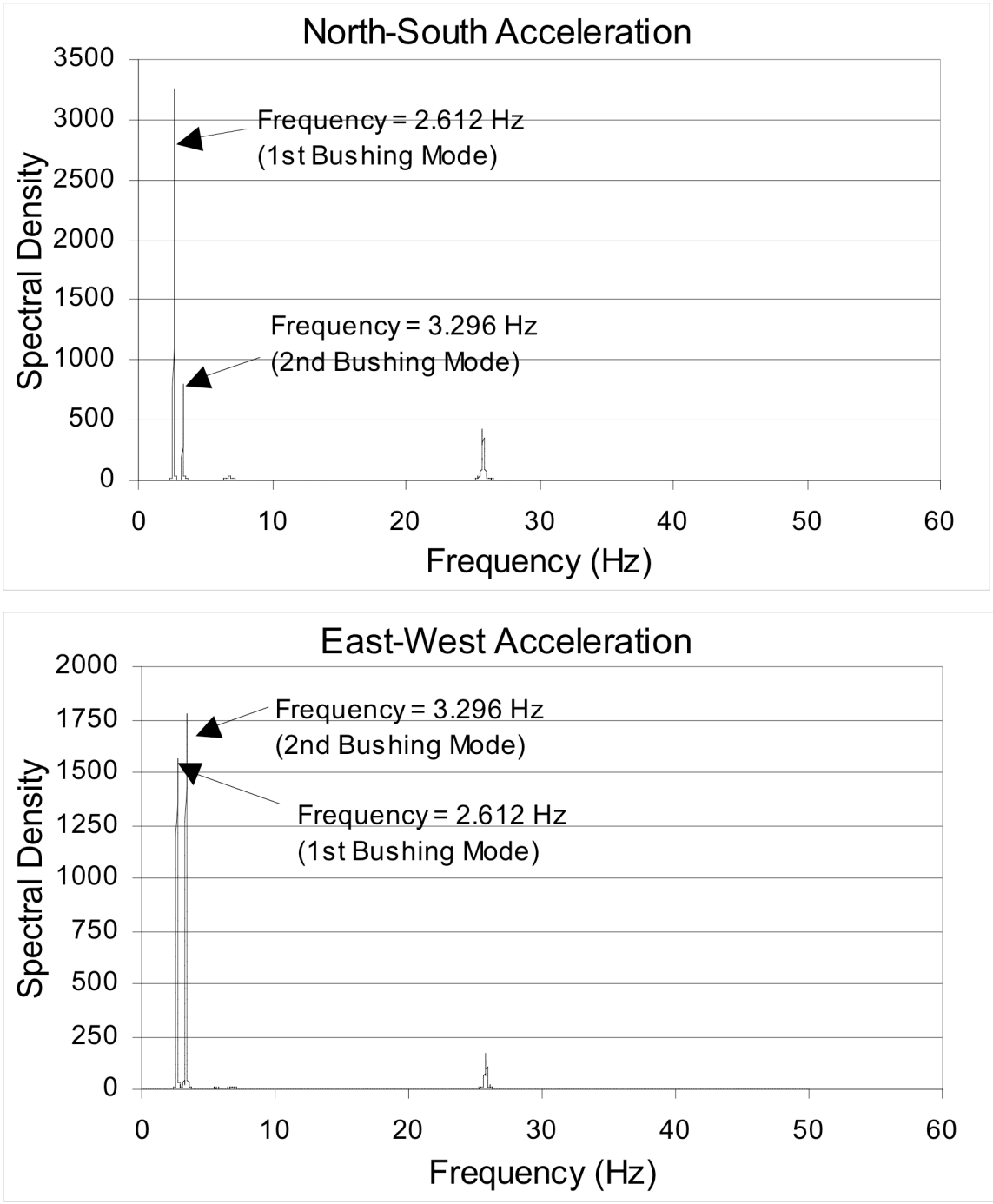

Figure 5.18 - Spectral Density Plots from Frequency Evaluation Test.

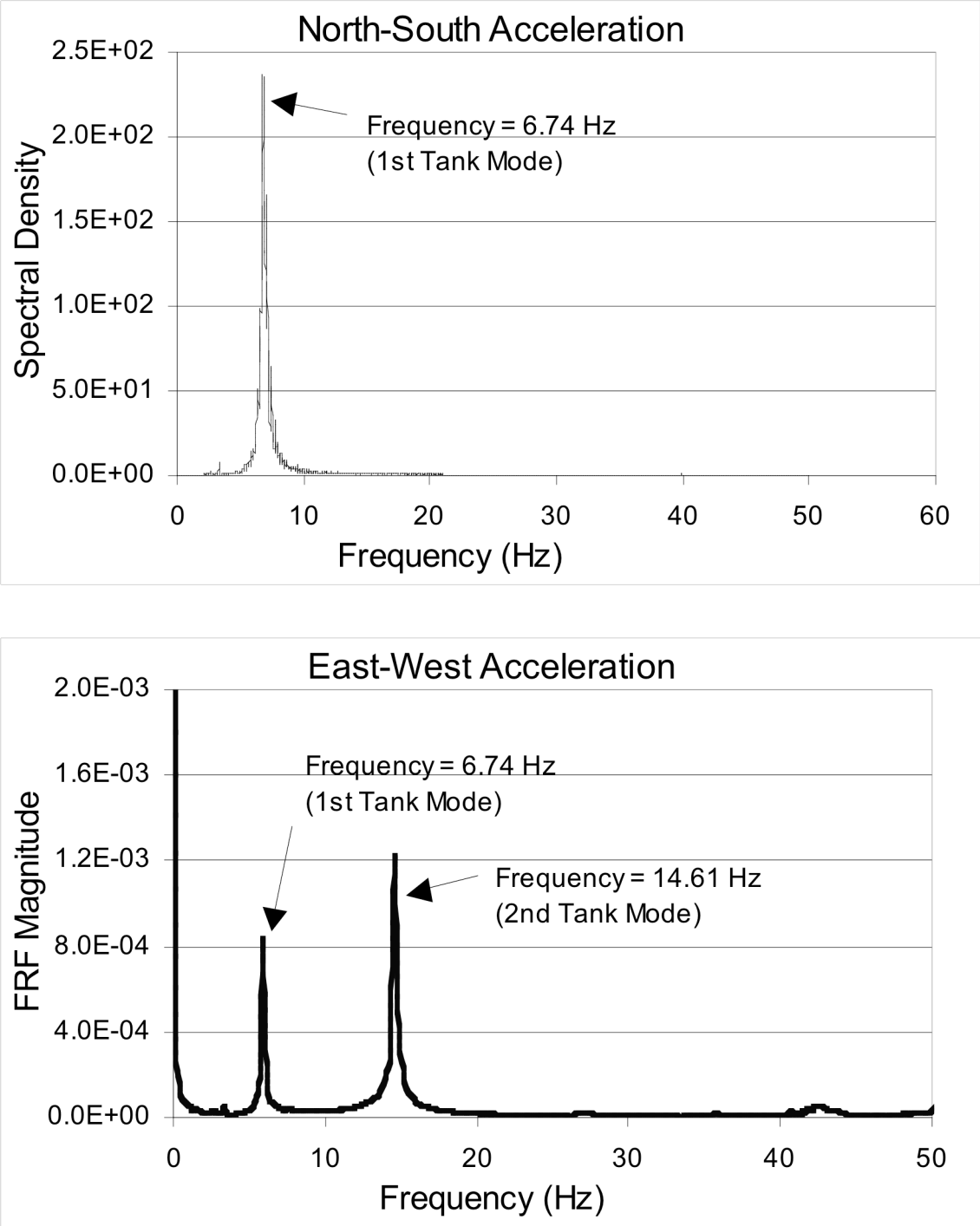

Figure 5.19 - Spectral Density and FRF Plots of Frequency Evaluation and Impact Hammer Tests.

The mode shapes were evaluated for the three lowest natural frequencies of the transformer-mock bushing system. Due to the difficulty in identifying the fourth mode of vibration (14.61 Hz) from the white noise test data, its mode shape could not be calculated. For the first three modes, the mode shapes were calculated by first computing the spectral density for seven accelerometers attached throughout the height of the transformer and mock bushing. The accelerometer channels A3, A5, and A7 measured the north-south acceleration of the transformer tank. Channels A14, and A15 measured the north-south acceleration of the bottom and top of the mock bushing tube respectively. Channels A16 and A17 measured the north-south and east-west motion of the mock bushing concrete block respectively.

In order to compute the mode shape for a particular mode, a reference channel had to be selected. The reference channel was selected by determining the accelerometer that resulted in the largest spectral density magnitude at that particular modes frequency. The modal value for a given channel was computed by taking the square root of the spectral density magnitude ratios at the natural frequency.

The U2 program was also utilized to determine the phase angle difference between the reference channel and the other selected channels at a given frequency. If two channels have the same positive direction of measurement and are in-phase with each other, then they both move in the same direction during the modal vibration. Likewise, if they are out of phase with each other, then one channel moves in the opposite direction of the other during the modal vibration. Phase angle differences of 0 degrees and 180 degrees correspond with in phase and out of phase scenarios

respectively. By knowing the modal values and phase differences for each accelerometer channel at a particular frequency, the mode shapes can be deduced.

The first mode of vibration corresponds to the bushing oscillating in the NW-SE plane. Each of the channels associated with the mock bushing were in phase with each other, meaning that the mock bushing vibrates like a single degree of freedom oscillator. The second mode is also associated with almost pure motion of the mock bushing. However, the mock bushing vibrated in a plane perpendicular to the first mode. The mode shape lied along the NE-SW plane. Again, all of the mock bushing accelerometers were in phase with one another. The third mode of vibration corresponds to the transformer tank vibrating in the longitudinal (North-South) direction. All of the channels associated with the mock bushing were out of phase with the transformer tank channels. Therefore, the mock bushing vibrated in the opposite direction of the tank in the north-south plane. The modes shapes detailed above are illustrated in Figs. 5.20 through 5.22. Note that the modal values for channels A14 and A15 are interpolated in the east-west direction since these accelerometers only measured north-south absolute accelerations. Table 5.4 summarizes the frequency evaluation test results described in this section.

Table 5.4 - Frequency Evaluation Results.

Mode	Natural Frequency (Hz)	Mode Shape
1	2.61	Mock Bushing (NW-SE)
2	3.30	Mock Bushing (NE-SW)
3	6.74	Transformer Tank (Longitudinal N-S)
4	14.61	Transformer Tank (Transverse E-W)

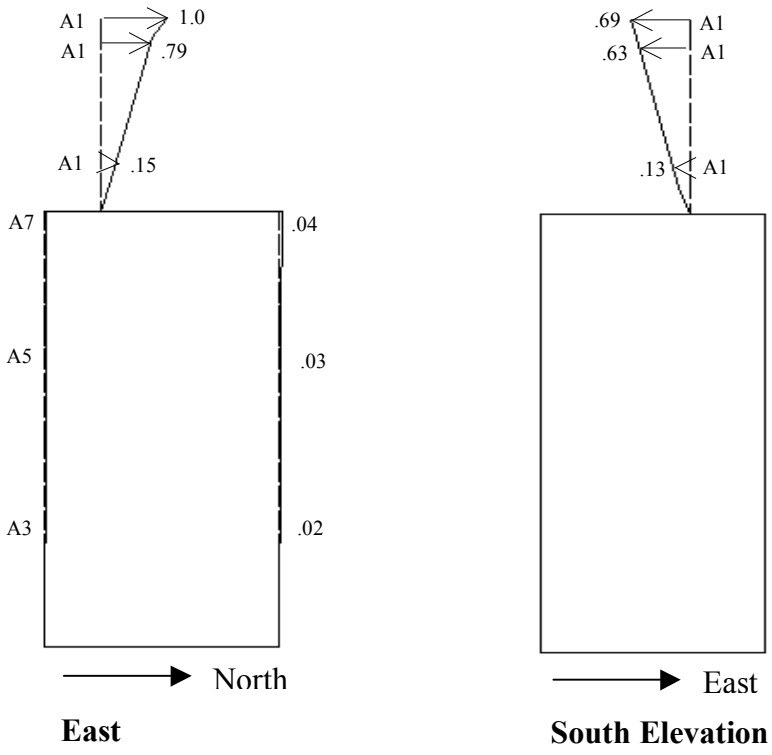

Figure 5.20 – First Mode of Mock Bushing, 2.61 Hz.

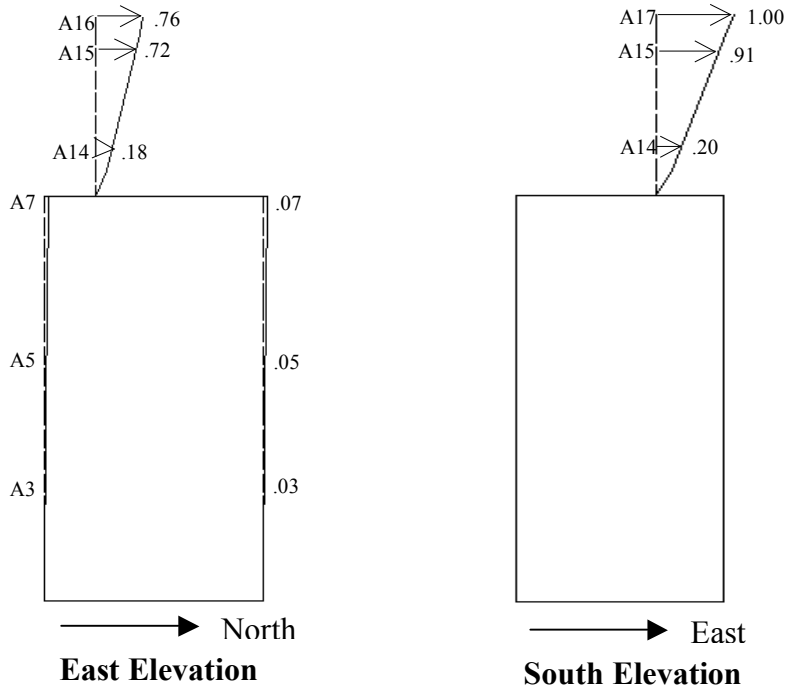

Figure 5.21 – Second Mode of Mock Bushing, 3.30 Hz.

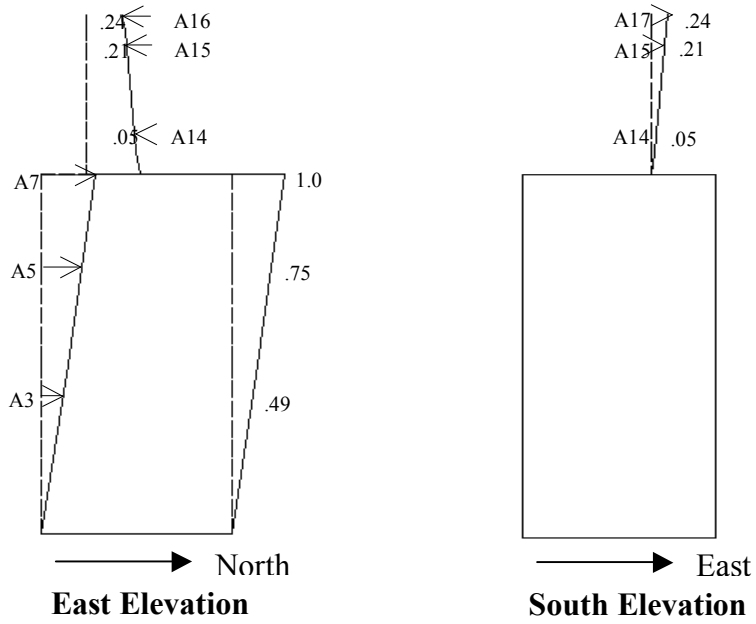

Figure 5.22 First Longitudinal Mode of Transformer Tank, 6.74 Hz.

5.9 Results of Damping Evaluation Tests

Damping evaluation tests were performed to determine the viscous damping ratios for the first three modes of vibration of the transformer-bushing system that were identified by the frequency evaluation tests. Each damping evaluation test was performed by introducing a low-amplitude sinusoidal excitation at each specific natural frequency of the system. Using selected acceleration time histories, the logarithmic decrement method was then used to calculate the viscous damping ratios associated with each mode after the excitation has been suddenly stopped and the system responded in free vibration.

The equivalent viscous damping varied depending upon the amplitude of the response. Therefore, the equivalent damping ratio was calculated at various amplitudes

recorded during the damping evaluation tests. Figure 5.23 shows the percentage of critical damping computed for each of the three modes as a function of acceleration amplitude. The damping appears to increase fairly linearly with increasing acceleration amplitude. Note also that the damping associated with the vibration of the transformer tank (Mode 3) is significantly higher than that associated with the vibration of the mock bushing (Modes 1 and 2).

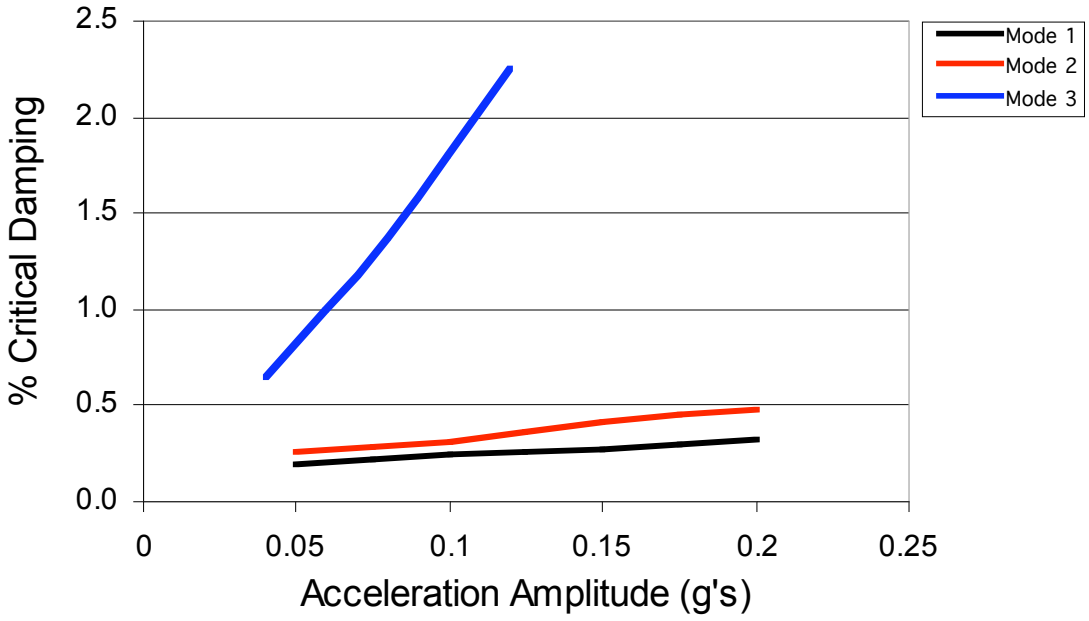

Figure 5.23 - Percentage of Damping for First Three Modes of Transformer-Mock Bushing System

Using the damping values at various amplitudes, the mean damping was computed. The mean damping ratio for the first and second mode of the mock bushing (Modes 1 and 2) was 0.26% and 0.37% of critical, respectively. The mean damping ratio computed for the longitudinal mode of the transformer (Mode 3) was 1.42% of critical. Table 5.5 summarizes the results from the damping evaluation tests.

Table 5.5 – Measured Mean Damping Ratios

Mode	Frequency (Hz)	Mean % Critical Damping
Mode 1 (Bushing NW-SE)	2.61	0.26
Mode 2 (Bushing NE-SW)	3.30	0.37
Mode 3 (Transformer N-S)	6.74	1.42

The construction of the transformer-mock bushing test setup was done in a manner such that it closely represents a true transformer-bushing system used in electrical substations. For this reason, it is important that the damping inherent on the mock bushing be representative of the true damping values for a real bushing. Dr. Gerald Pardoen from the University of California, Irvine conducted several damping tests on high voltage bushings attached to steel frames as part of another related research task of the PEER Lifelines Program. Results from these tests showed that the damping values of bushings are consistently low, generally ranging between .25% and 1% of critical. However, the bushings tested did not account for transformer mounting conditions and conducting cables that are attached to the top of transformer bushings. These additional factors will likely increase the damping associated with bushing vibration. Despite this, it was concluded that for the purposes of this study, the damping measured for the mock bushing modes is considered to be an adequate representation of the damping exhibited by a real transformer bushing.

5.10 Results of Seismic Tests

This section presents the results of all the shake table seismic tests performed. Five different earthquake records were inputted at seven different intensities. The ground motion intensities ranged from .05g to .35g PGA. Only the main seismic test

results of the transformer and mock bushing accelerations, displacements and stresses are presented in this section.

The peak shake table accelerations measured during the seismic tests were larger than the PGA of the input earthquake record. Ideally, the shake table peak absolute accelerations would match the input PGA. However, due to difficulty in obtaining high shake table fidelity as discussed in Section 5.6, the shake table response was always amplified. For this reason, results are presented in comparison with the measured shake table absolute acceleration rather than the input amplitude. Table 5.6 shows the measured peak absolute shake table acceleration for each of the seismic tests performed. It can clearly be seen that the measured shake table accelerations are larger than the desired input PGA.

The maximum peak absolute acceleration recorded at the top of the transformer tank for all of the seismic tests was 1.46 g. This acceleration was measured during the Northridge (Canoga Park) @ 25% PGA test. The minimum peak absolute acceleration at the top of the transformer tank was 0.27 g, recorded during the Northridge (Mulhol) @ 5% PGA test. The peak absolute accelerations measured at the top of the transformer tank for each earthquake record at the varying intensities are graphed in Fig. 5.24 as a function of peak shake table acceleration.

Table 5.6 - Peak Absolute Accelerations Measured on Shake Table.

Peak Input Accel. (g's)	Peak Abs.Shake Table Accel. (g's) (Cape Mendocino)	Peak Abs. Shake Table Accel. (g's) (Northridge - Mulhol)
0.05	0.120	0.17
0.1	0.210	0.25
0.15	0.280	0.34
0.2	0.340	0.44
0.25	0.420	0.51
0.3	------	0.54
0.35	------	0.59

Peak Input Accel. (g's)	Peak Abs.Shake Table Accel. (g's) (Northridge - Canoga)	Peak Abs. Shake Table Accel. (g's) (Landers)
0.05	0.15	0.15
0.1	0.25	0.26
0.15	0.38	0.38
0.2	0.49	0.43
0.25	0.52	0.56

Peak Input Accel. (g's)	Peak Abs. Shake Table Accel. (g's) (IEEE)
0.05	0.14
0.1	0.23
0.15	0.34
0.2	0.39
0.25	0.48

A solid and a dashed line were also plotted on this graph. The lower solid line represents a 1 to 1 slope line. The upper dashed line, which is the linear trend line of all the data, has a slope of 2.5 to 1. From this, it can be seen that the peak absolute acceleration can be approximated as a linear relationship with the peak transformer base excitation. The peak absolute acceleration of the transformer is amplified roughly by a factor of 2.5 from the transformer base to the top of the transformer.

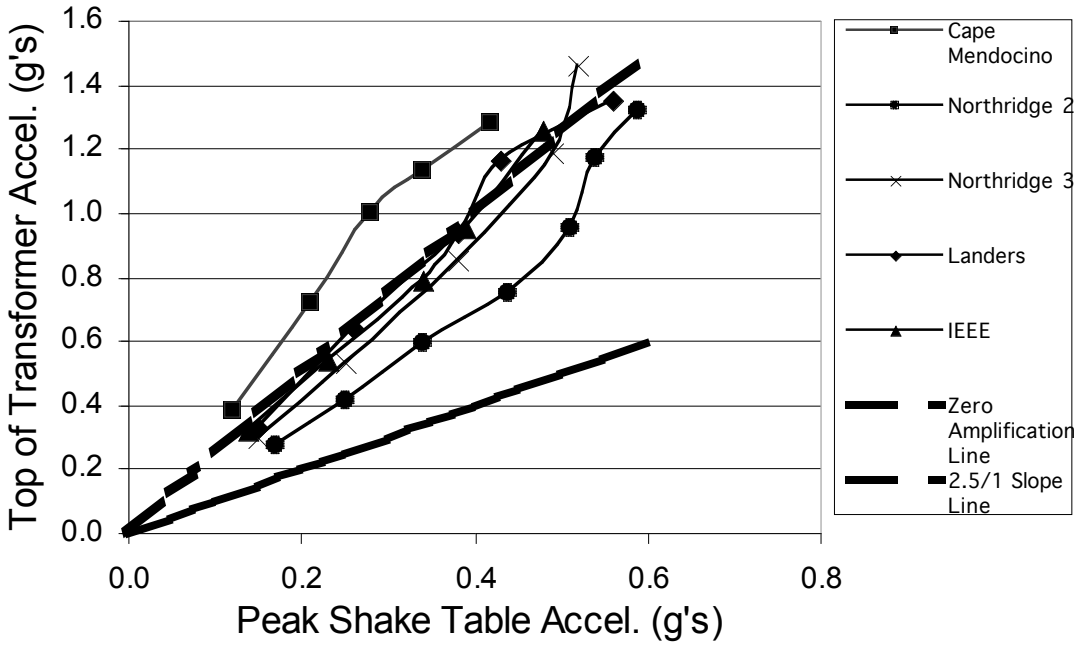

Figure 5.24 - Peak Absolute Accelerations at Top of Transformer Tank

The maximum peak absolute acceleration recorded at the base of the mock bushing for all of the seismic tests was 1.52 g. This acceleration was measured during the Northridge (Canoga Park) @ 25% PGA test. The minimum peak absolute acceleration at the base of the bushing was 0.26 g recorded during the Northridge (Mulhol) @ 5% PGA test. The peak absolute accelerations measured at the base of the mock bushing for each earthquake record at the varying intensities are graphed in Fig. 5.25 as a function of peak shake table acceleration. Again, the peak absolute acceleration at the base of the bushing appears to be linearly related to the peak base excitation. The peak absolute acceleration is amplified by an approximate factor of 2.25 from the transformer base to the base of the mock bushing. The maximum peak absolute acceleration at the base of the bushing was larger than that of the transformer tank. Interestingly though, the results show that the amplification in the base excitation

is slightly larger at the top of the transformer than at the base of the mock bushing. This is evident by comparing the dashed trend lines between the two cases.

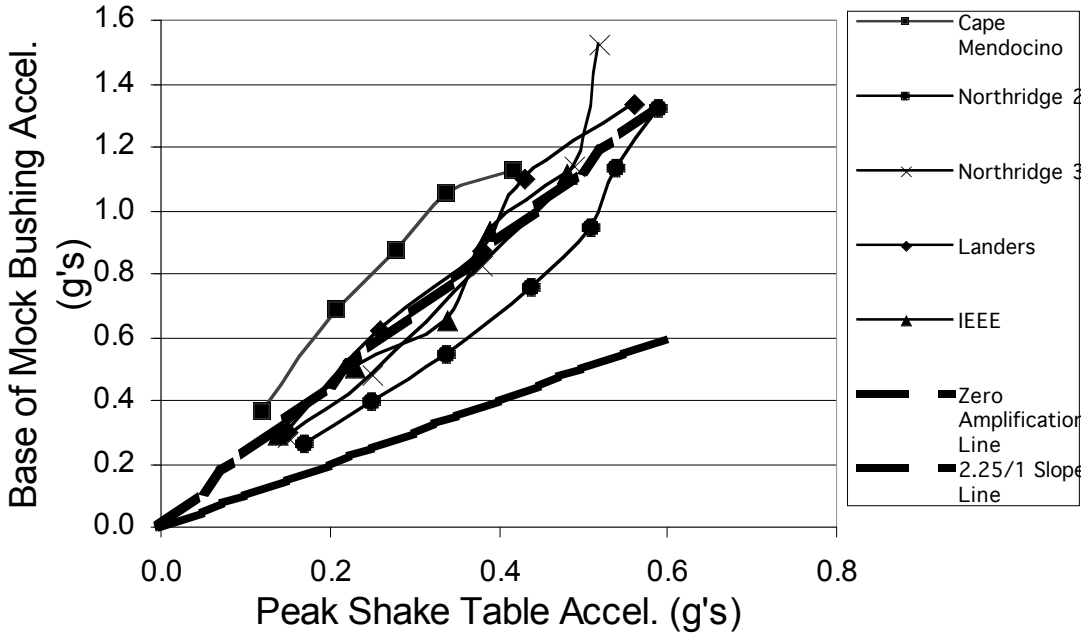

Figure 5.25 - Peak Absolute Accelerations at Base of Mock Bushing.

The maximum peak absolute acceleration recorded at the top of the mock bushing for all of the seismic tests was 1.72 g. This peak acceleration occurred during the Northridge (Canoga Park) @ 25% PGA test. The minimum peak absolute acceleration at the top of the bushing was 0.21 g, recorded during the Northridge (Mulhol) @ 5% PGA test. The peak absolute accelerations measured at the top of the bushing for each earthquake record at the varying intensities are graphed in Fig. 5.26 as a function of peak shake table acceleration. The peak accelerations follow a linear trend line with a slope of 3.0 to 1. The peak absolute acceleration is amplified by an approximate factor of 3.0 from the transformer base to the top of the mock bushing. As expected, the peak

acceleration amplification is larger at the top of the mock bushing than at the other two locations.

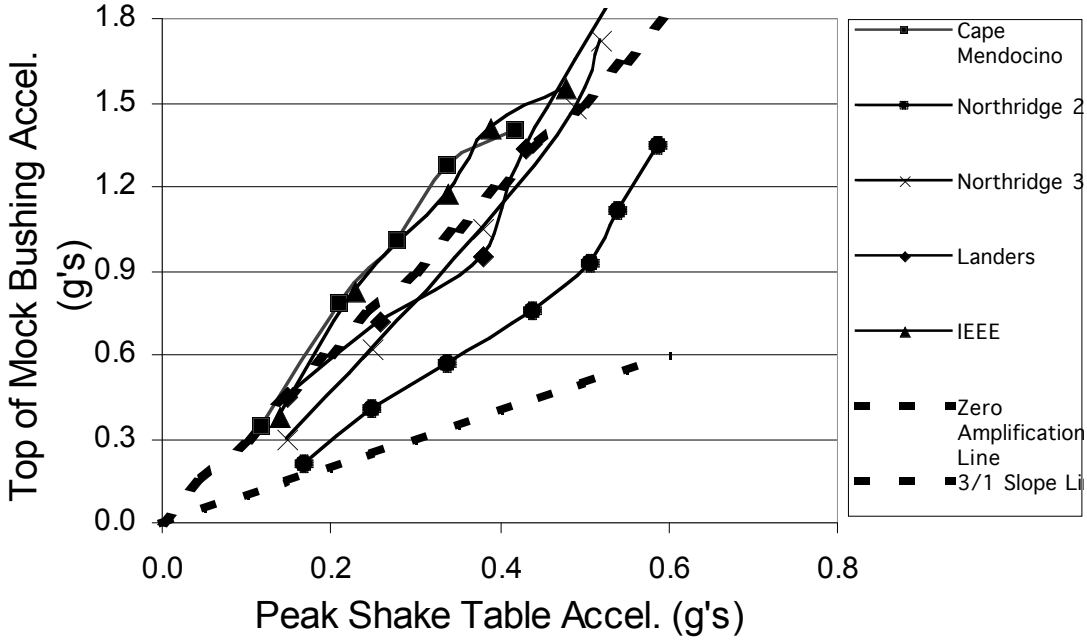

Figure 5.26 - Peak Absolute Accelerations at Top of Mock Bushing.

The maximum peak relative displacement recorded at the top of the transformer for all of the seismic tests was 0.38 in. This peak displacement occurred during the Northridge (Canoga Park) @ 25% PGA test. The minimum peak relative displacement at the top of the transformer was .03 in. recorded during the Landers @ 5% PGA test. The peak relative displacements measured at the top of the transformer for each earthquake record at the varying intensities are graphed in Fig. 5.27 as a function of peak shake table acceleration. The results show that the peak relative displacement at the top of the transformer tank varies linearly with respect to the peak base excitation.

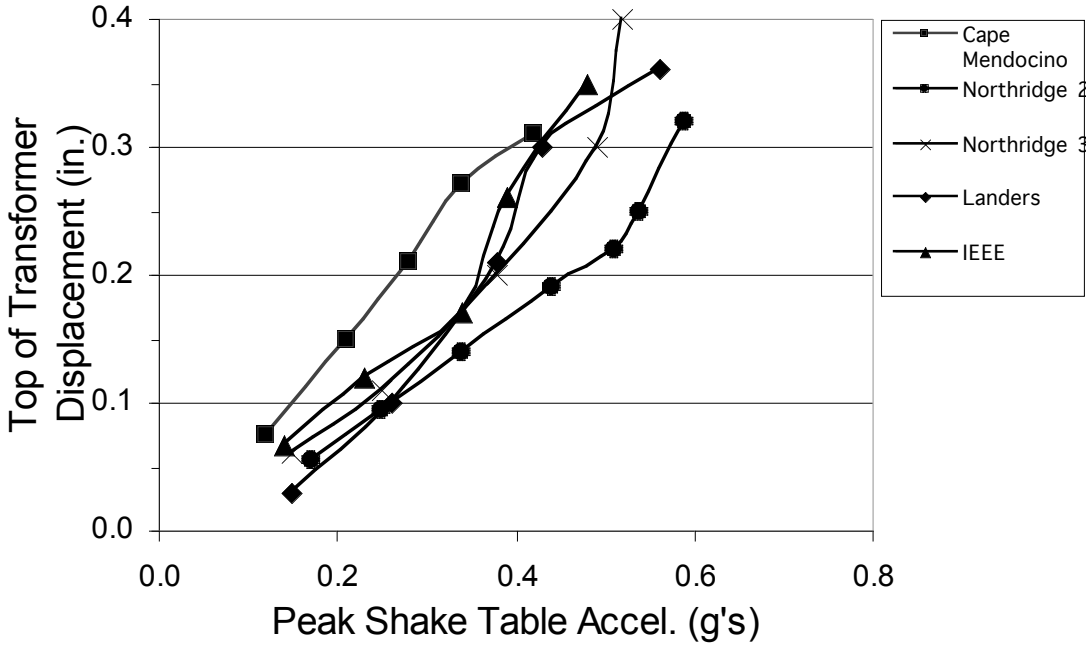

Figure 5.27 - Peak Relative Displacement at Top of Transformer Tank.

The maximum peak relative displacement recorded at the top of mock bushing for all of the seismic tests was 1.74 in. This peak displacement occurred during the Landers @ 25% PGA test. The minimum peak relative displacement at the top of the mock bushing was 0.21 in. recorded during the Northridge (Mulhol) @ 5% PGA test. The peak relative displacements measured at the top of the mock bushing for each earthquake record at the varying intensities are graphed in Fig. 5.28 as a function of peak shake table acceleration. Again, the results show that the peak relative displacement at the top of the mock bushing varies linearly with respect to the peak base excitation.

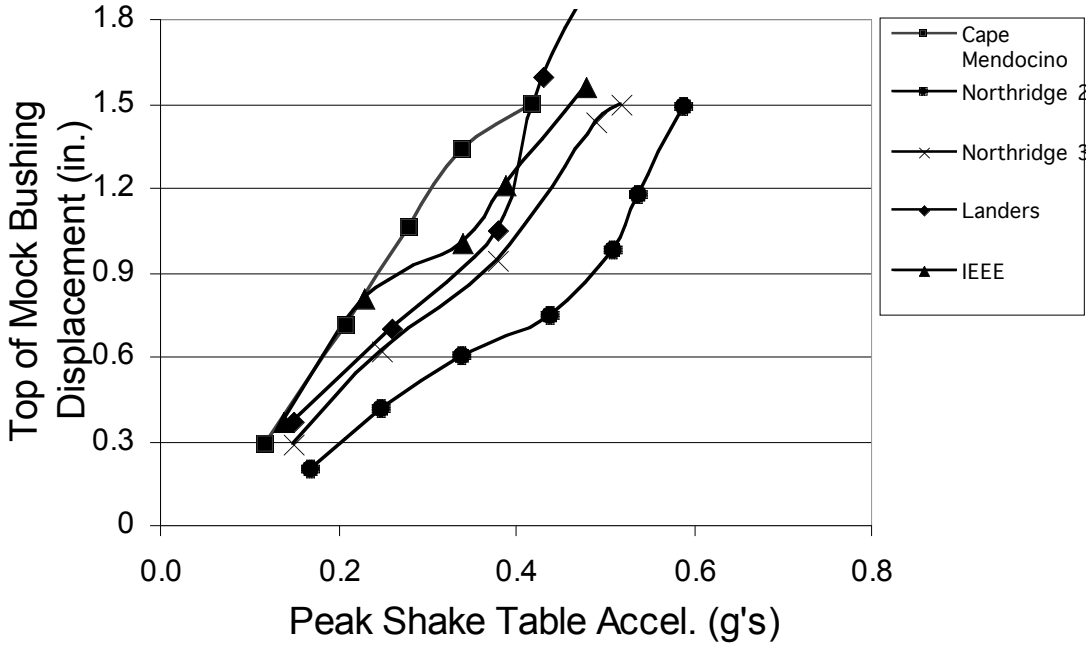

Figure 5.28 - Peak Relative Displacement at Top of Mock Bushing.

The maximum peak relative vertical displacement of the transformer top plate for all of the seismic tests was 0.13 in. This peak vertical displacement occurred during the Landers @ 25% PGA test. The minimum peak relative vertical displacement of the transformer top plate was .02 in. recorded during the Northridge (Mulhol) @ 5% PGA test. The peak vertical displacements measured on the top plate for each earthquake record at the varying intensities are graphed in Fig. 5.29 as a function of peak shake table acceleration. From the results, it can be seen that the peak relative vertical displacement of the top plate varies linearly with respect to the peak base excitation.

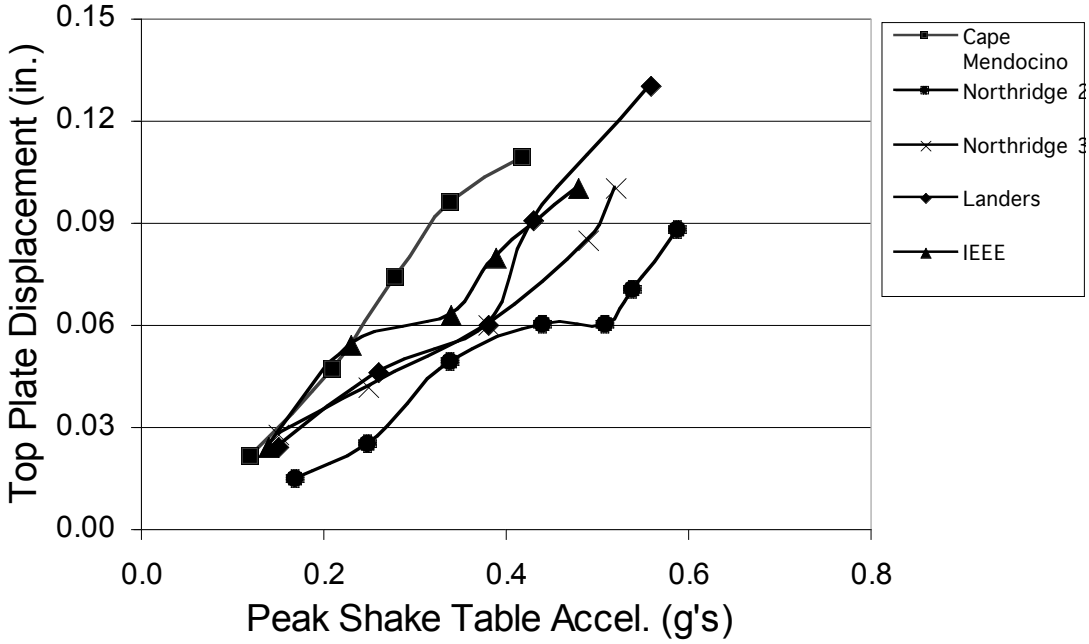

Figure 5.29 - Peak Relative Vertical Displacement at Top Plate.

The peak principal stresses at the base of the turret were calculated using the eight strain gauge rosettes described in Section 5.5. The maximum peak principal stress experienced at the base of the turret for all of the seismic tests was 23.6 ksi. This peak stress value occurred during the Landers @ 25% PGA test. The minimum peak principal stress experienced at the base of the turret was 2.7 ksi recorded during the Northridge (Mulhol) @ 5% PGA test. The peak principal stresses experienced at the base of the turret for each earthquake record at the varying intensities are graphed in Fig. 5.30 as a function of peak shake table acceleration. It can be seen that the peak principal stresses experienced at the base of the turret varies linearly with respect to the peak base excitation.

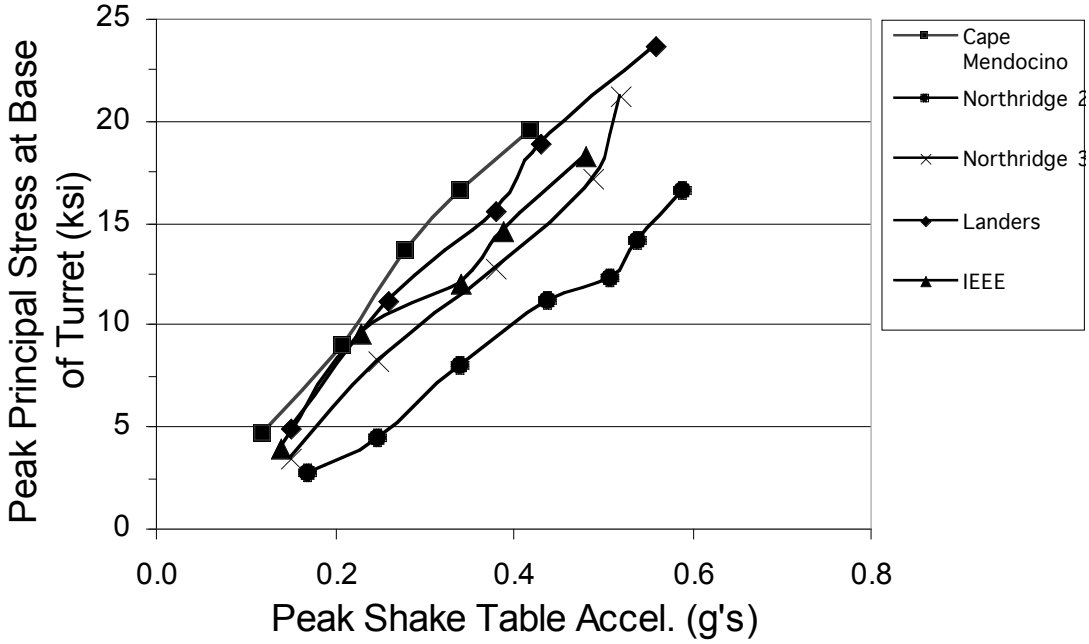

Figure 5.30 - Peak Principal Stresses at Base of Turret.

The peak bending stresses at the base of the mock bushing were obtained using the readings from the six uniaxial strain gauges attached at the bottom of the steel tube, just above the turret. The maximum peak bending stress experienced at the base of the mock bushing for all of the seismic tests was 21.8 ksi. This peak stress value occurred during the Landers @ 25% PGA test. The minimum peak bending stress at the base of the mock bushing was 2.1 ksi recorded during the Northridge (Mulhol) @ 5% PGA test. The peak bending stresses experienced at the base of the mock bushing for each earthquake record at the varying intensities are graphed in Fig. 5.31 as a function of peak shake table acceleration. The amplitudes of the peak bending stress values at the base of the bushing were similar to the amplitudes of the principal stresses experienced at the base of the turret. Similar to the previous results, the peak

bending stresses occurring at the base of the mock bushing varies linearly with respect to the peak base excitation.

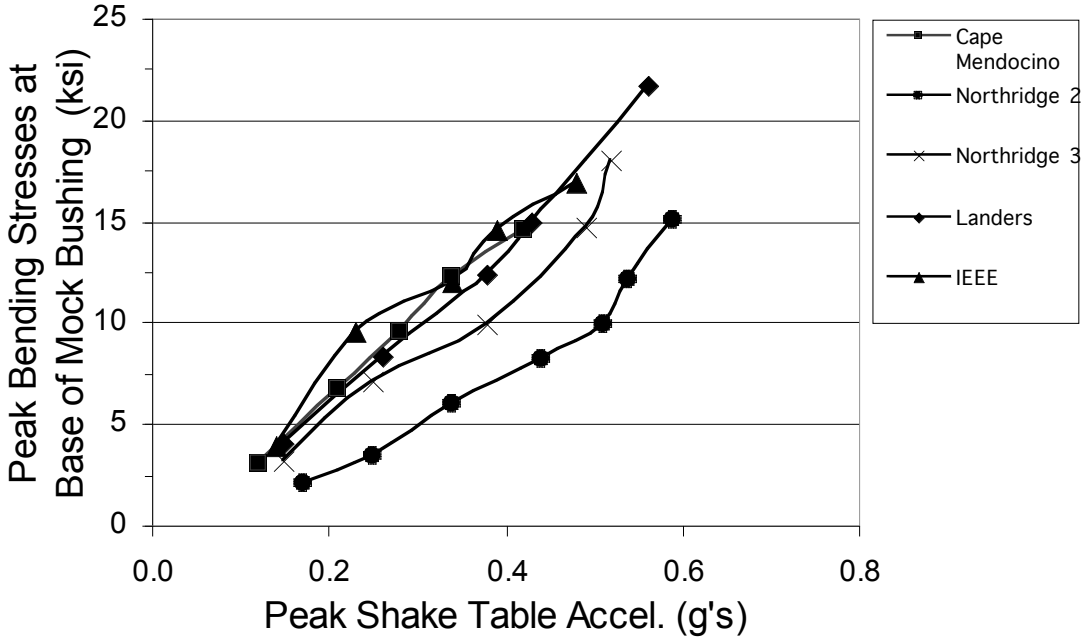

Figure 5.31 - Peak Bending Stresses at Base of Mock Bushing.

The final experimental results presented in this section are of the calculated spectral amplifications. Just as was done for the numerical studies, the spectral amplification was calculated by taking the ratio of the shake table absolute acceleration response spectrum and the acceleration response spectrum calculated from the absolute acceleration measured at the base of the bushing. The spectral amplification therefore shows the spectral acceleration amplification as a function of frequency. Figure 5.32 shows the spectral amplification plot from the Landers @ 25% PGA test. Note that there are three distinct peaks in the spectral amplification. These peaks occur at the first two natural frequencies of the bushing, and the longitudinal

natural frequency of the transformer. The constant line shown at 2.0 represents the maximum allowable amplification as defined within the IEEE-693 standard.

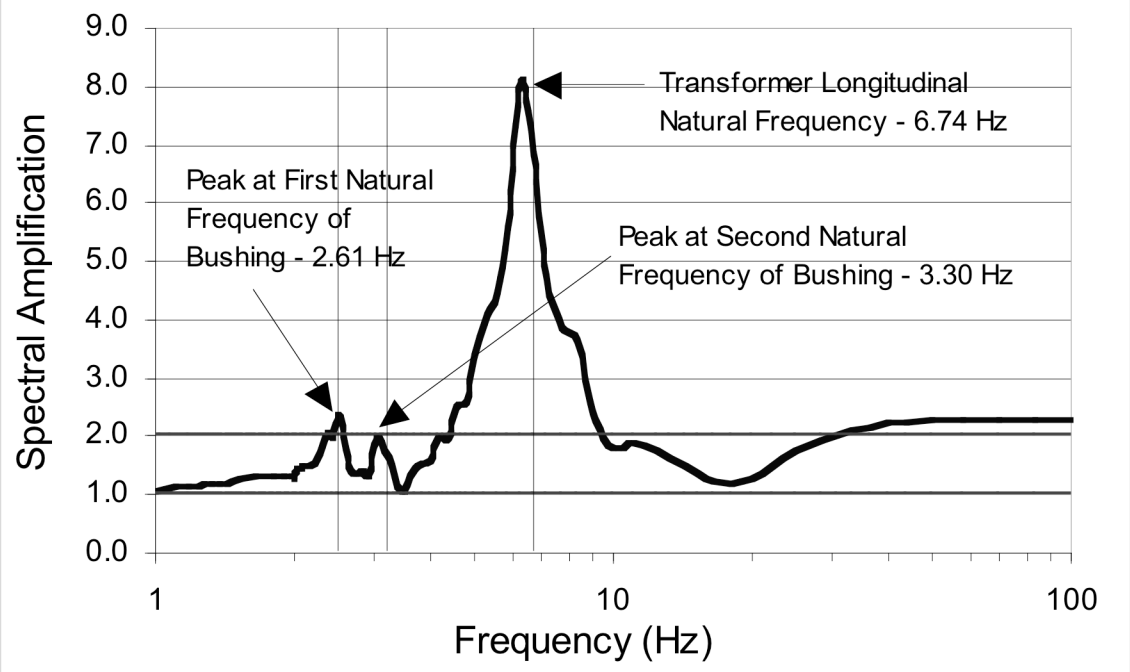

Figure 5.32 - Spectral Amplification Plot for Landers Test @ 25% PGA.

The spectral amplification values occurring at the frequencies of the mock bushing are of highest interest since this dictates the bushing response. When comparing the two peaks associated with the bushing frequencies, the spectral amplification was generally larger at the first natural frequency of the mock bushing.

The spectral amplification values occurring at the first natural frequency of the mock bushing were identified for all of the seismic tests. The maximum spectral amplification was 3.05 and resulted from the Cape Mendocino test @ 10% PGA. The minimum spectral amplification at the first natural frequency of the mock bushing was 1.55, resulting from the Northridge (Mulhol) test @ 20% PGA. Figure 5.33 shows a plot of the spectral amplification values at the first natural frequency of the mock

bushing for each earthquake record at the varying shakes table intensities. In addition, the mean spectral amplification of all records is also plotted. The maximum allowable amplification as defined within the IEEE-693 is shown as the constant line at 2.0.

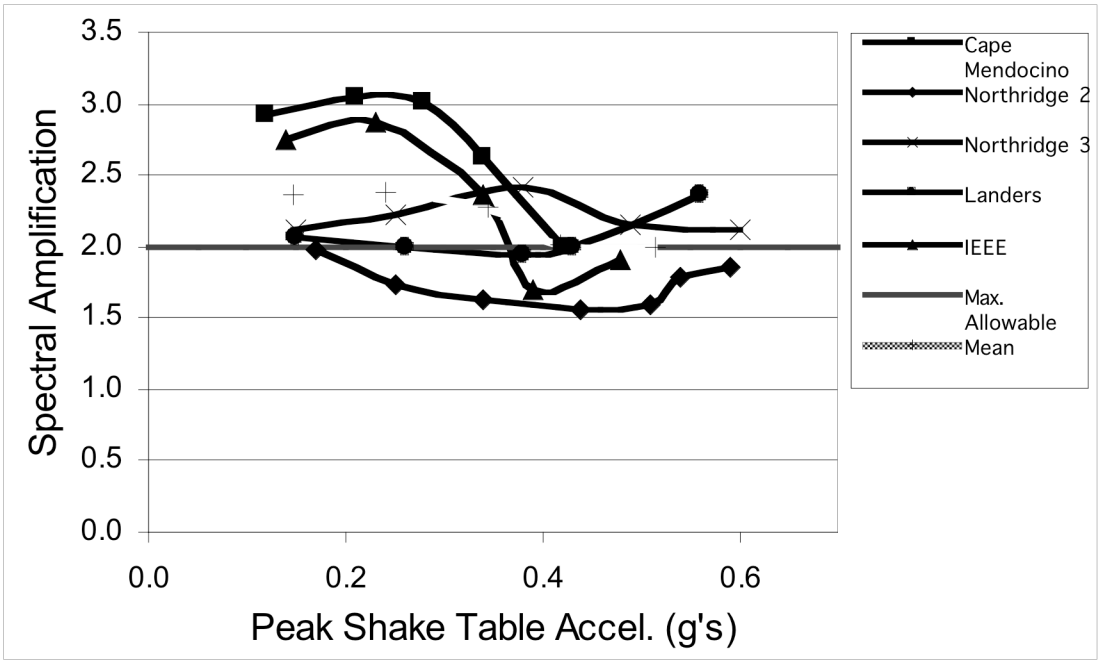

Figure 5.33 - Spectral Amplification Values at First Natural Frequency of Mock Bushing

Since the spectral amplification is based on the ratio of input acceleration and the acceleration at the base of the bushing, it is expected that the spectral amplification should remain constant for a given ground motion regardless of its amplitude. Although this is apparently clear for the Northridge (Mulhol), Northridge (Canoga Park), and Landers earthquake records, the IEEE and Cape Mendocino records show a decline in spectral amplification as the ground motion intensity increases.

Interestingly, every seismic record with exception of the Northridge (Mulhol) record resulted in spectral amplification values larger than 2.0 at the first natural

frequency of the mock bushing. The mean spectral amplification computed from all five records was above the maximum allowable amplification value of 2.0 for all amplitudes. The maximum mean spectral amplification at the first frequency of the bushing is 2.38 and occurs at an intensity of 0.24 g. As expected, the mean spectral amplification remains fairly constant with respect to the ground motion intensity

5.11 Numerical Modeling of Test Structure

A finite element model was initially developed in an attempt to predict the results obtained during the shake table tests. The model was developed from the 525 kV Transformer A finite element model previously used in the first and third numerical studies (see Chapters 2 and 4). This model was modified to represent the transformer test specimen used during the shake table tests.

After obtaining shake table test data, the model was then calibrated according to the test results. The objective was to replicate as accurately as possible the experimental results, thereby further validating the results and conclusions of the numerical studies.

Initially, the finite element model of the transformer test specimen was essentially the same as the 525 kV Transformer A used during the first numerical study. However, unlike a fully equipped transformer, the test specimen did not contain any oil, nor did it have the external appendages such as the radiators and surge arrestors. Therefore, the model of the transformer test specimen did not include any mass from the oil. In addition the surge arrestor and low voltage bushing that was modeled in the first numerical study was eliminated. In place of the 525 kV bushing, the mock

bushing was modeled by using the appropriate frame elements representative of the mock bushing components. Point masses at the top of the mock bushing were added to account for the concrete block mass. The boundary conditions for the model remained the same since the transformer was welded onto the shake table frame. Figure 5.34 shows the initial finite element mesh of the transformer test specimen.

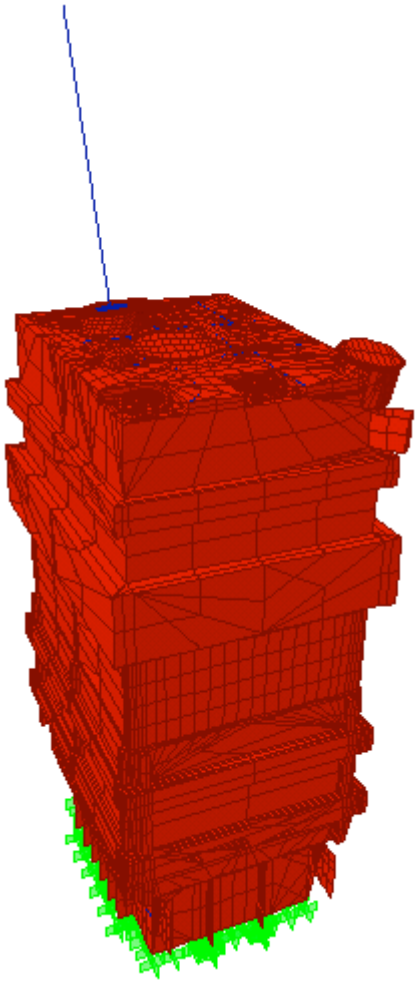

Figure 5.34 Initial Finite Element Mesh of Transformer Test Specimen.

Using this initial model, a free-vibration analysis was performed to obtain the fundamental frequencies of the system as well as obtain their corresponding mode shapes. The first and second natural frequencies of the bushing were computed to be

2.5 Hz and 3.0Hz respectively. The first natural frequency of the transformer was computed to be 13.8 Hz and was related to the tank vibrating in the transverse direction. The second natural frequency of the transformer was computed to be 20.2 Hz. This frequency corresponded to vibration of the tank in the longitudinal direction. These modal analysis results as well as the results obtained from the frequency evaluation tests described in Section 5.8 are summarized in Table 5.7.

Table 5.7 - Comparison between Measured and Predicted Natural Frequencies by Initial Finite Element Model.

Frequency Evaluation Test Results

Mode	Natural Frequency (Hz)
Mock Bushing Mode 1 (NW-SE)	2.6
Mock Bushing Mode 2 (NE-SW)	3.3
Tank Mode 1 (Transverse)	14.6
Tank Mode 2 (Longitudinal)	6.7

Finite Element Model Modal Analysis Results

Mode	Natural Frequency (Hz)
Mock Bushing Mode 1 (NW-SE)	2.5
Mock Bushing Mode 2 (NE-SW)	3.0
Tank Mode 1 (Transverse)	13.8
Tank Mode 2 (Longitudinal)	20.2

Although the natural frequencies and mode shapes for the mock bushing were very similar, there was a large discrepancy between the predicted and measured longitudinal frequencies of the transformer tank. Yet, the transverse frequencies seemed to match fairly well. Clearly, the initial finite element model was not capturing all of the details of the test setup.

It was mentioned earlier that the longitudinal frequency of the transformer obtained from the frequency evaluation tests was much lower than anticipated. By definition, the longitudinal direction of the transformer is always stiffer than the transverse direction. Therefore, it was expected that the measured longitudinal frequency of the tank would be higher than the transverse frequency. However, this was not the case. The longitudinal frequency of the test specimen was found to be 6.74 Hz compared to its transverse frequency of 14.6 Hz. It became apparent that something was greatly reducing the stiffness of the transformer tank in its longitudinal direction. It was concluded that the shake table frame and the transformer-mounting frame were the sources of this reduction in stiffness. In fact, due to the large overturning moment induced, the transformer tank and shake table frame were thought to be experiencing a rotating or rocking motion response.

The shake table frame and the transformer-mounting frame were not considered in the initial model of the transformer test specimen. Instead, rigid boundary conditions were applied to the transformer model. Therefore, the model was modified to capture the seemingly large flexibility in the true boundary conditions.

The W14X26 I-beams supporting the transformer were included as the mounting frame in the model. The I-sections were modeled as a steel plate element with the proper web dimensions sandwiched between two beam elements representing the top and bottom flange. The shake table was modeled as 5/8 in. thick steel plate elements. The shake table frame is made up of several W18X35 I-beams. These beams are supported by eight bearings that slide along two stationary steel shafts having a diameter of 8in. The W18X35 I-beams were modeled as plate elements for the webs

and beam elements for the flanges. The eight bearings were included as beam elements. The boundary conditions for the bearings were such that all rotations and the horizontal displacement perpendicular to the shaft axis were restricted. The bearings could freely translate along the axis of the shaft. Vertical springs with a stiffness corresponding to the bending stiffness of the shaft were also introduced at the base of the bearings. The model was constrained in the direction of shaking at the location of the hydraulic actuator. Figure 5.35 shows the finite element mesh of the model before and after introducing its support frame on the shake table.

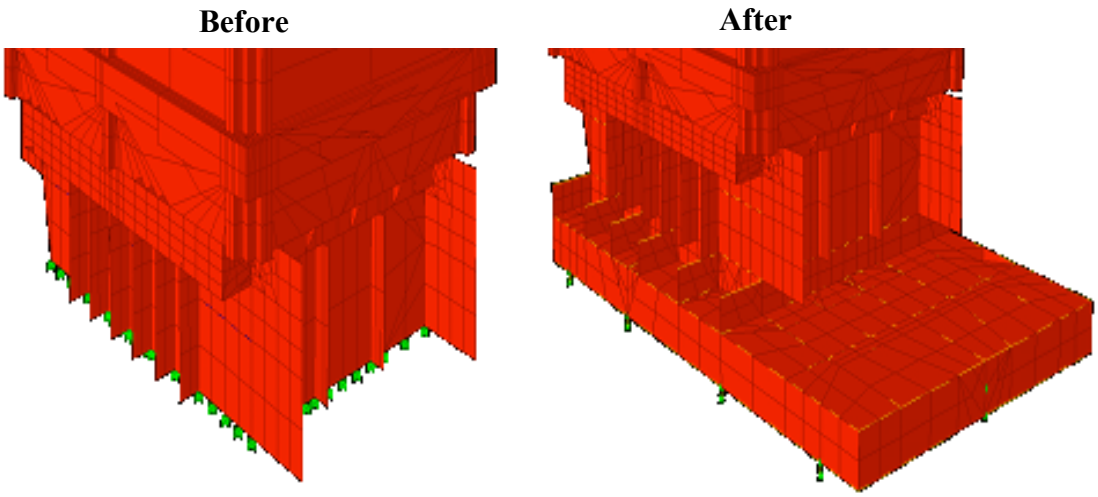

Figure 5.35 - Transformer Base Before and After Adjustments.

After making the modifications stated above, another modal analysis was performed to identify the fundamental frequencies of the transformer-mock bushing system. The shake table frame incorporated into the model greatly reduced the natural frequency of the longitudinal frequency of the transformer. The longitudinal natural frequency of the modified model was reduced to 9.3 Hz. The first two natural frequencies for the mock bushing were 2.6 Hz and 3.0 Hz. Table 5.8 presents the

modal results obtained from the frequency evaluation tests and from the prediction of the modified finite element model. As can be seen, the modified model produced modal results much closer to those measured during the frequency evaluation tests.

Table 5.8 - Comparison between Measured and Predicted Natural Frequencies by Modified Finite Element Model

Frequency Evaluation Test Results

Mode	Natural Frequency (Hz)
Mock Bushing Mode 1 (NW-SE)	2.6
Mock Bushing Mode 2 (NE-SW)	3.3
Tank Mode 1 (Longitudinal)	6.7
Tank Mode 2 (Transverse)	14.6

Modified Finite Element Model Modal Analysis Results

Mode	Natural Frequency (Hz)
Mock Bushing Mode 1 (NW-SE)	2.6
Mock Bushing Mode 2 (NE-SW)	3.0
Tank Mode 2 (Longitudinal)	9.3
Tank Mode 1 (Transverse)	12.4

After predicting the modal properties with the modified finite element model of the test structure, dynamic time-history analyses were performed. The input ground motions used for the model were the actual shake table time-histories recorded for each of the seismic tests performed at an intensity of 25% g. By doing this, a direct comparison between the seismic test results and the numerical results could be obtained. The mean modal damping ratios measured during the damping tests were used in the numerical model. These values were 0.26% and 0.37% of critical for the first and second modes of the mock bushing, respectively and 1.42% of critical for the longitudinal mode of the transformer tank. All other modes of vibration were assigned a damping ratio of 2% of critical. The numerical results were compared by looking at

the peak values of each 25% g seismic test presented in the previous section. Tables 5.9 to 5.11 summarize these peak numerical and experimental results. In addition, selected relative displacement, and absolute acceleration time-histories were also compared with the respective time-histories measured during the seismic tests. All displacements and accelerations are in the North-South direction.

In general, the model predicted the seismic results fairly well. The peak absolute acceleration values were typically slightly larger for the numerical model as seen in Table 5.9. The maximum peak absolute accelerations predicted by the model at the transformer top, base of bushing, and top of bushing were 2.20, 2.18, and 2.29 g, respectively. The corresponding measured peak absolute accelerations at the transformer top, base of bushing, and top of bushing were 1.46, 1.52, and 2.0 g, respectively.

Table 5.10 presents the peak displacement results for the seismic tests and model time history analyses. The relative displacement values predicted by the model were generally slightly larger than those recorded during the seismic tests. The predicted peak relative displacements at the transformer top, top plate and top of bushing were 0.28 in., 0.28 in., and 2.44 in., respectively. The measured peak relative displacements at the transformer top, top plate and top of bushing were 0.40 in., 0.13 in., and 2.33 in., respectively.

Table 5.9 - Peak Absolute Acceleration Results from Numerical Model and Seismic Tests at 25% g.

Seismic Test Results

Record	Peak Accel. @ Top of transformer (g's)	Peak Accel. @ Base of Bushing (g's)
Cape Mendocino	1.28	1.12
Northridge (Mulhol)	0.95	0.94
Northridge (Canoga Park)	1.46	1.52
Landers	1.35	1.33
IEEE	1.26	1.11

Record	Peak Accel. @ Top of Bushing (g's)
Cape Mendocino	1.40
Northridge (Mulhol)	0.92
Northridge (Canoga Park)	1.72
Landers	2.00
IEEE	1.55

Numerical Model Results

Record	Peak Accel. @ Top of transformer (g's)	Peak Accel. @ Base of Bushing (g's)
Cape Mendocino	1.46	1.39
Northridge (Mulhol)	1.53	1.48
Northridge (Canoga Park)	1.81	1.75
Landers	2.20	2.18
IEEE	1.97	1.94

Record	Peak Accel. @ Top of Bushing (g's)
Cape Mendocino	1.21
Northridge (Mulhol)	1.09
Northridge (Canoga Park)	1.18
Landers	2.17
IEEE	2.29

Table 5.10 - Peak Relative Displacement Results from Numerical Model and Seismic Tests at 25% g.

Seismic Test Results

Record	Peak Rel. Disp. @ Top of Transformer (in)	Peak Rel. Vert. Displ. of Top plate (in)
Cape Mendocino	0.31	0.11
Northridge (Mulhol)	0.22	0.06
Northridge (Canoga Park)	0.40	0.10
Landers	0.36	0.13
IEEE	0.35	0.10

Record	Peak Rel. Displ. @ Top of Bushing (in)
Cape Mendocino	1.50
Northridge (Mulhol)	0.98
Northridge (Canoga Park)	1.50
Landers	2.33
IEEE	1.56

Numerical Model Results

Record	Peak Rel. Disp. @ Top of Transformer (in)	Peak Rel. Vert. Displ. of Top plate (in)
Cape Mendocino	0.17	0.22
Northridge (Mulhol)	0.18	0.12
Northridge (Canoga Park)	0.22	0.15
Landers	0.28	0.23
IEEE	0.24	0.28

Record	Peak Rel. Displ. @ Top of Bushing (in)
Cape Mendocino	1.45
Northridge (Mulhol)	1.30
Northridge (Canoga Park)	1.19
Landers	2.14
IEEE	2.44

Table 5.11 presents the peak stress results for the seismic tests and model time-history analyses. The principal stresses found at the base of turret were over-predicted by the model while the peak bending stress at the base of the bushing tended to be less

than the results from the seismic tests. The principal stress at the turret base and bending stress at the base of the bushing predicted by the model were 38.2 ksi and 17.4 ksi, respectively. The measured peak principal stress at the turret base, and maximum peak bending stress at the base of the bushing were 23.6 ksi and 21.8 ksi, respectively.

Table 5.11 - Peak Stress Results from Numerical Model and Seismic Tests at 25% g.

Seismic Test Results

Record	Max. Princ. Stress @ Base of Turret (ksi)	Max. Bending Stress @ Base of Bushing (ksi)
Cape Mendocino	19.5	14.6
Northridge (Mulhol)	12.3	9.9
Northridge (Canoga Park)	21.2	18.0
Landers	23.6	21.8
IEEE	18.2	17.0

Numerical Model Results

Record	Max. Princ. Stress @ Base of Turret (ksi)	Max. Bending Stress @ Base of Bushing (ksi)
Cape Mendocino	27.4	9.8
Northridge (Mulhol)	18.9	6.4
Northridge (Canoga Park)	24.1	14.2
Landers	36.3	15.8
IEEE	38.2	17.4

Table 5.12 summarizes the predicted and measured spectral amplification results. The spectral amplification was computed for each record after performing the time-history analysis. Compared to the results from the seismic tests, the predicted spectral amplification values at the first natural frequency of the mock bushing were slightly lower. At this frequency, the measured mean spectral amplification computed for all earthquake records is 2.00, while the predicted mean spectral amplification 1.83.

Table 5.12 - Numerical and Experimental Spectral Amplification Results.

Seismic Test Results

Record	Spectral Amplification (2.6 Hz)	Spectral Amplification (3.0 Hz)	Spectral Amplification (6.7 Hz)
Cape Mendocino	2.0	1.8	11.1
Northridge (Mulhol)	1.6	1.6	7.4
Northridge (Canoga Park)	2.1	2.2	6.8
Landers	2.4	2.0	8.1
IEEE	1.9	2.0	8.5
	Mean	**Mean**	**Mean**
	2.00	**1.91**	**8.38**

Numerical Model Results

Record	Spectral Amplification (2.6 Hz)	Spectral Amplification (3.0 Hz)	Spectral Amplification (9.3 Hz)
Cape Mendocino	1.71	1.7	10.5
Northridge (Mulhol)	1.86	1.9	9.4
Northridge (Canoga Park)	1.74	1.6	8.8
Landers	1.63	1.6	11.1
IEEE	2.22	1.8	14.3
	Mean	**Mean**	**Mean**
	1.83	**1.73**	**10.82**

Figures 5.36 through 5.38 present the numerical and experimental time-history results for the Cape Mendocino record at 25% g. Considering the complexity of the test specimen, the measured and predicted acceleration and displacement time-histories are in relatively good agreement with one another. However, higher frequency content is present in the predicted time-histories. This is to be expected because of the fact that the longitudinal frequency of the transformer model was higher than the actual longitudinal frequency of the test specimen.

Comparing the Cape Mendocino record results, it can be seen that the peak absolute acceleration at the base of the bushing tends to be slightly larger for the

model. The magnitudes of the peak absolute accelerations and peak relative displacements at the top of the bushing appear to match fairly well; however, the time at which these peaks occur do not coincide.

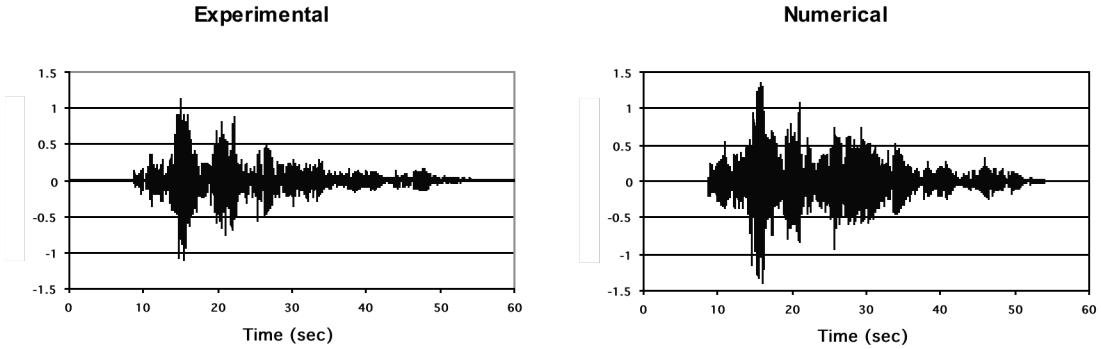

Figure 5.36 - Comparison of Numerical and Experimental Absolute Acceleration at Base of Mock Bushing for Cape Mendocino @ 25% g.

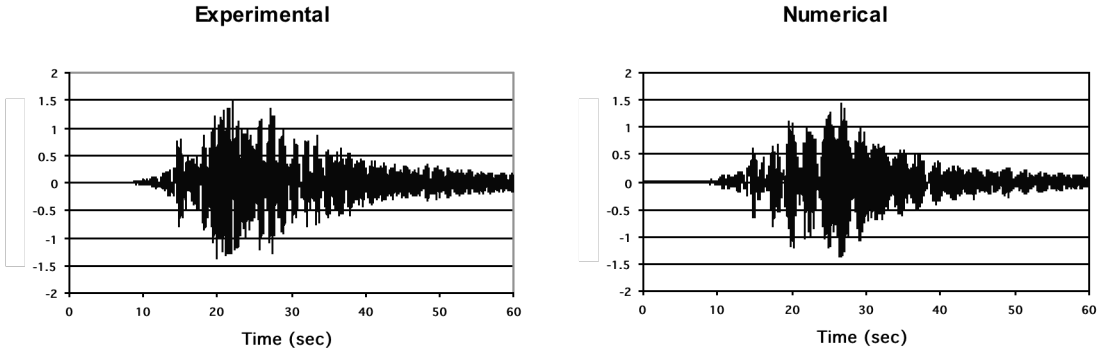

Figure 5.37 - Comparison of Numerical and Experimental Relative Displacement at Top of Mock Bushing for Cape Mendocino @ 25% g.

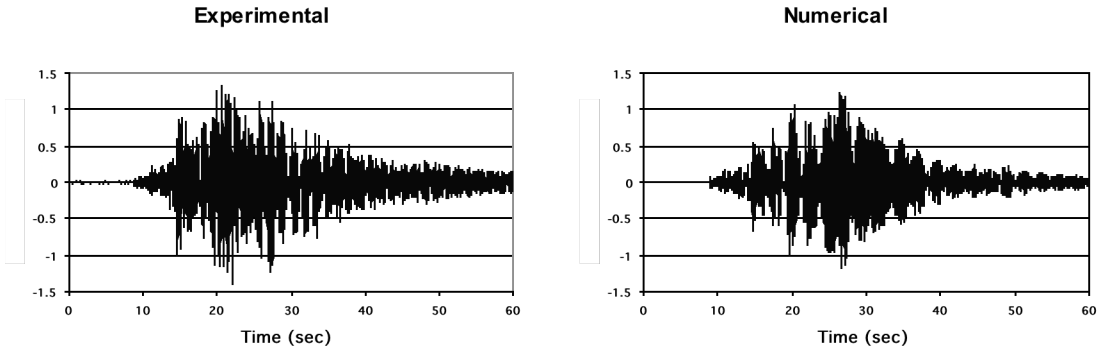

Figure 5.38 - Comparison of Numerical and Experimental Absolute Acceleration at Top of Mock Bushing for Cape Mendocino @ 25% g.

Figures 5.39 through 5.41 present the numerical and experimental results for the Northridge (Mulhol) record @ 25% g. The model absolute acceleration and peak relative displacement time-histories at the top of the mock bushing are both fairly consistent with the experimental results. Again, higher frequency content is prevalent in the model that was not present for the experimental results. The results also indicate that the model overestimates the peak absolute acceleration magnitude at the base of the mock bushing.

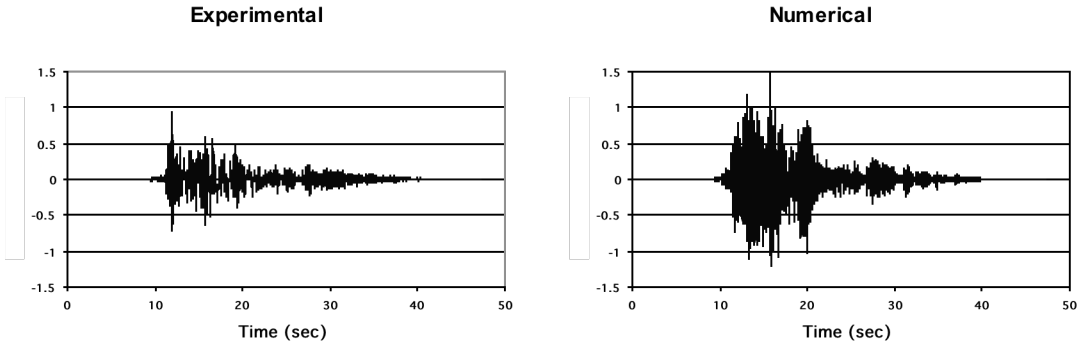

Figure 5.39 - Comparison of Numerical and Experimental Absolute Acceleration at Base of Mock Bushing for Northridge (Mulhol) @ 25% g.

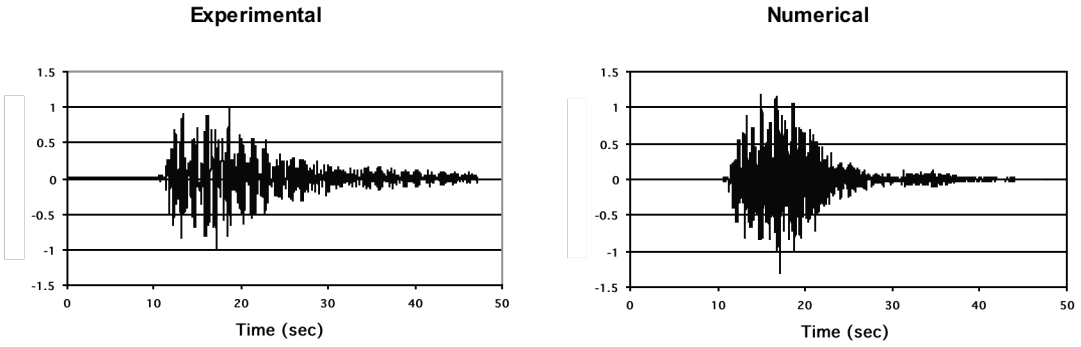

Figure 5.40 - Comparison of Numerical and Experimental Relative Displacement at Top of Mock Bushing for Cape Mendocino @ 25% g.

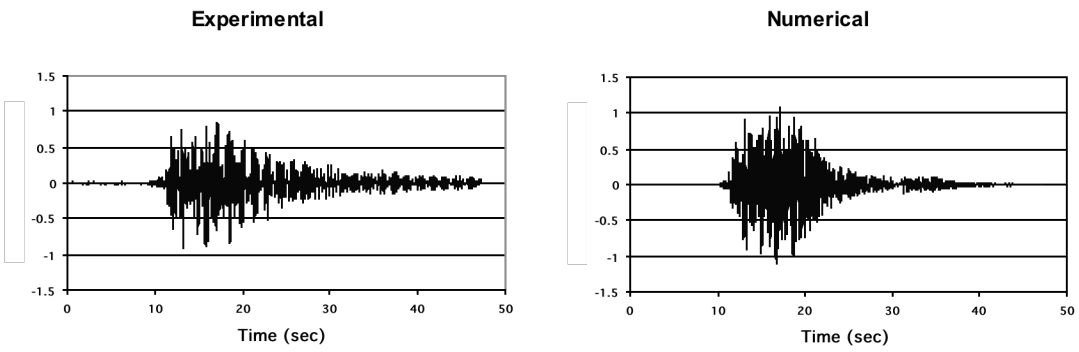

Figure 5.41 - Comparison of Numerical and Experimental Absolute Acceleration at Top of Mock Bushing for Cape Mendocino @ 25% g.

In summary, the numerical analysis presented within this section show that the model predicts the experimental results with relatively good accuracy considering the complexity of the test specimen. The mode shapes and natural frequencies of the mock bushing predicted by the model closely matched the corresponding measured values. After improving its support boundary conditions, most of the flexibility of the shake table frame was captured by the finite element model. The model had difficulty in predicting with great accuracy the peak absolute accelerations at the top of the transformer and mock bushing; however, even the largest discrepancy was reasonable considering the complexity of the system. The experimental and numerical acceleration and displacement time-histories corresponded fairly well, despite the fact that the longitudinal transformer frequency was slightly larger for the numerical model.

6. REPORT SUMMARY, CONCLUSIONS AND RECOMMENDATIONS FOR FUTURE WORK

6.1. Summary

This Research Task 406, initiated as part of the PEER lifelines Task 4 program, investigated the factors that most greatly influence an increase in the dynamic response of high voltage bushings as well as quantified the amplification for various transformers from numerical and experimental results.

Three numerical studies were performed on four different high voltage transformers: the 525 kV Transformer A, the 500 kV Transformer D, the 230 kV Transformer C, and the 500 kV Transformer B. Using an ensemble of 20 acceleration time-histories recorded during recent seismic events, dynamic time-history analyses were performed during a first numerical study to determine the spectral amplification for each of the four transformer models. A second numerical study looked into various methods of retrofit in order to improve the dynamic response of the 230 kV Transformer C bushing under seismic loading. A third and final numerical study utilized dynamic time-history analyses to define the amplification in bending stress experienced by the bushings when mounted on its respective transformer.

Experimental shake table tests were conducted on the full scale 525 kV Transformer A using the UC-San Diego uniaxial earthquake simulation system. Frequency and damping evaluation tests were performed to determine the dynamic properties such as predominant natural frequencies and modal viscous damping ratios of the transformer and mock bushing. In addition, shake table time-history tests were performed using five different earthquake ground motions at various input amplitudes.

The shake table tests were used to determine the true dynamic amplification and influencing factors of the mock bushing response.

A numerical finite element model of the test configuration was developed to predict the modal properties of the system as well as the seismic test results through modal and dynamic time-history analyses. The shake table absolute acceleration time-histories recorded during the 25% g seismic tests were utilized for the numerical analysis.

6.2. Conclusions

From the results of the three numerical studies, experimental tests, and numerical model of the testing configuration, many conclusions can be drawn regarding the dynamic response of high voltage transformer mounted bushings subjected to seismic excitation. The key conclusions from this study are summarized below:

- The transformer structure cannot be considered rigid if the tank is not braced to the interior core.
- The flexibility of the top plate of the transformer tank greatly reduces the fundamental natural frequency of a transformer-mounted bushing.
- The top plate flexibility of the transformer tank should be accounted for during seismic qualification tests in order to better represent the true dynamic characteristics as well as to obtain more accurate seismic forces.
- In a given direction, the spectral amplification occurs at two predominant frequencies, the natural frequency of the transformer frame and the natural frequency of the bushing.

- The lower frequency transverse direction of the transformer tank consistently results in larger spectral and bending stress amplifications that the higher frequency longitudinal direction.
- The motion amplification factor of 2.0 defined in the IEEE-693 seismic qualification document is not necessarily conservative for all transformers.
- Very large spectral and bending stress amplifications may occur when the predominant frequency of the transformer tank and bushing are relatively close to one another.
- For transformer tanks with predominant modes near the natural frequencies of the high voltage bushing, simple bracing members attached near the turret of the bushing effectively reduce the spectral and bending stress amplifications as well as improve the overall bushing response.
- The bending stress amplifications were consistently less than the corresponding spectral amplifications at the frequency of the bushing for all transformers.
- The bending stress amplification may be larger than the allowable amplification factor of 2.0, as was the case for the 230 kV Transformer C.
- Methods to recognize cases (such as the 230 kV Transformer C) where the bushing stresses experienced during the design earthquake will be much larger than the peak stresses induced during the seismic qualification testing should be adopted.
- The mean equivalent viscous damping of the mock bushing varies with amplitude of acceleration. The mean values of damping ratios measured were 0.26% and 0.37% of critical for the first two modes of vibration. These values are reasonable for the purpose of studying bushing response.

- Due to the large overturning moment of the test specimen, the shake table-transformer frame interaction greatly reduced the natural frequency of the 525 kV Transformer A in the longitudinal direction. This behavior highlights the fact that transformer rocking or site effects may significantly influence the seismic response of transformer tanks. These effects are generally ignored in typical design practice.
- The peak absolute accelerations at the base of the mock bushing were only slightly larger than the peak absolute accelerations measured at the top of the transformer.
- The measured spectral amplifications at the first natural frequency of the mock bushing were generally larger than at the second natural frequency of the mock bushing.
- The spectral amplifications at the first natural frequency of the mock bushing were generally slightly larger than 2.0.
- Depending upon the earthquake record, the spectral amplification may not be constant for all seismic intensities.
- The transformer top plate of the test specimen had fairly significant flexibility despite the presence of stiffening members on the top interior of the transformer.
- Rocking motion of the mock bushing and turret, facilitated by the top plate flexibility caused noticeable relative displacements at the top of the mock bushing.
- The bending stresses in the mock bushing base and at the base of the turret were nearly the same during the seismic tests
- The numerical model was able to predict peak absolute acceleration, relative displacement and stress values with reasonable accuracy considering the complexity of the system.

- The ability to numerically reproduce the shake table results with reasonable accuracy further validated the results and conclusions from the three numerical studies

6.3 Recommendations for Future Work

Based on the results obtained in this study, the following two issues should be urgently investigated in the future in order to improve the seismic design and behavior of transformer-bushing systems.

1. A simple procedure needs to be developed to insure that the bushing natural frequency is not tuned to the transformer tank frequency. Some simple design tools and/or testing procedures need to be elaborated to help transformer tank manufacturers design tank and bushing supports that detune the transformer structural frequency from the bushing natural frequency. Some criteria on adequate spacing between tank and bushing frequencies need to be established.
2. Changes to the IEEE 693 design standards may need to be considered to reflect the fact that the dynamic properties of a bushing mounted on a transformer tank are significantly different that of the same bushing mounted on a rigid support. Two different paths may be considered. The first path could be to keep the current rigid test stand, as currently specified in the IEEE 663 standard, and to introduce some transformer tank design requirements to insure that the bushing support is sufficiently stiff. Another approach could be to modify both the bushing qualification procedure in the IEE-693 standard, along with the introduction of

new transformer tank design requirements. In either case, it seems practical to anchor the seismic qualification testing on a standard test stand since bushings and transformers are usually supplied by different manufacturers and utilities need to have bushings that are interchangeable. Transformer manufacturers input will be needed in these modifications of the IEE 693 standard.

REFERENCES

[1] Schiff, Anshel, 1998. "Guide to Improved Earthquake Performance of Electrical Power Systems," Report NIST GCR 98-757, National Institute for Standards and Testing, Washington, DC.

[2] Institute of Electrical and Electronics Engineers, 1997. "Recommended Practice for Seismic Design of Substations," IEEE Standards Department Copyright and Permissions, Piscataway, NJ.

[3] Gilani, A., Whittaker, A. Fenves, G., 1999. "Seismic Evaluation and Retrofit of 230-kV Porcelain Transformer Bushings," PEER Report 1999/14, University of California, Berkeley, CA.

[4] Gilani, A., Chavez, J., Fenves, G., Whittaker, A., 1998. "Seismic Evaluation of 196 kV Porcelain Transformer Bushings", PEER Report 1998/02, University of California, Berkeley, CA.

[5] Gilani, A., Whittaker, A., Fenves, G., 1999. "Seismic Evaluation of 550 kV Porcelain Transformer Bushings," PEER Report 1999/05, University of California, Berkeley, CA.

[6] Computers and Structures, Inc., 2003. "SAP2000 Nonlinear V. 8.2.6," Berkeley, CA.

[7] Gundy, W., 2002. "Seismic Qualification of a 500 kV Power Transformer," Report 1018-58, W.E. Gundy & Associates, Inc., Hailey, ID.

[8] Gundy, W., 2000. "Seismic Qualification of a 230 kV Power Transformer," Report 1018-54, W.E. Gundy & Associates, Inc., Hailey, ID.

[9] Westinghouse Electric Corporation, 1966. "Westinghouse Transformers Instruction Book," Power Transformer Division, Muncie, IN.

[10] Krawinkler, H., Parisi, F., Ibarra, L., Ayoub, A., Medina, R., 2000. "Development of a Testing Protocol for Woodframe Structures," CUREE Publication No. W-02, Richmond, CA.

[11] Fischer, D., Filiatrault, A., Folz, B., Uang, C., Seible, F., 2001. "Shake Table Tests of a Two-Story Woodframe House," University of California, San Diego, CA.

[12] Experimental Dynamic Investigations, 1993. "U2 Program User's Manual," Vancouver, BC.

[13] Filiatrault, A., 1998. "Elements of Earthquake Engineering and Structural Dynamics," Polytechnic International Press, Montreal, Canada.

[14] Clough, R.W., Penzien, J., 1993. "Dynamic of Structures, Second Edition, McGraw-Hill, New York.

[15] Ersoy, S., Saadeghvaziri, M. Ala., 2002. "Seismic Response of Transformer-Bushing Systems," National Science Foundation Award No. EEC-9701471.

[16] Filiatrault, A., Christopoulos, C., Stearns, C., 2001. "Guidelines, Specifications, and Seismic Performance Characterization of Nonstructural Building Components and Equipment," Report No. SSRP – 2001/13, University of California, San Diego, CA.

[17] Villaverda, R., Pardoen, G., Carnalla, S., 1999. "Ground Motion Amplification at Base of Bushings Mounted on Electric Substation Transformers," PEER/PG&E Award No. PGE-09566, University of California, Irvine, CA.

[18] Schiff, A., Kempner, J., 2003. "Issues and Guidance for IEEE 693 Equipment Qualification Tests," PMI, Los Altos Hills, CA.

APPENDIX A: TRANSFORMER MODEL DRAWINGS

Appendix A – 525 kV Transformer A

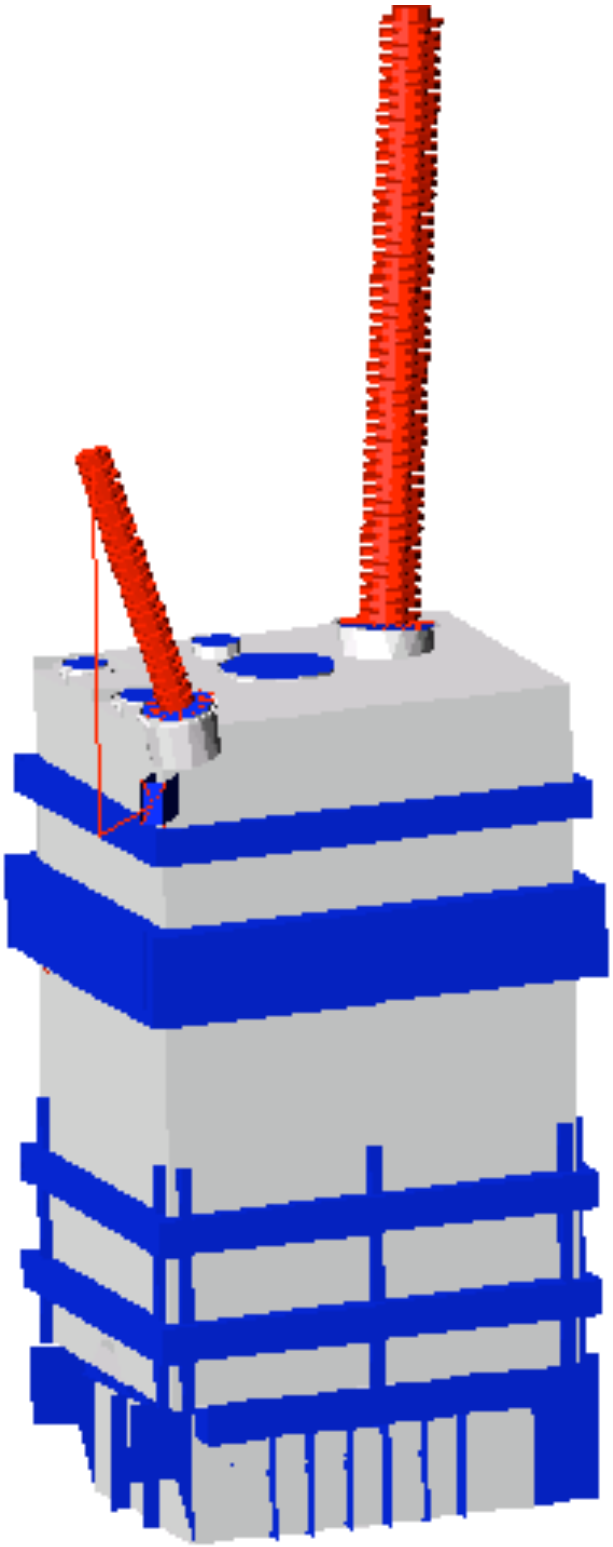

Appendix A – 500 kV Transformer B

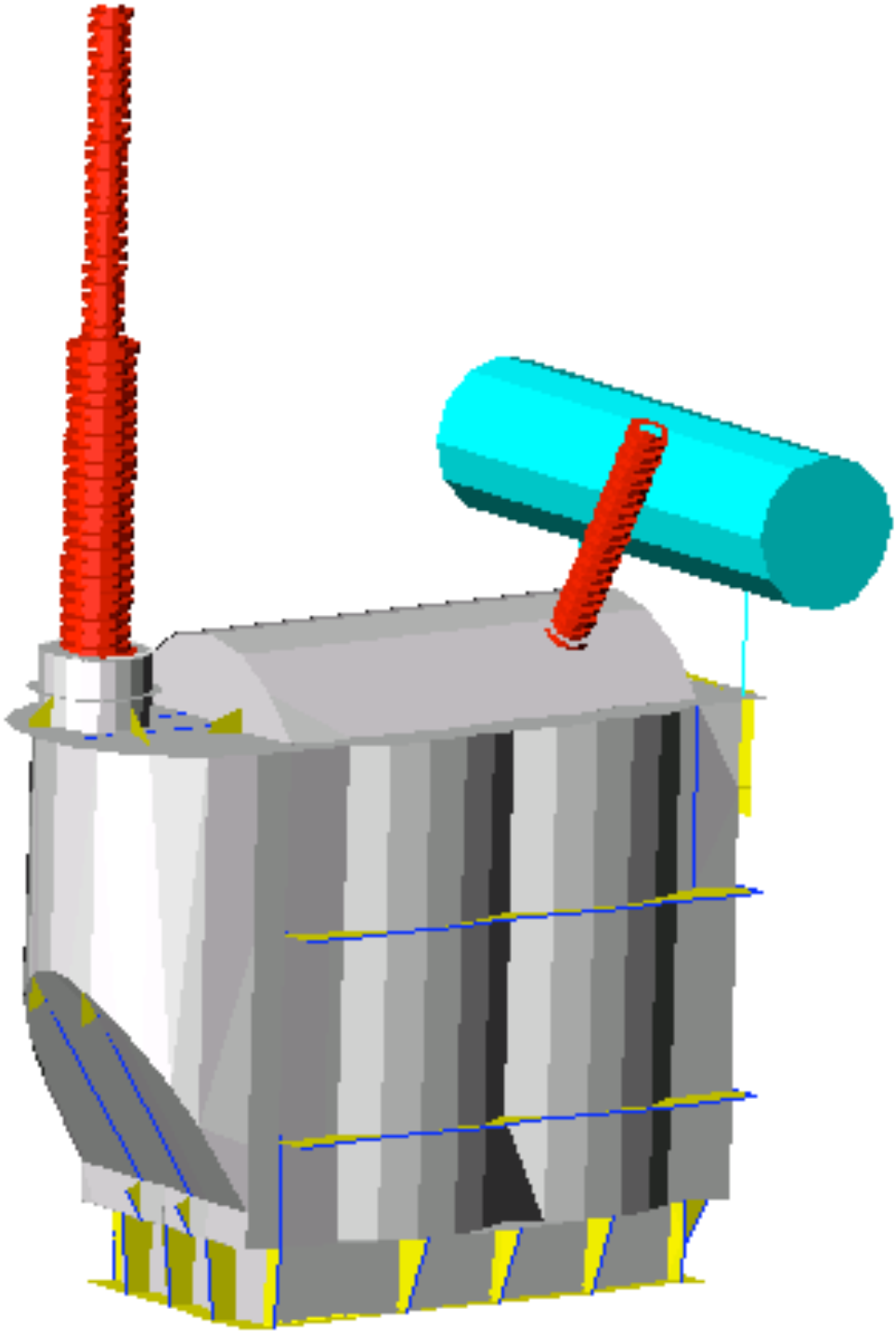

Appendix A – 230 kV Transformer C

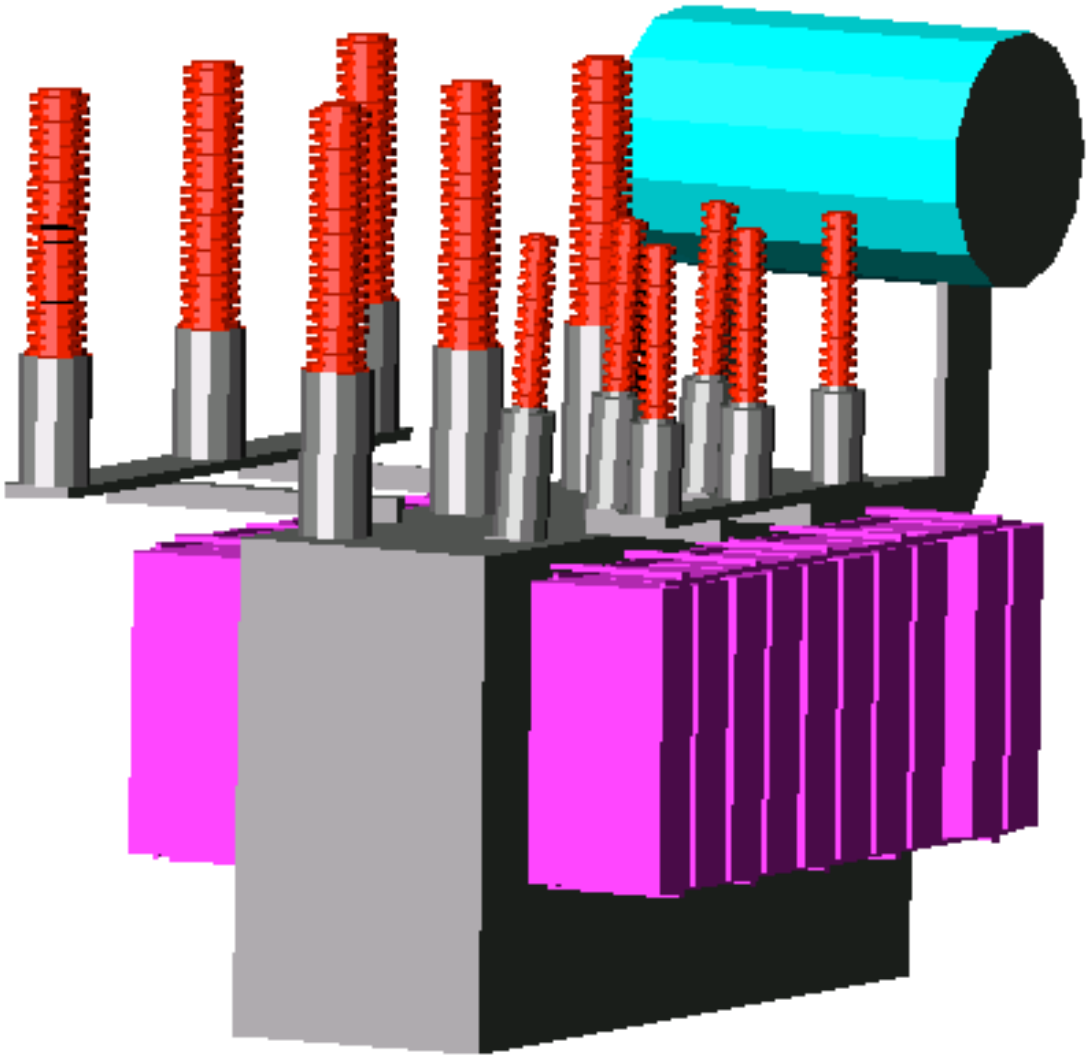

Appendix A – 500 kV Transformer D

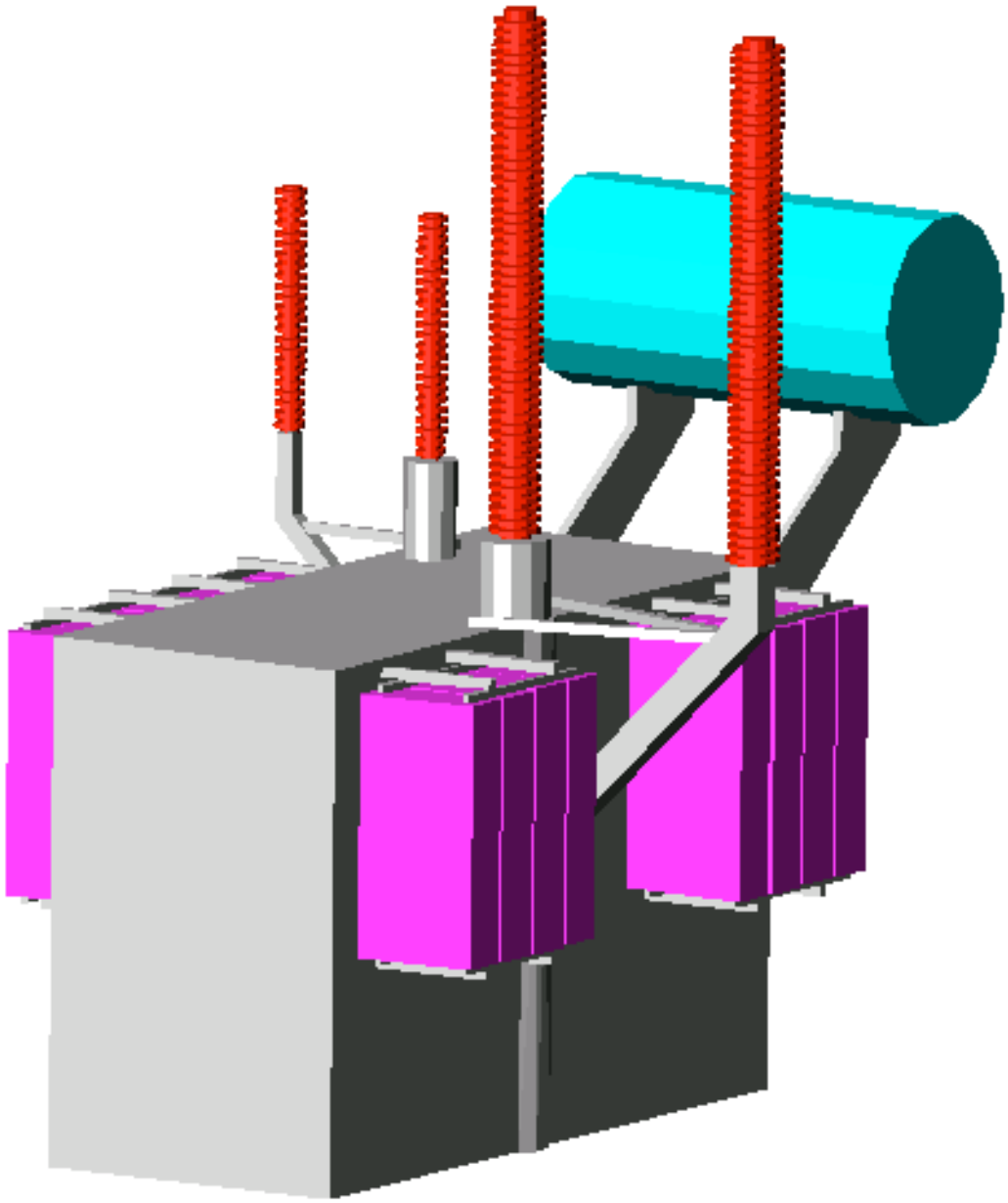

APPENDIX B: BUSHING AND TRANSFORMER MODE SHAPES

Appendix B – 525kV Transformer A

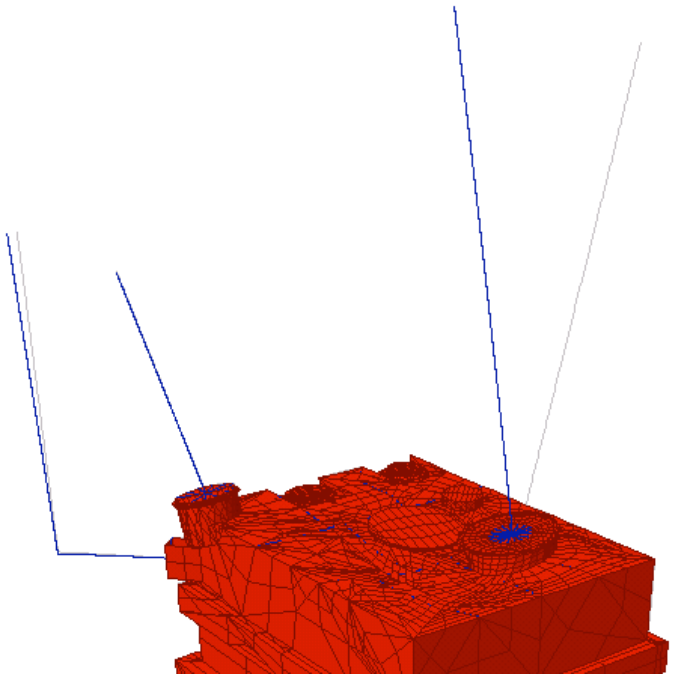

Mode 2 - Bushing 1st Mode (2.9 Hz)

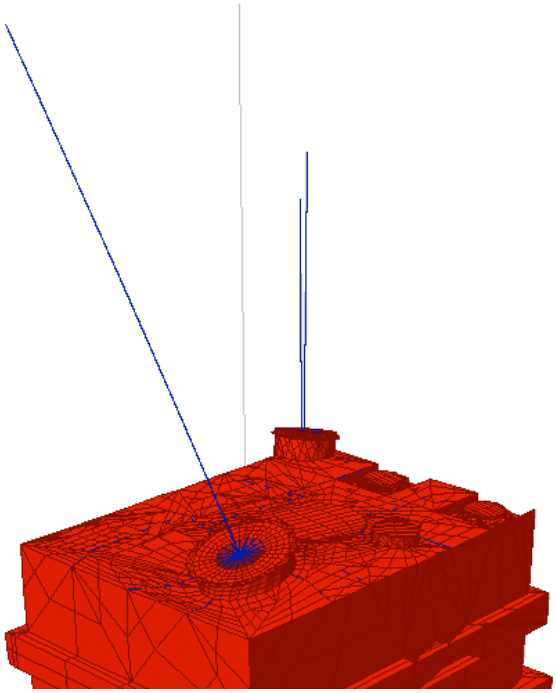

Mode 4 - Bushing 2nd Mode (3.4 Hz)

Appendix B – 525kV Transformer A

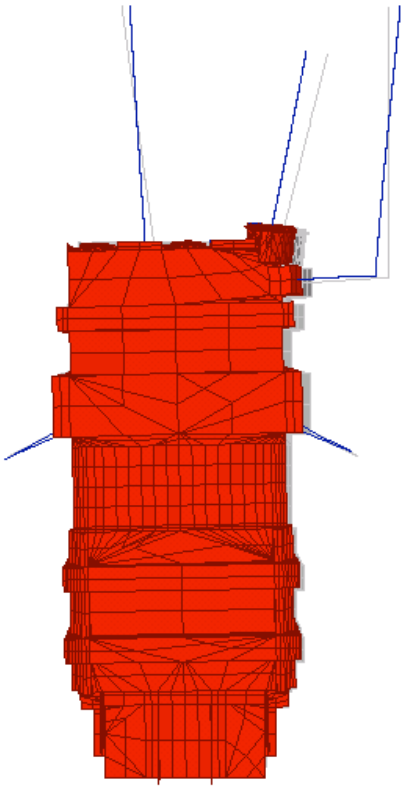

Mode 5 – Transformer Transverse (8.4 Hz)

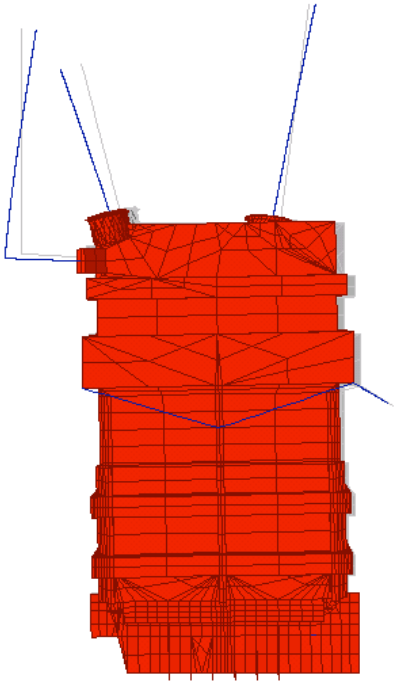

Mode 6 – Transformer Longitudinal (11.4 Hz)

Appendix B – 500 kV Transformer B

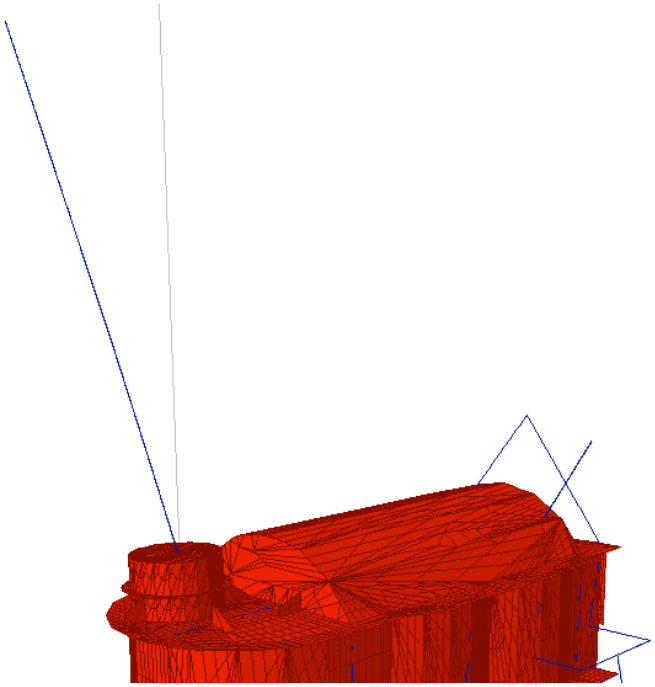

Mode 1 - Bushing Transverse (3.2 Hz)

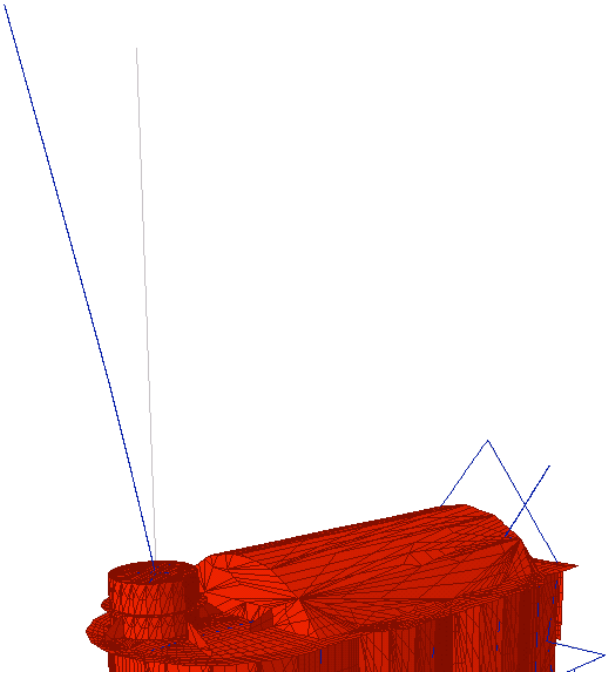

Mode 2 - Bushing Longitudinal (4.9 Hz)

Appendix B – 500 kV Transformer B

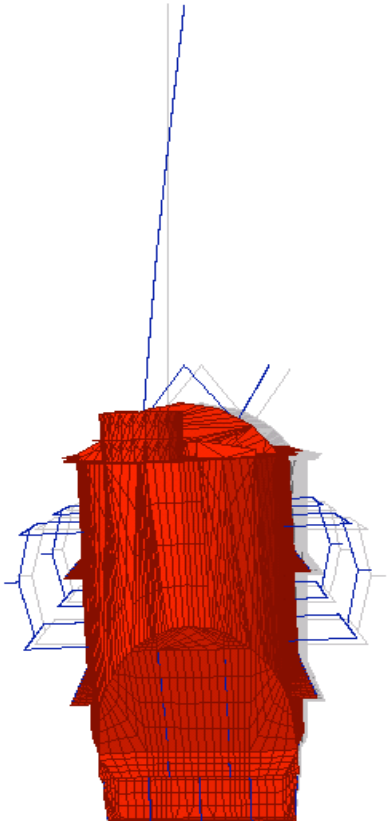

Mode 3 - Transformer Transverse (14.2 Hz)

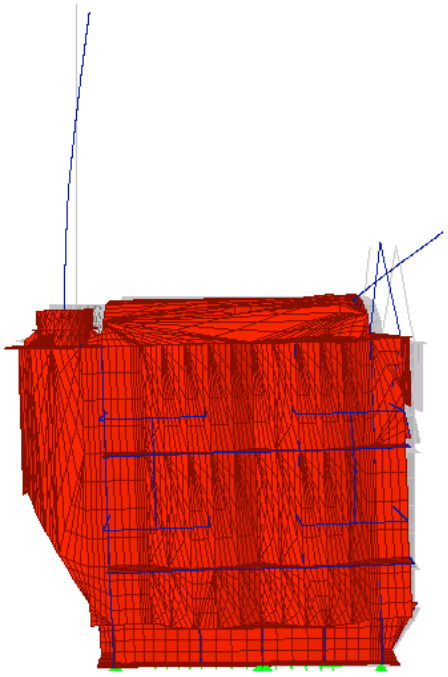

Mode 4 - Transformer Longitudinal (25.3 Hz)

Appendix B – 230 kV Transformer C

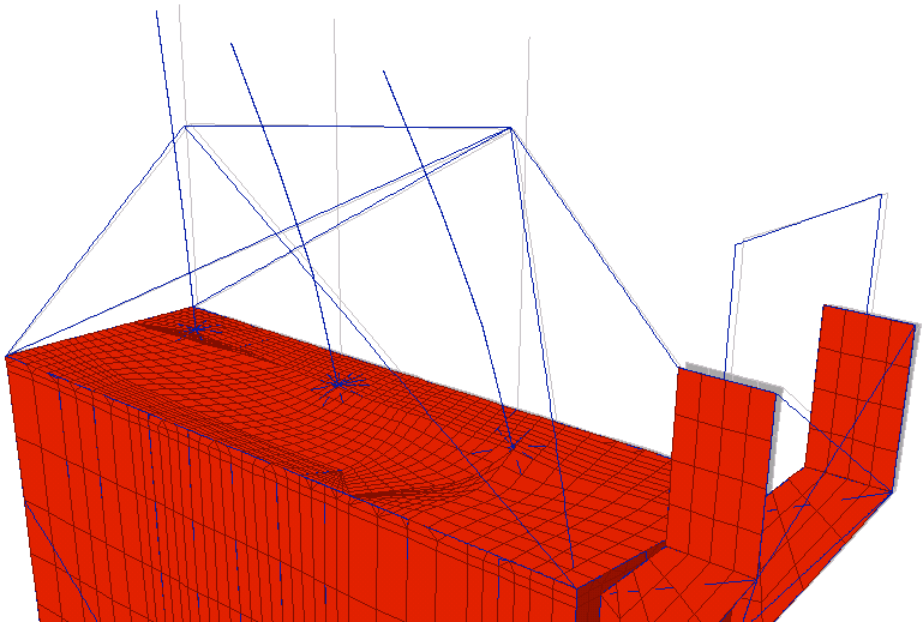

Mode 1 - Bushing Transverse (9.1 Hz)

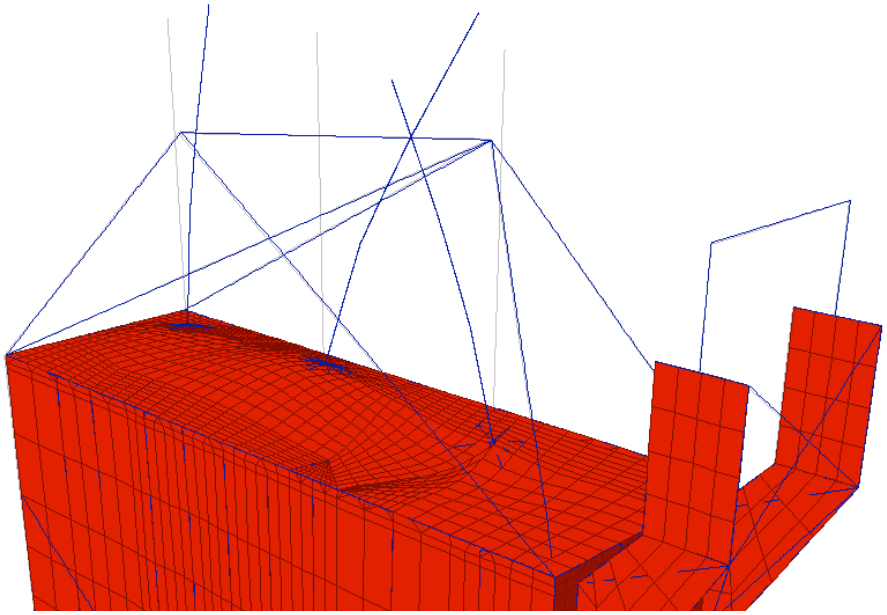

Mode 2 - Bushing Longitudinal (10.3 Hz)

Appendix B – 230 kV Transformer C

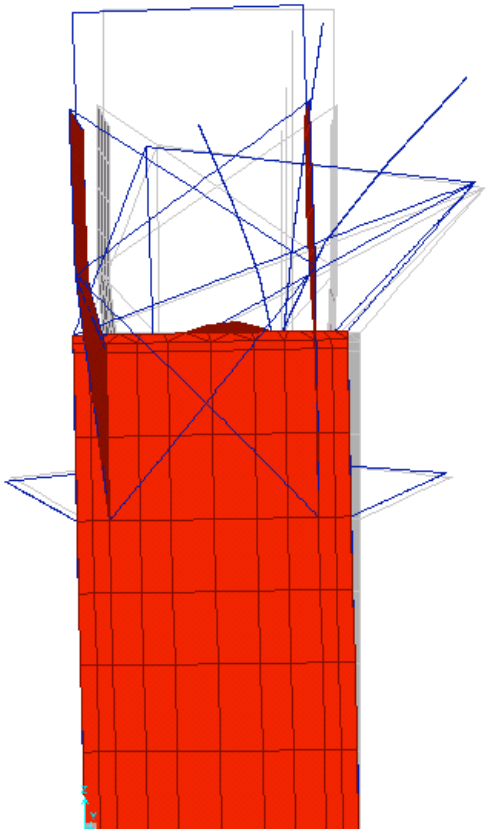

Mode 3 - Transformer Transverse (10.8 Hz)

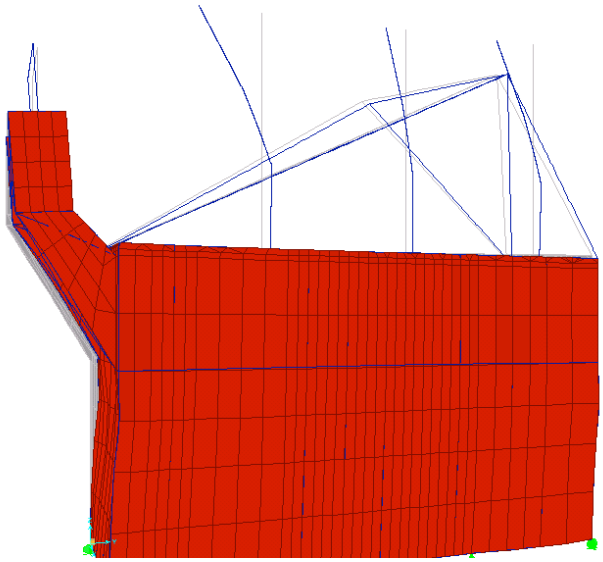

Mode 10 – Transformer Longitudinal (25.1 Hz)

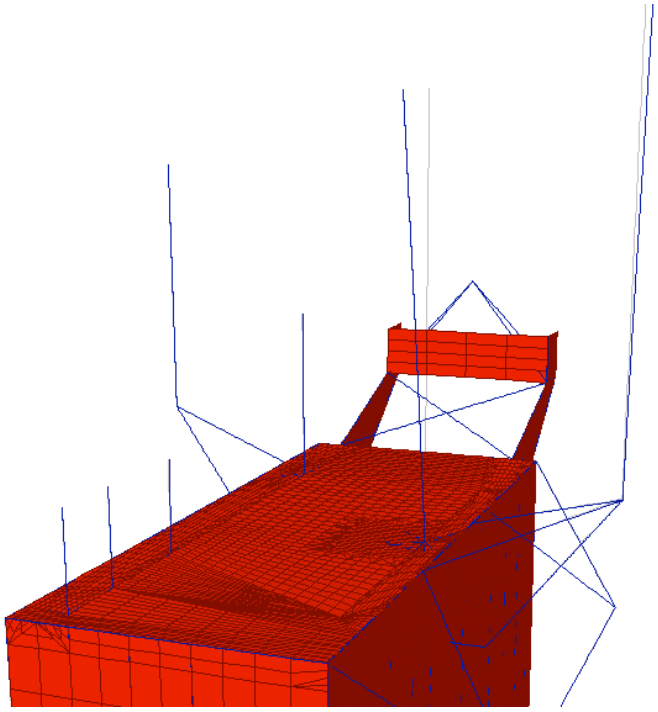

Mode 3 – Bushing Transverse (3.4 Hz)

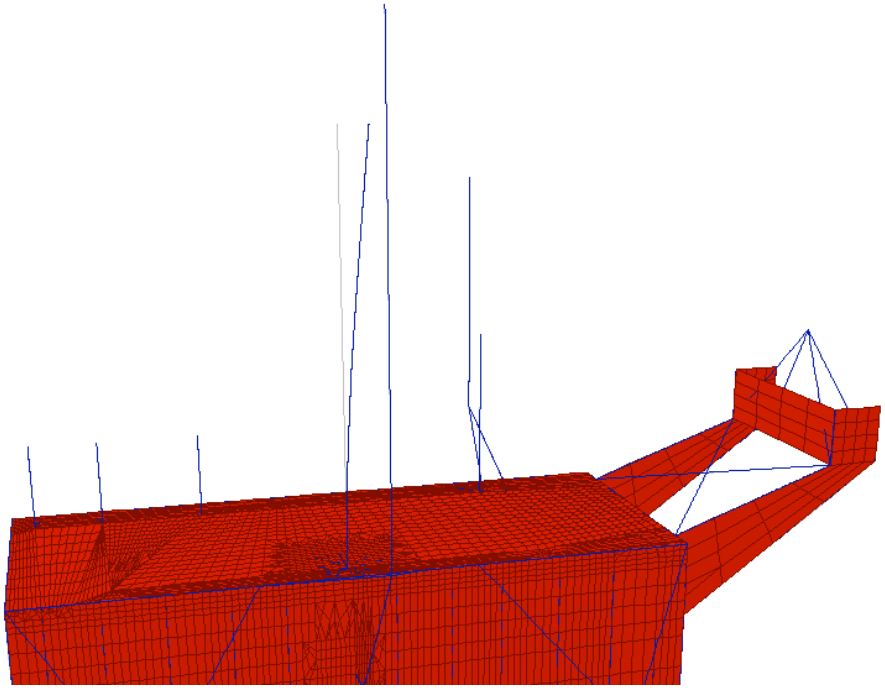

Mode 8 – Bushing Transverse (8.4 Hz)

Appendix B –500 kV Transformer D

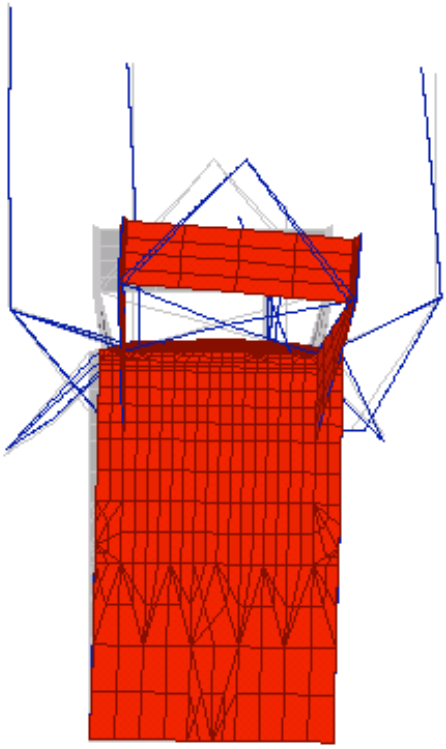

Mode 11 – Transformer Transverse (10.5 Hz)

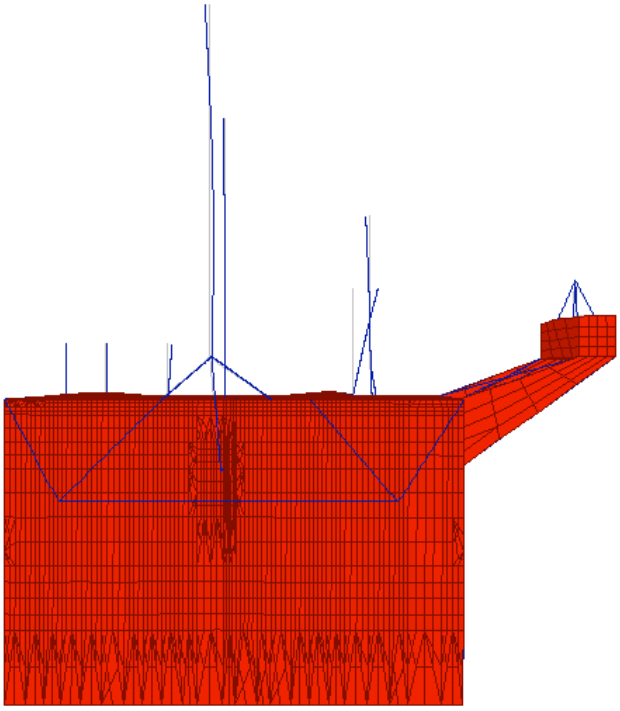

Mode 18 – Transformer Longitudinal (10.5 Hz)

APPENDIX C: DATABASE OF TRANSFORMER BUSHING FREQUENCIES

Appendix C - Database Transformer Bushing Frequencies

Source	Voltage Rating (kV)	Weight* (lbs)	Insulator Material	Length* (ft)	Support	1st Mode (Hz)
PEER Database	550	NA	Porcelain	NA	Rigid	8.2
PEER Database	550	NA	Porcelain	NA	Rigid	8.0
PEER Database	550	NA	Porcelain	NA	Rigid	8.0
SDG&E Seismic Qualification Report	550	2200	Composite	16.37	Rigid	3.8
550 kV Seismic Eval. (PEER)	550	2895	Porcelain	15.96	Rigid	8.0
Westinghouse 525 kV Transformer	525	3089	Porcelain	13.48	Transformer	3.1
Westinghouse 525 kV Transformer	525	3089	Porcelain	13.48	Rigid	8.9
SDG&E Report	500	2900	Porcelain	14.33	Rigid	3.3
Siemens 500 kV Transformer	500	1321	Composite	13.08	Rigid	8.9
Siemens 500 kV Transformer	500	1321	Composite	13.08	Transformer	3.5
Brown Boveri 500 kV Transformer	500	2900	Porcelain	14.33	Rigid	8.7
Brown Boveri 500 kV Transformer	500	2900	Porcelain	14.33	Transformer	3.2
UC-Irvene Report	500	4190	Porcelain	15.86	Transformer	3.1
UC-Irvene Report	500	NA	Porcelain	NA	Transformer	3.4
UC-Irvene Report	500	4190	Porcelain	15.86	Transformer	3.4
PEER Database	500	NA	Composite	NA	Rigid	3.9
PEER Database	500	NA	Composite	NA	Rigid	3.9
UC-Irvene Report	275	NA	Porcelain	NA	Transformer	7.5
UC-Irvene Report	230	1100	Porcelain	8.5	Transformer	4.6
Westinghouse 525 kV Transformer	230	1129	Porcelain	7.17	Transformer	25.6
Westinghouse 525 kV Transformer	230	1129	Porcelain	7.17	Rigid	29.3
230 kV Seismic Eval. (PEER)	230	560	Porcelain	7.08	Rigid	20.0
Siemens 230 kV Transformer	230	600	Porcelain	6.83	Rigid	18.9
Siemens 230 kV Transformer	230	600	Porcelain	6.83	Transformer	9.1
UC-Irvene Report	230	1100	Porcelain	15.86	Transformer	5.6
PEER Database	230	200	Composite	NA	Rigid	9.8
PEER Database	230	NA	Porcelain	NA	Rigid	18.0
PEER Database	230	NA	Porcelain	NA	Rigid	18.0
PEER Database	230	NA	Porcelain	NA	Rigid	18.0
PEER Database	230	NA	Porcelain	NA	Rigid	18.0
PEER Database	230	NA	Composite	NA	Rigid	14.0
PEER Database	230	NA	Composite	NA	Rigid	5.3
PEER Database	230	NA	Composite	NA	Rigid	5.3
SDG&E Report	196	900	Porcelain	6.33	Rigid	9.1
PEER Database	196	836	Porcelain	NA	Rigid	8.6
PEER Database	196	836	Porcelain	NA	Rigid	8.6
Bushing Response Report	196	NA	Porcelain	NA	Transformer	10.0
Bushing Response Report	196	NA	Porcelain	NA	Rigid	14.4

APPENDIX D: GROUND MOTION TIME-HISTORIES

Appendix D – Time Histories

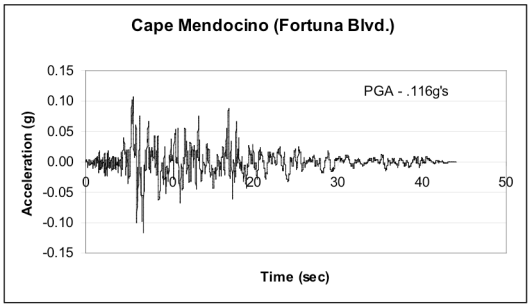

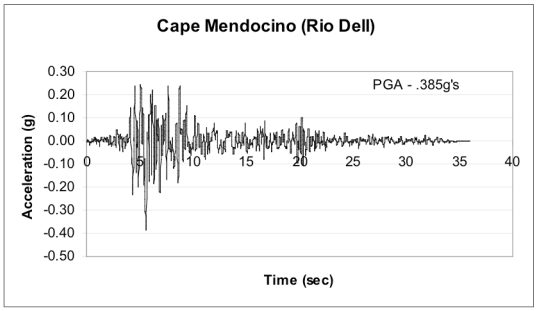

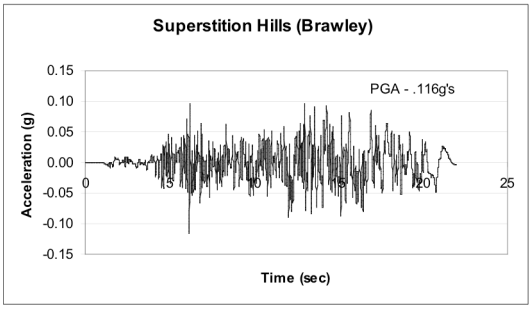

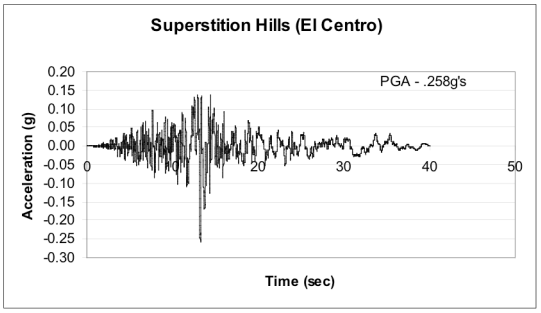

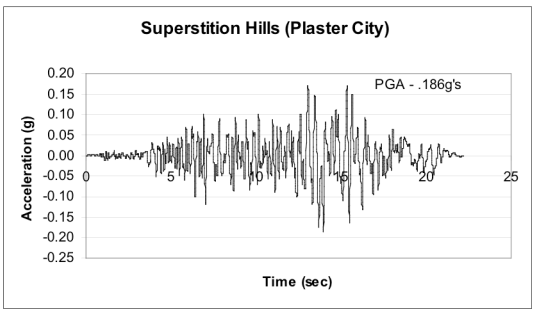

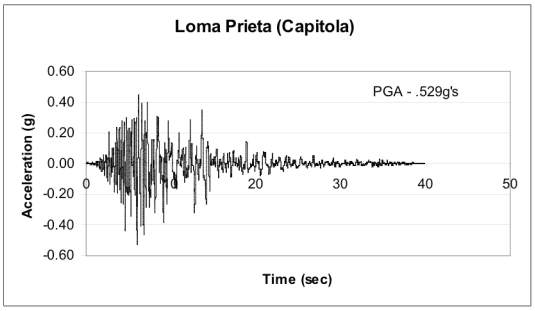

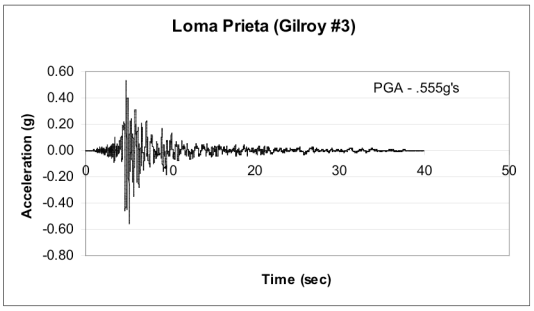

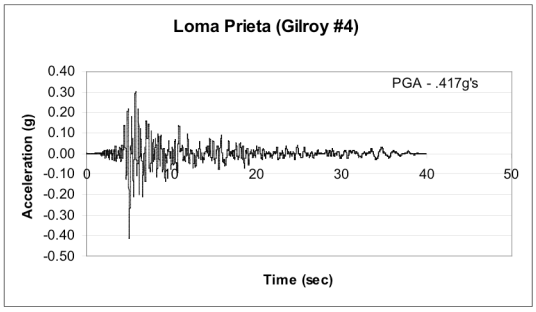

Appendix D – Time Histories

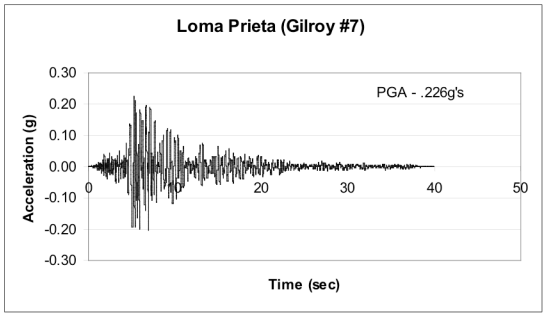

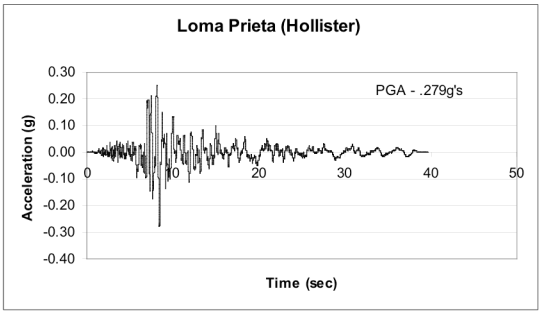

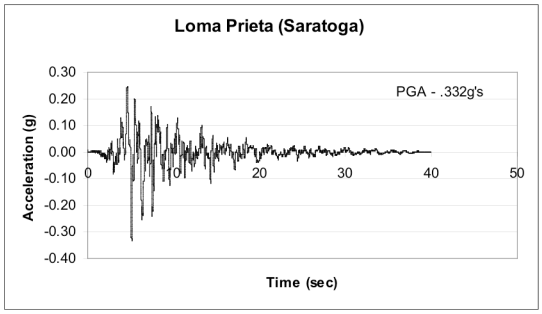

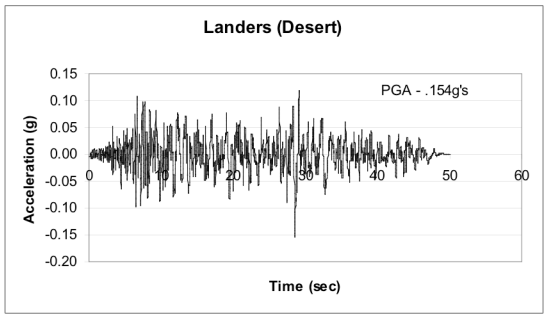

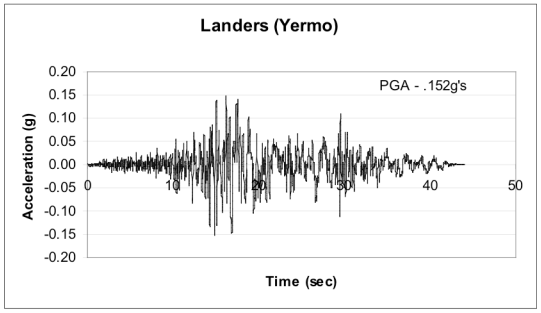

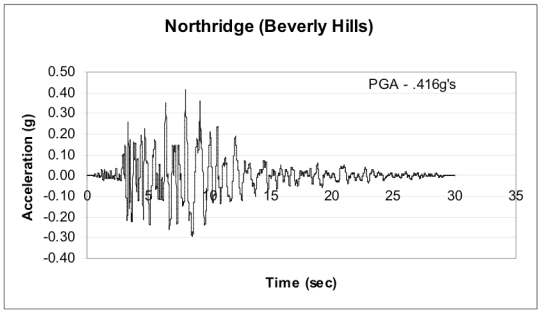

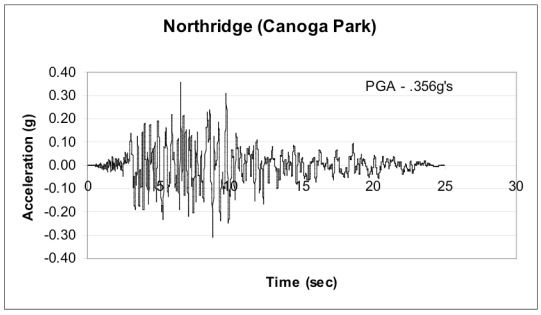

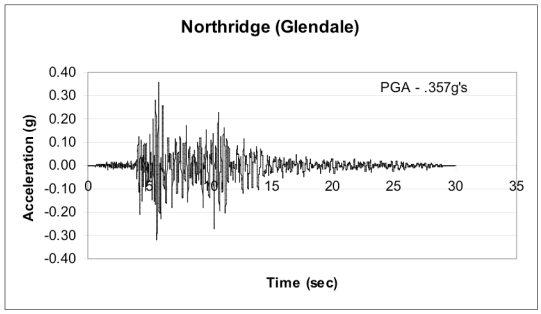

Appendix D – Time Histories

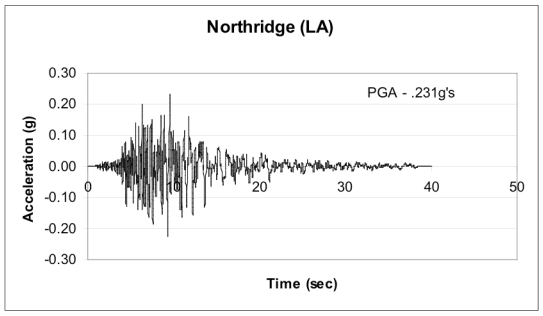

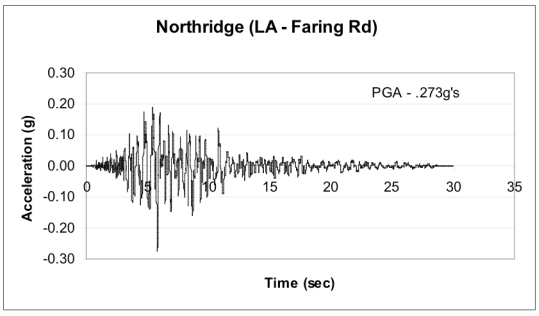

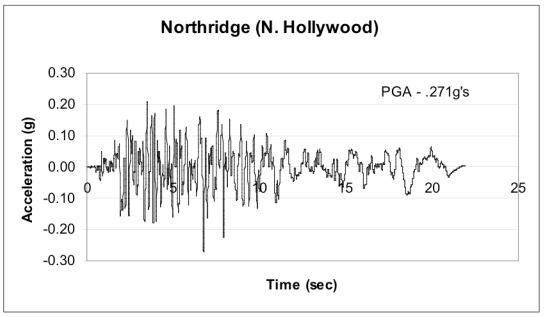

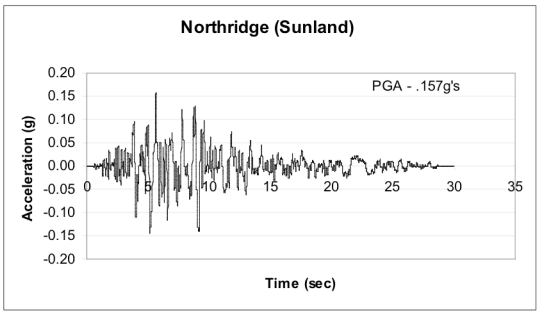

APPENDIX E: GROUND MOTION RESPONSE SPECTRA

Appendix E –Ground Motion Response Spectra

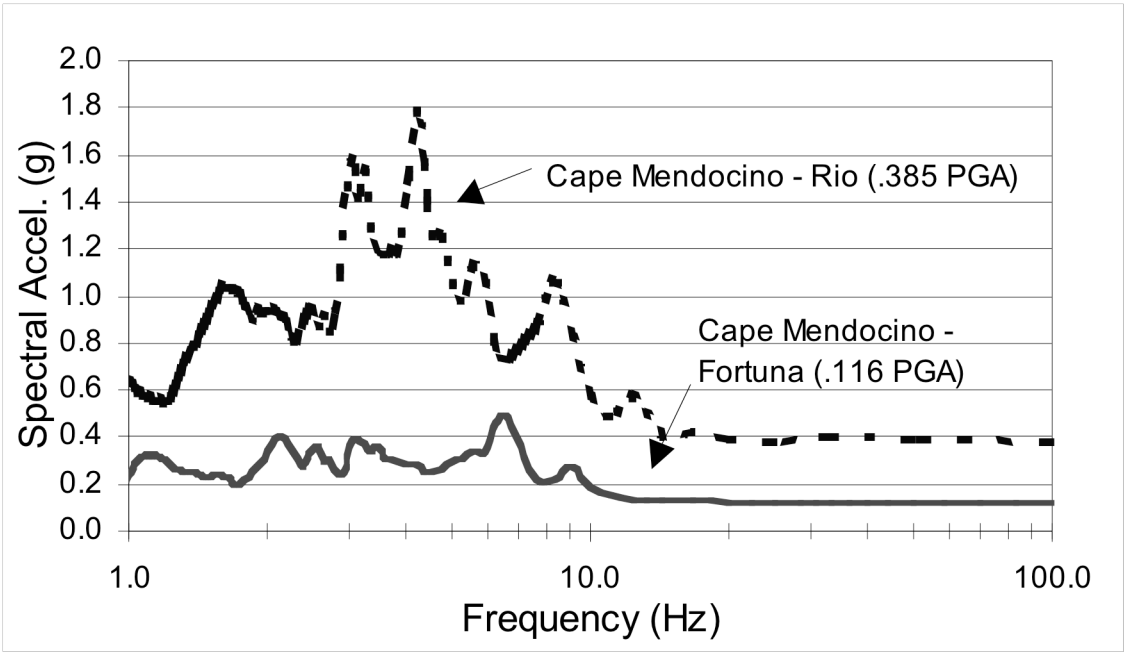

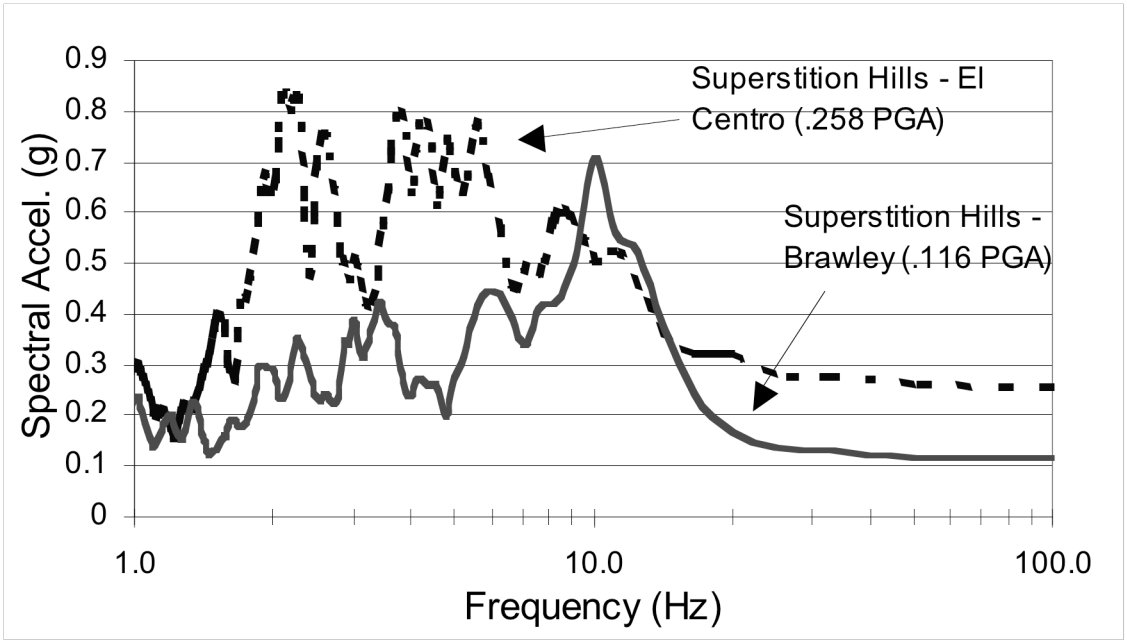

Appendix E –Ground Motion Response Spectra

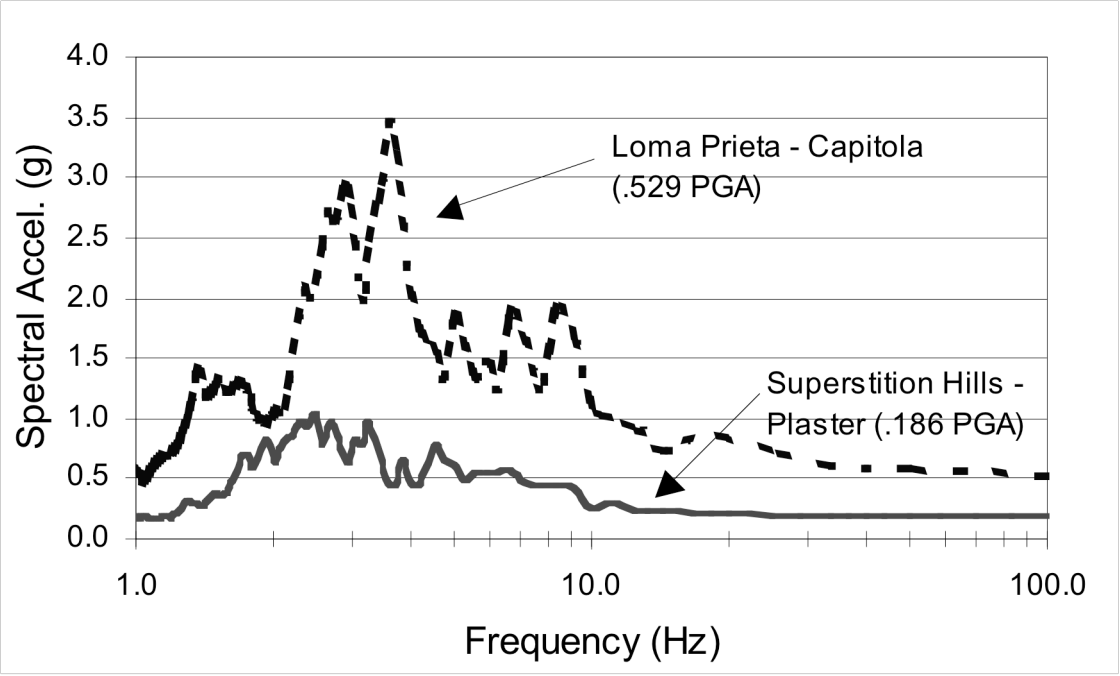

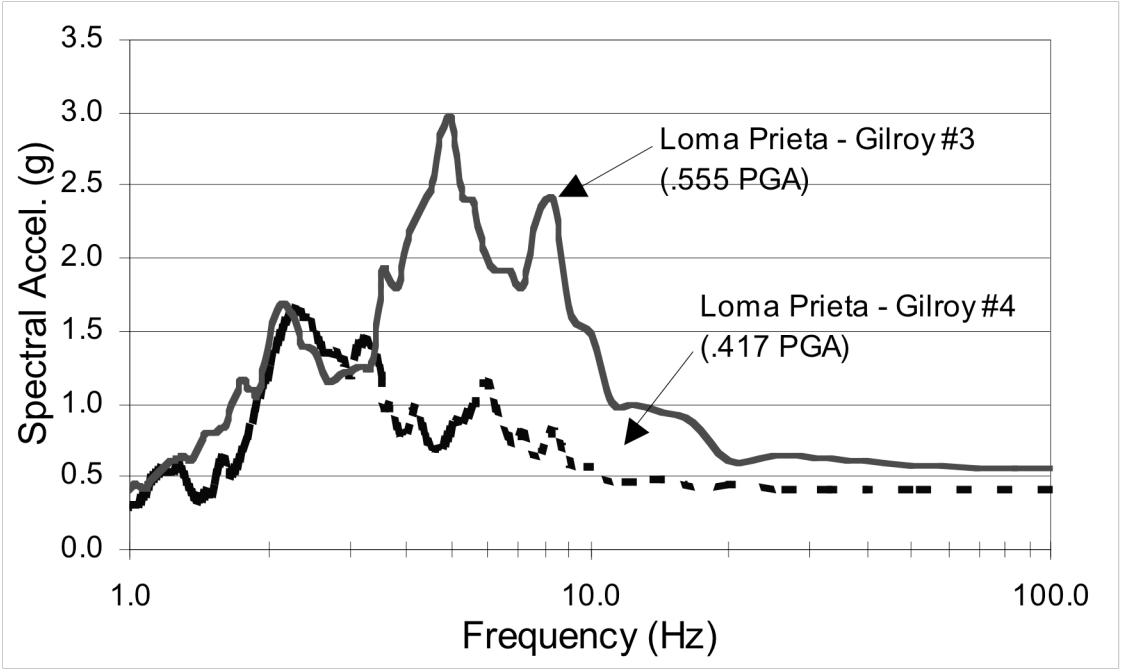

Appendix E –Ground Motion Response Spectra

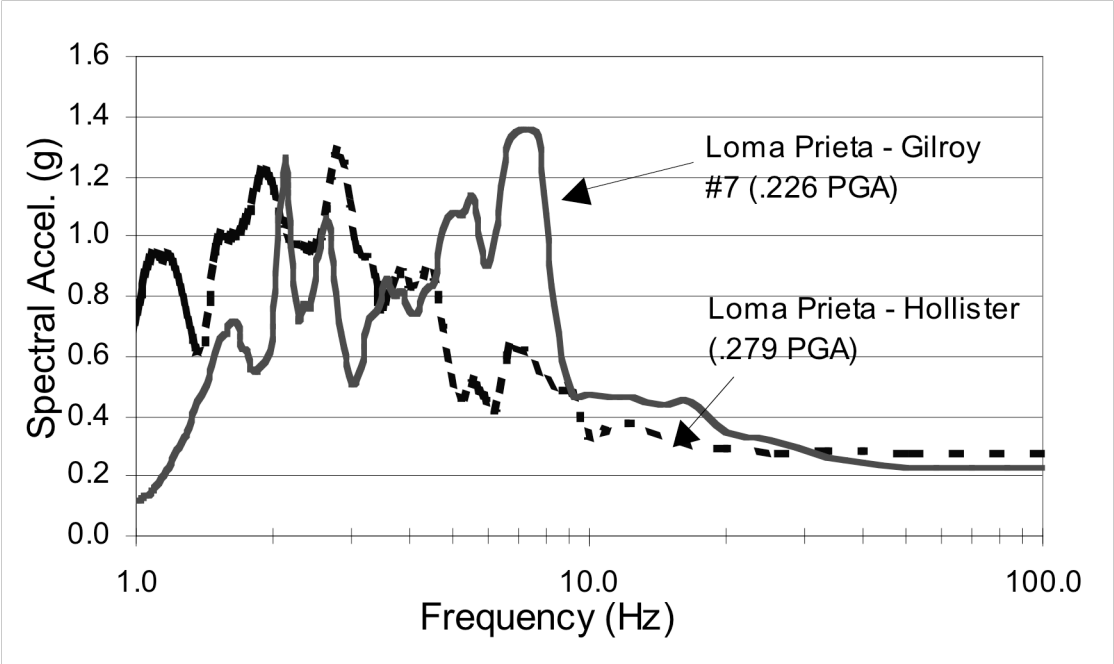

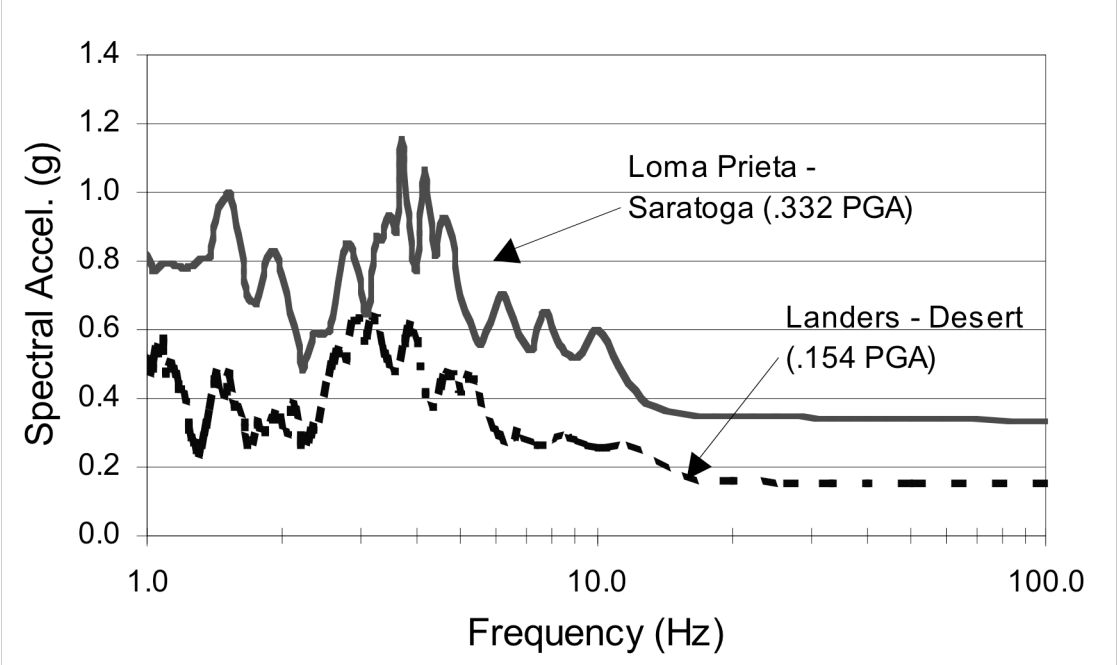

Appendix E –Ground Motion Response Spectra

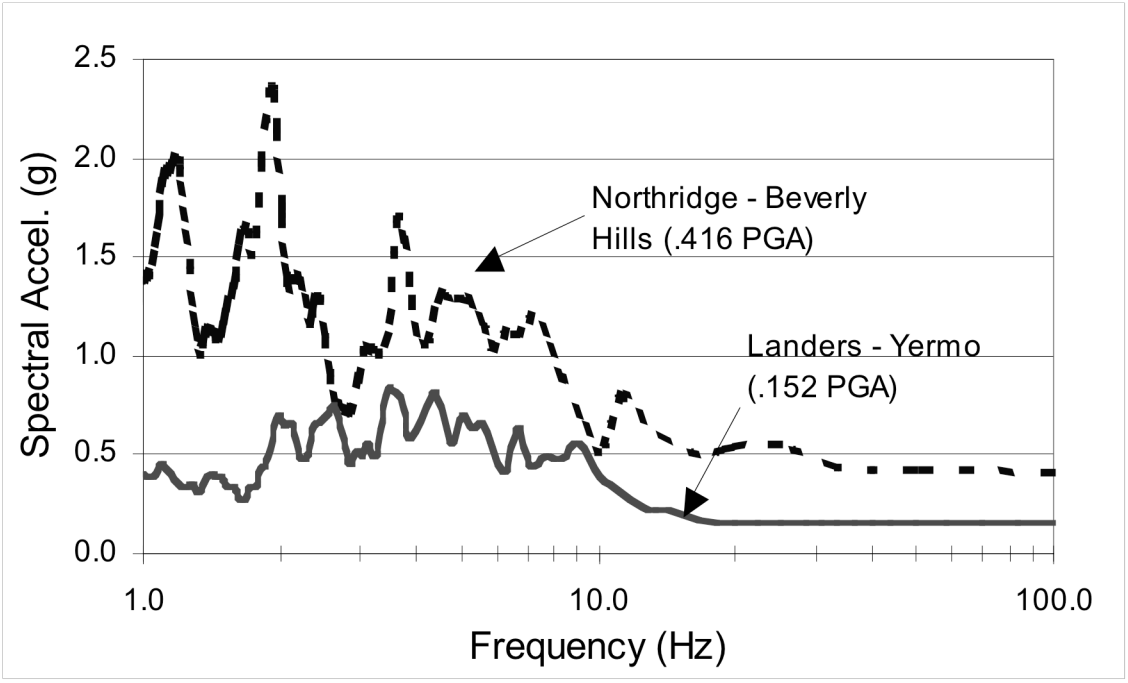

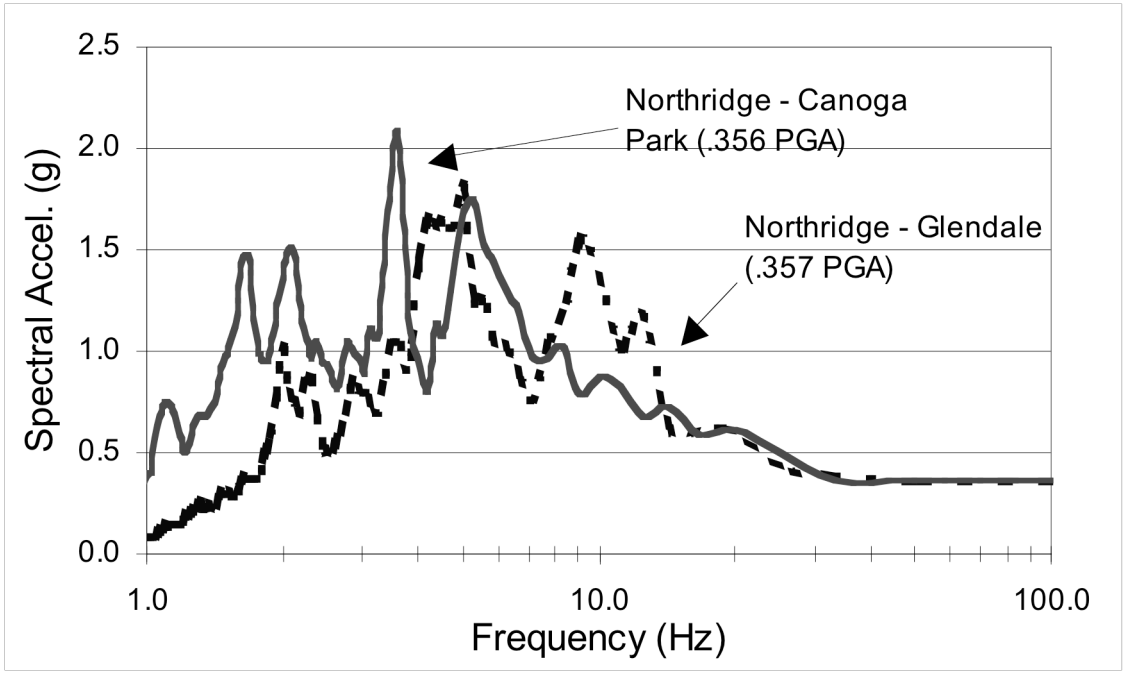

Appendix E –Ground Motion Response Spectra

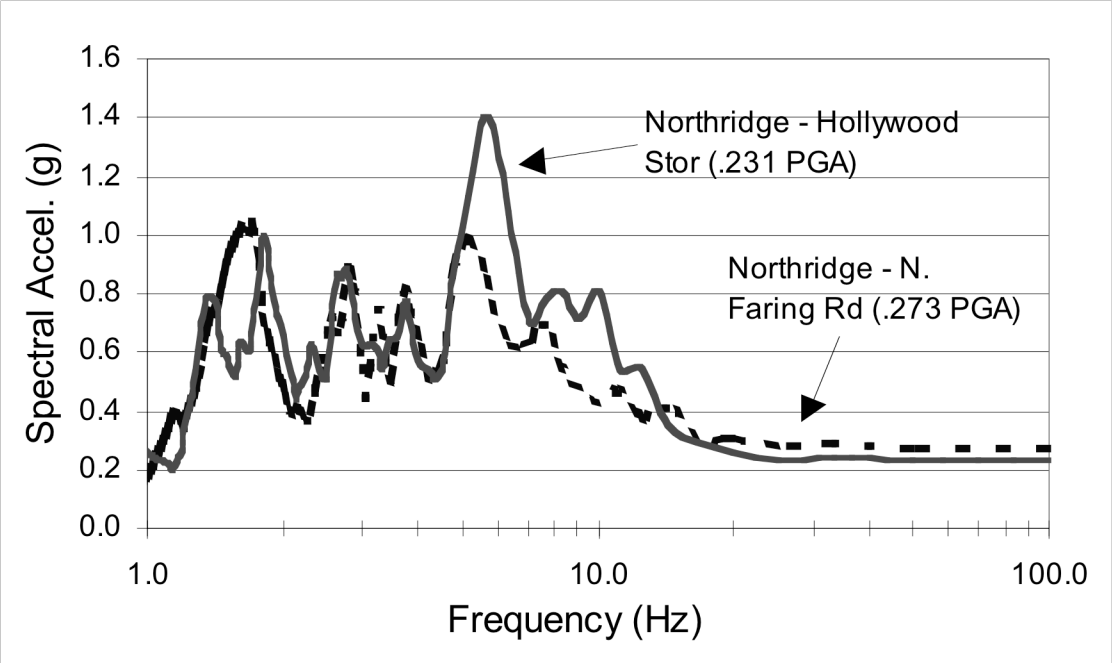

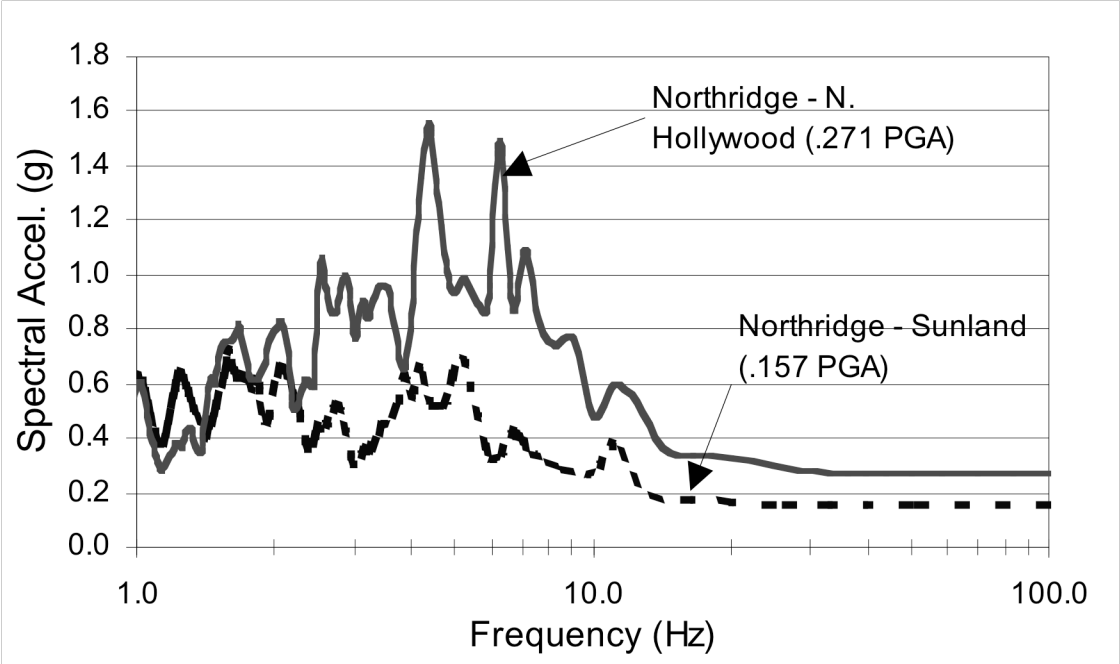

APPENDIX F: SCALED PEAK GROUND ACCELERATIONS

Appendix F – Scaled Peak Ground Accelerations

Earthquake Event	Station	525 kV Transformer A Transverse Scaled PGA (g)	525 kV Transformer A Longitudinal Scaled PGA (g)	500 kV Transformer B Transverse Scaled PGA (g)
Superstition Hills	Brawley	0.232	0.255	0.418
Superstition Hills	El Centro Imp. Co. Cent.	0.671	0.645	0.629
Superstition Hills	Plaster City	0.874	0.837	0.695
Northridge	Beverly Hills 14145 Mulhol	0.998	0.707	0.632
Northridge	Canoga Park - Topanga Can	0.570	0.545	0.466
Northridge	Glendale - Las Palmas	0.714	0.357	0.459
Northridge	LA - Hollywood Stor FF #	0.393	0.501	0.652
Northridge	LA - N Faring Rd	1.037	0.764	0.707
Northridge	N. Hollywood - Coldwater Can	0.678	0.596	0.644
Northridge	Sunland - Mt Gleason Ave	0.754	0.754	0.702
Loma Prieta	Capitola	0.582	0.635	0.490
Loma Prieta	Gilroy Array # 3	0.500	0.611	0.547
Loma Prieta	Gilroy Array # 4	1.001	0.917	0.744
Loma Prieta	Gilroy Array # 7	0.633	0.520	0.426
Loma Prieta	Hollister Diff. Array	1.060	0.809	0.734
Loma Prieta	Saratoga - W Valley Coll.	0.764	0.896	0.748
Cape Mendocino	Fortuna Fortuna Blvd #	0.766	0.931	0.704
Cape Mendocino	Rio Dell Overpass - FF #	0.847	0.770	0.722
Landers	Desert Hot Springs #	0.785	0.678	0.738
Landers	Yermo Fire Station #	0.486	0.699	0.728

Appendix F – Scaled Peak Ground Accelerations

Earthquake Event	Station	500 kV Transformer B Longitudinal Scaled PGA (g)	230 kV Transformer C Transverse Scaled PGA (g)	230 kV Transformer C Longitudinal Scaled PGA (g)
Superstition Hills	Brawley	0.470	0.203	0.411
Superstition Hills	El Centro Imp. Co. Cent.	0.203	0.216	0.210
Superstition Hills	Plaster City	0.527	0.669	0.572
Northridge	Beverly Hills 14145 Mulhol	0.439	0.623	0.523
Northridge	Canoga Park - Topanga Can	0.428	0.511	0.411
Northridge	Glendale - Las Palmas	0.463	0.412	0.422
Northridge	LA - Hollywood Stor FF #	0.540	0.503	0.632
Northridge	LA - N Faring Rd	0.523	0.482	0.421
Northridge	N. Hollywood - Coldwater Can	0.515	0.418	0.455
Northridge	Sunland - Mt Gleason Ave	0.543	0.501	0.657
Loma Prieta	Capitola	0.412	0.520	0.370
Loma Prieta	Gilroy Array # 3	0.478	0.623	0.593
Loma Prieta	Gilroy Array # 4	0.542	0.750	0.472
Loma Prieta	Gilroy Array # 7	0.413	0.569	0.452
Loma Prieta	Hollister Diff. Array	0.540	0.822	0.594
Loma Prieta	Saratoga - W Valley Coll.	0.524	0.588	0.488
Cape Mendocino	Fortuna Fortuna Blvd #	0.530	0.819	0.623
Cape Mendocino	Rio Dell Overpass - FF #	0.536	0.575	0.429
Landers	Desert Hot Springs #	0.544	0.526	0.504
Landers	Yermo Fire Station #	0.544	0.553	0.636

Appendix F – Scaled Peak Ground Accelerations

Earthquake Event	Station	500 kV Transformer D Transverse Scaled PGA (g)	500 kV Transformer D Longitudinal Scaled PGA (g)
Superstition Hills	Brawley	0.259	0.376
Superstition Hills	El Centro Imp. Co. Cent.	0.250	0.179
Superstition Hills	Plaster City	0.664	0.460
Northridge	Beverly Hills 14145	0.681	0.438
Northridge	Canoga Park - Topanga Can	0.469	0.436
Northridge	Glendale - Las Palmas	0.519	0.451
Northridge	LA - Hollywood Stor FF #	0.629	0.504
Northridge	LA - N Faring Rd	0.449	0.340
Northridge	N. Hollywood - Coldwater Can	0.538	0.388
Northridge	Sunland - Mt Gleason Ave	0.794	0.511
Loma Prieta	Capitola	0.526	0.348
Loma Prieta	Gilroy Array # 3	0.530	0.440
Loma Prieta	Gilroy Array # 4	0.578	0.373
Loma Prieta	Gilroy Array # 7	0.466	0.411
Loma Prieta	Hollister Diff. Array	0.691	0.458
Loma Prieta	Saratoga - W Valley Coll.	0.624	0.373
Cape Mendocino	Fortuna Fortuna Blvd #	0.754	0.459
Cape Mendocino	Rio Dell Overpass - FF #	0.534	0.316
Landers	Desert Hot Springs #	0.577	0.397
Landers	Yermo Fire Station #	0.652	0.497

APPENDIX G: MODAL RESULTS OF RETROFITED TRANFORMERS

Appendix G – Modal Results of Retrofit

Natural Frequencies, Mode Shape Descriptions, and Modal Mass Participation for Modes Considered in 230 kV Transformer C Analysis (Retrofit Scheme 1)

Mode	Frequency (Hz)	Description	Individual Mode (% Participation)		Cumulative Mode (% Participation Summation)	
			Transverse	Longitudinal	Transverse	Longitudinal
1	10.3	Transformer Frame (Tran)	54.7	0.0	54.7	0.0
2	12.0	Oil Conservator Tank (Vertical)	0.1	10.8	54.7	10.9
3	12.7	H.V. Bushings (Tran)	2.8	0.1	57.5	10.9
4	13.5	H.V. Bushings (2nd Mode Tran)	0.0	0.0	57.5	10.9
5	15.3	H.V. Bushings (Long)	0.0	2.4	57.5	13.3
6	16.7	Oil Conservator Tank + Transformer (Tran)	12.1	0.1	69.6	13.4
7	18.6	H.V. Bushings (2nd Mode Long)	4.4	0.2	73.9	13.6
8	18.9	H.V. Bushings + Transformer	4.4	1.1	78.3	14.7
9	22.9	H.V. Bushings + Transformer	7.5	0.4	85.8	15.1
10	25.1	Transformer Frame (Long)	0.2	61.5	86.0	76.6
11	27.0	N.A.	4.7	0.5	90.7	77.1
12	39.0	N.A.	2.3	0.0	93.0	77.1
13	39.7	N.A.	0.0	10.5	93.0	87.7
14	42.3	N.A.	0.1	3.8	93.1	91.5

Appendix G – Modal Results of Retrofit

Natural Frequencies, Mode Shape Descriptions, and Modal Mass Participation for Modes Considered in 525 kV Transformer A Analysis (Retrofit Scheme 2)

Mode	Frequency (Hz)	Description	Individual Mode (% Participation)		Cumulative Mode (% Participation Summation)	
			Transverse	Longitudinal	Transverse	Longitudinal
1	12.1	Oil Conservator Tank (Vertical)	0.2	10.0	0.2	10.0
2	12.4	H.V. Bushings (Tran)	3.3	0.0	3.4	10.0
3	13.5	H.V. Bushings (2nd Mode Tran)	0.3	0.0	3.7	10.0
4	14.4	Oil Conservator Tank (Tran)	17.4	0.0	21.1	10.0
5	15.4	H.V. Bushings (3rd Mode Tran)	0.0	2.0	21.1	12.0
6	17.5	H.V. Bushings (Long)	0.7	0.9	21.7	13.0
7	18.6	H.V. Bushings	0.1	0.1	21.8	13.0
8	21.5	Transformer Frame (Tran)	65.4	0.0	87.2	13.1
9	24.0	Transformer tank + Bushings	0.9	1.9	88.1	15.0
10	25.7	Transformer Frame (Long)	0.0	65.1	88.1	80.1
11	31.0	N.A.	1.6	1.5	89.7	81.6
12	42.4	N.A.	0.2	7.7	89.9	89.4
13	45.0	N.A.	0.0	1.7	89.9	91.0
14	58.4	N.A.	2.4	0.3	92.3	91.3

APPENDIX H: MEAN RESPONSE SPECTRA RESULTS FOR RETROFITTED TRANSFORMERS

Appendix H – Mean Response Spectrum Results of Retrofit

230 kV Transformer C Mean Response Spectrum Results in Transverse Direction (Retrofit Scheme 1)

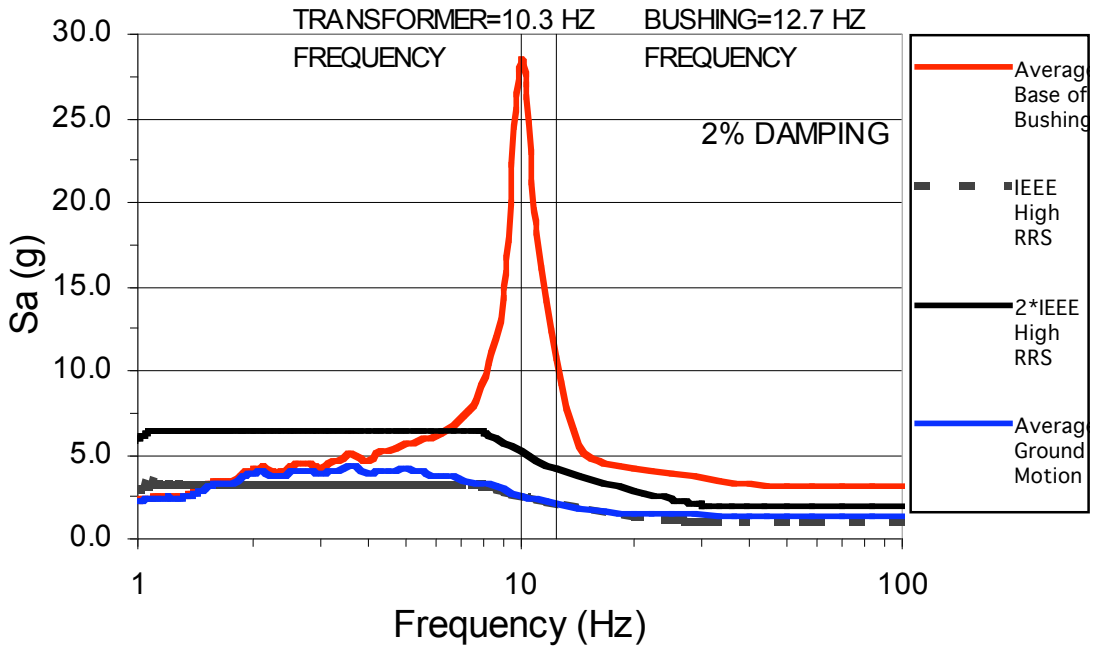

Siemens 230 kV Mean Response Spectrum Results in Longitudinal Direction (Retrofit Scheme 1)

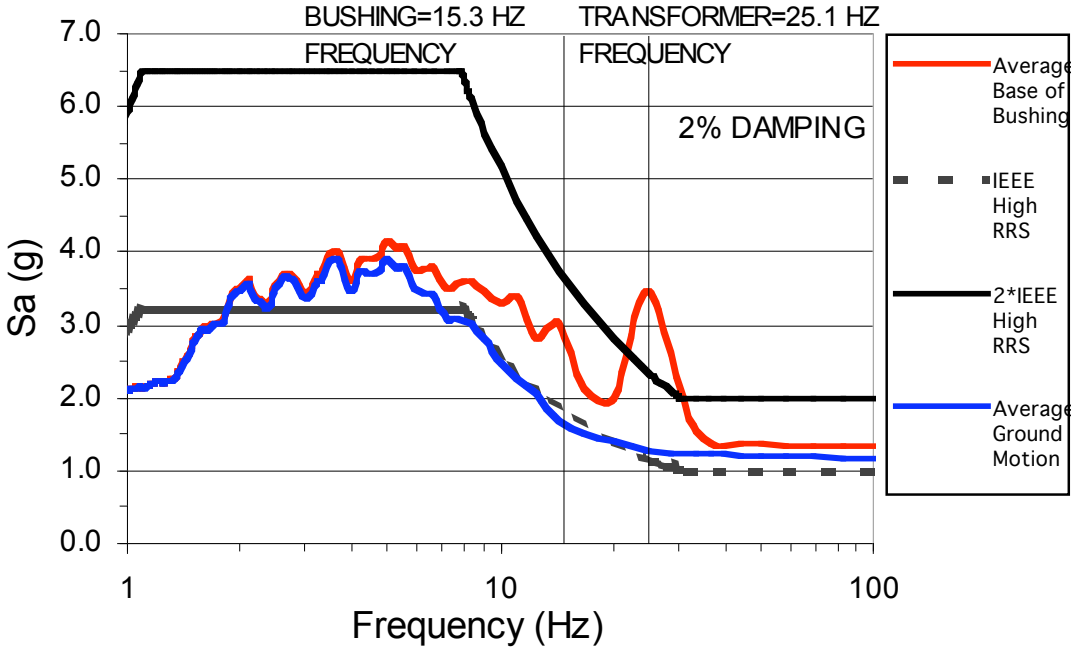

Appendix H – Mean Response Spectrum Results of Retrofit

230 kV Transformer C Mean Response Spectrum Results in Transverse Direction (Retrofit Scheme 2)

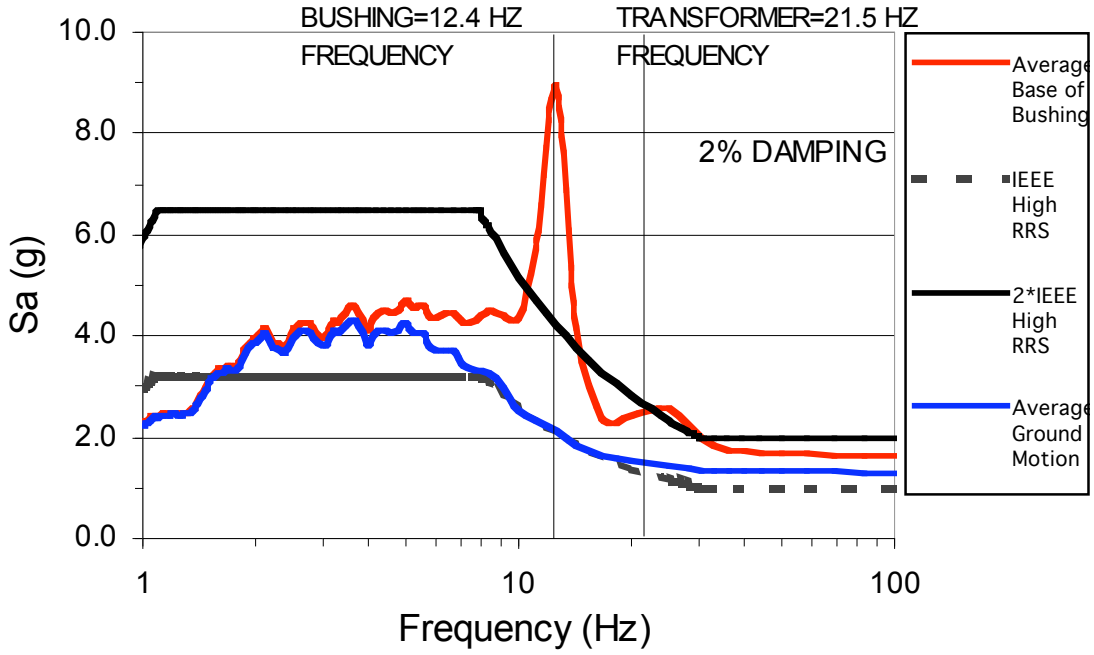

Siemens 230 kV Mean Response Spectrum Results in Longitudinal Direction (Retrofit Scheme 2)

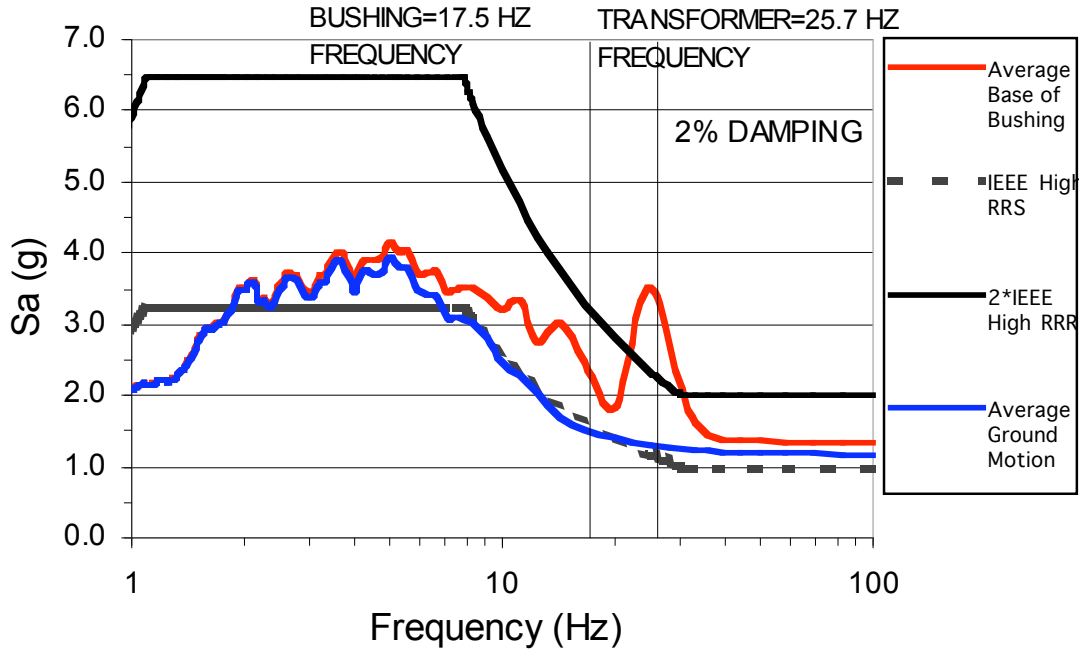

APPENDIX I: INSTRUMENTATION DETAILS

Appendix I – Instrumentation Details

Instrument	Measurement	Physical Location (overhead observer)	Positive Direction of Measurement
A1	Shake Table Absolute Acceleration, North-South Direction	Shake Table	South
A2	Transformer Absolute Acceleration, North-South Direction	Middle of Transformer (South-West)	South
A3	Transformer Absolute Acceleration, North-South Direction	Middle of Transformer (South-East)	South
A4	Transformer Absolute Acceleration, North-South Direction	Upper half of tank (South-West)	South
A5	Transformer Absolute Acceleration, North-South Direction	Upper half of tank (South-East)	South
A6	Transformer Absolute Acceleration, North-South Direction	Top of Tank (South-West)	South
A7	Transformer Absolute Acceleration, North-South Direction	Top of Tank (South-East)	South
A8	Transformer Absolute Acceleration, East-West Direction	Middle of Transformer (West-South)	East
A9	Transformer Absolute Acceleration, East-West Direction	Middle of Transformer (West-North)	East
A10	Transformer Absolute Acceleration, East-West Direction	Upper half of tank (West-North)	East
A11	Transformer Absolute Acceleration, East-West Direction	Upper half of tank (West-South)	East
A12	Transformer Absolute Acceleration, East-West Direction	Top of Tank (West-North)	East
A13	Transformer Absolute Acceleration, East-West Direction	Top of Tank (West-South)	East
A14	Mock Bushing Absolute Acceleration, North-South Direction	Bottom of Bushing	North
A15	Mock Bushing Absolute Acceleration, North-South Direction	Top of Bushing	North
A16	Mock Bushing Absolute Acceleration, North-South Direction	Concrete Block (West)	North
A17	Mock Bushing Absolute Acceleration, East-West Direction	Concrete Block (South)	East
A18	Turret Absolute Acceleration, East-West Direction	Turret (West-Top)	West
A19	Turret Absolute Acceleration, Vertical Direction	Turret (West-Top)	Up
A20	Turret Absolute Acceleration, North-South Direction	Turret (North-Top)	South
A21	Turret Absolute Acceleration, Vertical Direction	Turret (North-Top)	Down
A22	Turret Absolute Acceleration, East-West Direction	Turret (East-Top)	West
A23	Turret Absolute Acceleration, Vertical Direction	Turret (East-Top)	Down
A24	Turret Absolute Acceleration, North-South Direction	Turret (South-Top)	North
A25	Turret Absolute Acceleration, Vertical Direction	Turret (South-Top)	Up
P1	Relative Displacement of Top Plate, Vertical Direction	Transformer Top Plate	Inward buckling of plate
P2	Relative Displacement of Top Plate, Vertical Direction	Transformer Top Plate	Inward buckling of plate
P3	Relative Displacement of Top Plate, Vertical Direction	Transformer Top Plate	Inward buckling of plate
P4	Relative Displacement of Top Plate, Vertical Direction	Transformer Top Plate	Inward buckling of plate
P5	Relative Displacement of Top Plate, Vertical Direction	Transformer Top Plate	Inward buckling of plate
P6	Relative Displacement of Top Plate, Vertical Direction	Transformer Top Plate	Inward buckling of plate
P7	Relative Displacement of Top Plate, Vertical Direction	Transformer Top Plate	Inward buckling of plate
P8	Relative Displacement of Top Plate, Vertical Direction	Transformer Top Plate	Inward buckling of plate
P9	Relative Displacement of Turret, Vertical Direction	Top of Turret	Upward rocking of turret
P10	Relative Displacement of Turret, Vertical Direction	Top of Turret	Upward rocking of turret
P11	Relative Displacement of Turret, Vertical Direction	Top of Turret	Upward rocking of turret
P12	Relative Displacement of Turret, Vertical Direction	Top of Turret	Upward rocking of turret
S1-90	Top Plate Strain	Base of Turret (NorthWest)	Tension
S1-45	Top Plate Strain	Base of Turret (NorthWest)	Tension
S1-0	Top Plate Strain	Base of Turret (NorthWest)	Tension
S2-90	Turret Strain	Base of Turret (NorthWest)	Tension
S2-45	Turret Strain	Base of Turret (NorthWest)	Tension
S2-0	Turret Strain	Base of Turret (NorthWest)	Tension
S3-90	Top Plate Strain	Base of Turret (SouthWest)	Tension
S3-45	Top Plate Strain	Base of Turret (SouthWest)	Tension
S3-0	Top Plate Strain	Base of Turret (SouthWest)	Tension
S4-90	Turret Strain	Base of Turret (SouthWest)	Tension
S4-45	Turret Strain	Base of Turret (SouthWest)	Tension
S4-0	Turret Strain	Base of Turret (SouthWest)	Tension
S5-90	Top Plate Strain	Base of Turret (SouthEast)	Tension
S5-45	Top Plate Strain	Base of Turret (SouthEast)	Tension
S5-0	Top Plate Strain	Base of Turret (SouthEast)	Tension
S6-90	Turret Strain	Base of Turret (SouthEast)	Tension
S6-45	Turret Strain	Base of Turret (SouthEast)	Tension
S6-0	Turret Strain	Base of Turret (SouthEast)	Tension
S7-90	Top Plate Strain	Base of Turret (NorthEast)	Tension
S7-45	Top Plate Strain	Base of Turret (NorthEast)	Tension
S7-0	Top Plate Strain	Base of Turret (NorthEast)	Tension
S8-90	Turret Strain	Base of Turret (NorthEast)	Tension
S8-45	Turret Strain	Base of Turret (NorthEast)	Tension
S8-0	Turret Strain	Base of Turret (NorthEast)	Tension
S9	Mock Bushing Bending Strain	Base of Steel Tube (NorthWest)	Tension
S10	Mock Bushing Bending Strain	Base of Steel Tube (NorthEast)	Tension
S11	Mock Bushing Bending Strain	Base of Steel Tube (SouthWest)	Tension
S12	Mock Bushing Bending Strain	Base of Steel Tube (SouthEast)	Tension
S13	Mock Bushing Bending Strain	Base of Steel Tube (South)	Tension
S14	Mock Bushing Bending Strain	Base of Steel Tube (North)	Tension
D1	Transformer Absolute Displacement, North-South Direction	Shake Table	North
D2	Transformer Absolute Displacement, North-South Direction	Middle of Transformer (South-West)	North
D3	Transformer Absolute Displacement, North-South Direction	Middle of Transformer (South-East)	North
D4	Transformer Absolute Displacement, North-South Direction	Upper half of tank (South-West)	North
D5	Transformer Absolute Displacement, North-South Direction	Upper half of tank (South-East)	North
D6	Transformer Absolute Displacement, North-South Direction	Top of Tank (South-West)	North

APPENDIX J: ABSOLUTE ACCELERATION RESPONSE SPECTRA OF GROUND MOTIONS USED FOR SHAKE TABLE TESTING

Appendix J - Absolute Acceleration Response Spectra of Ground Motions Used for Shake Table Testing.

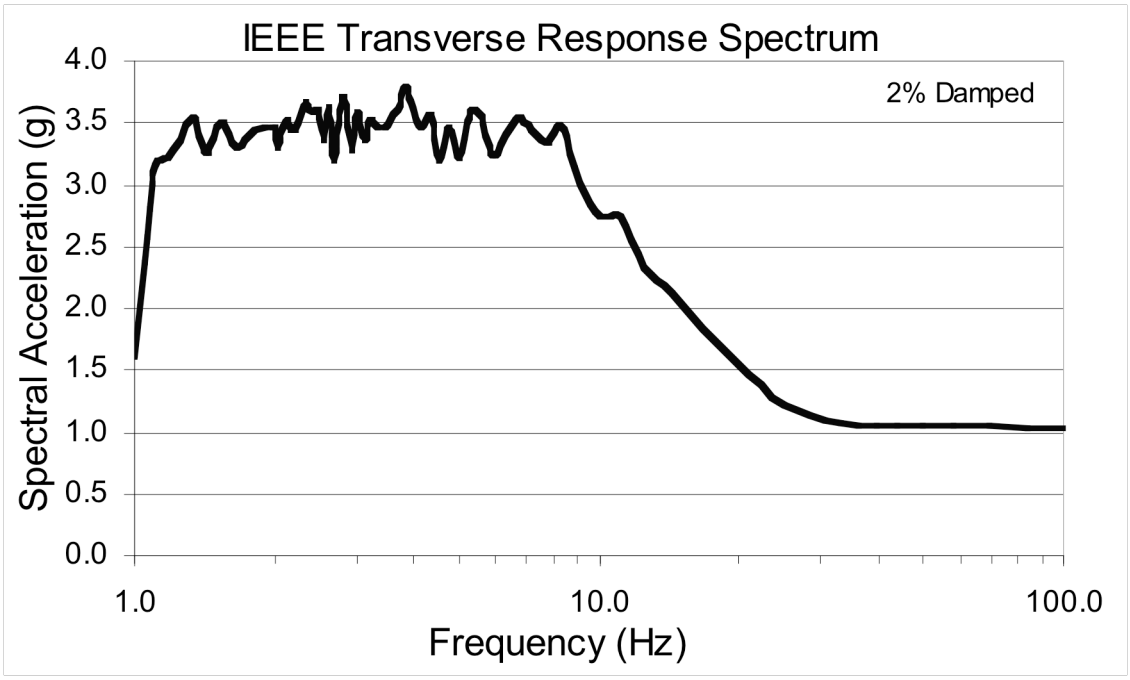

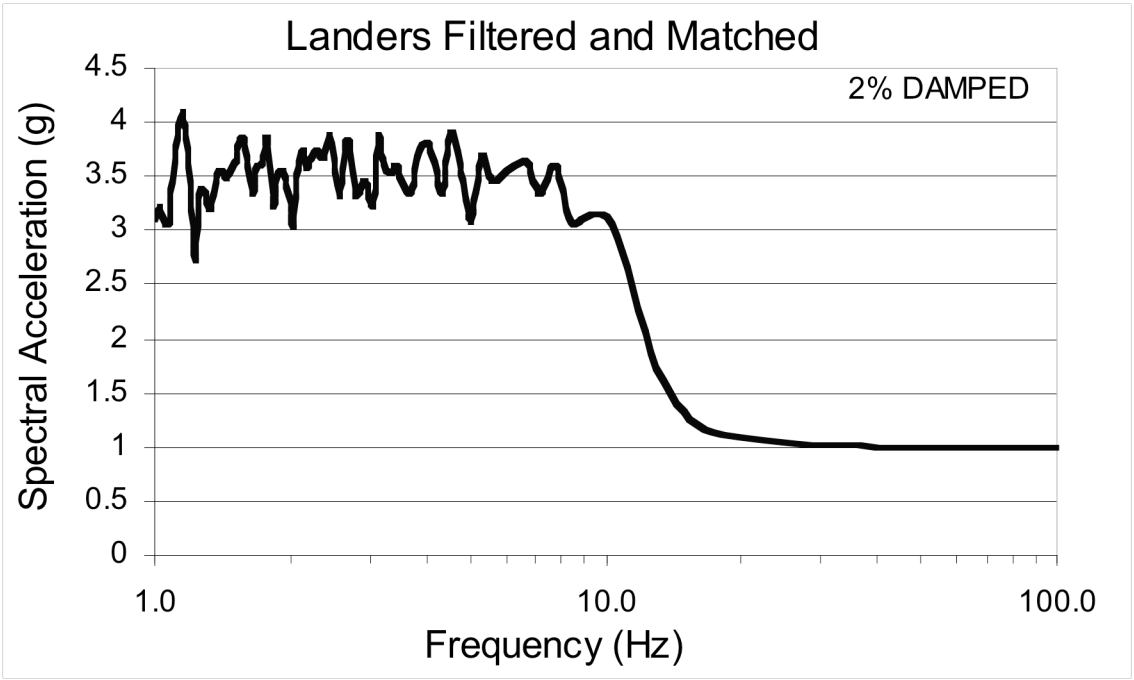

Appendix J - Absolute Acceleration Response Spectra of Ground Motions Used for Shake Table Testing.

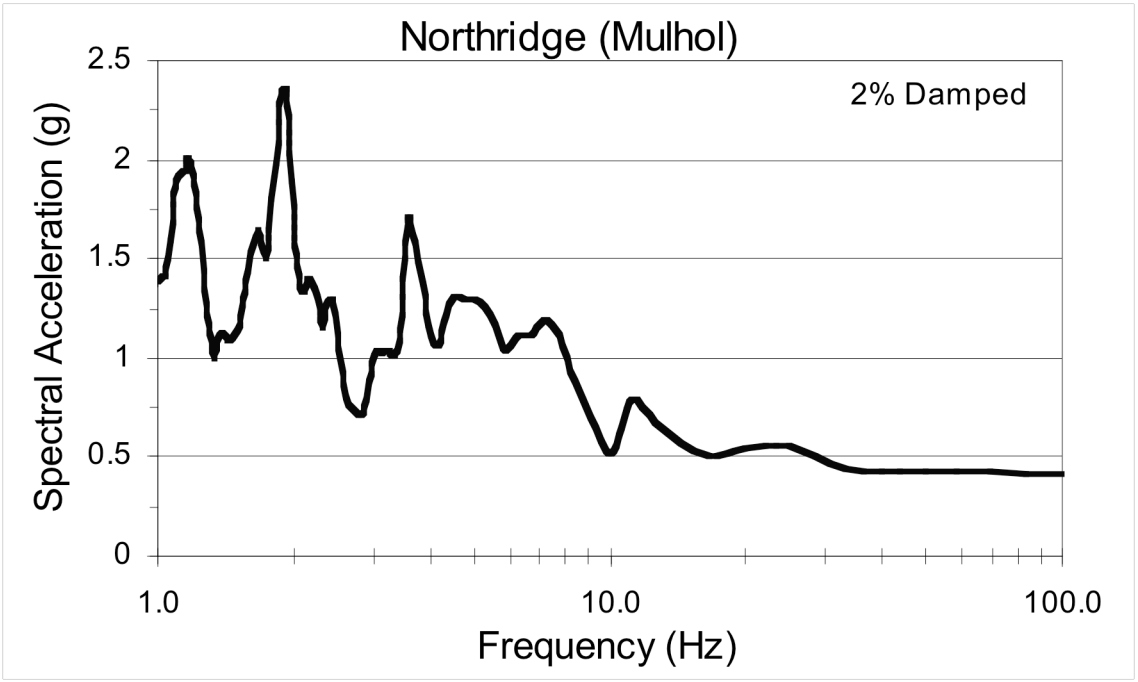

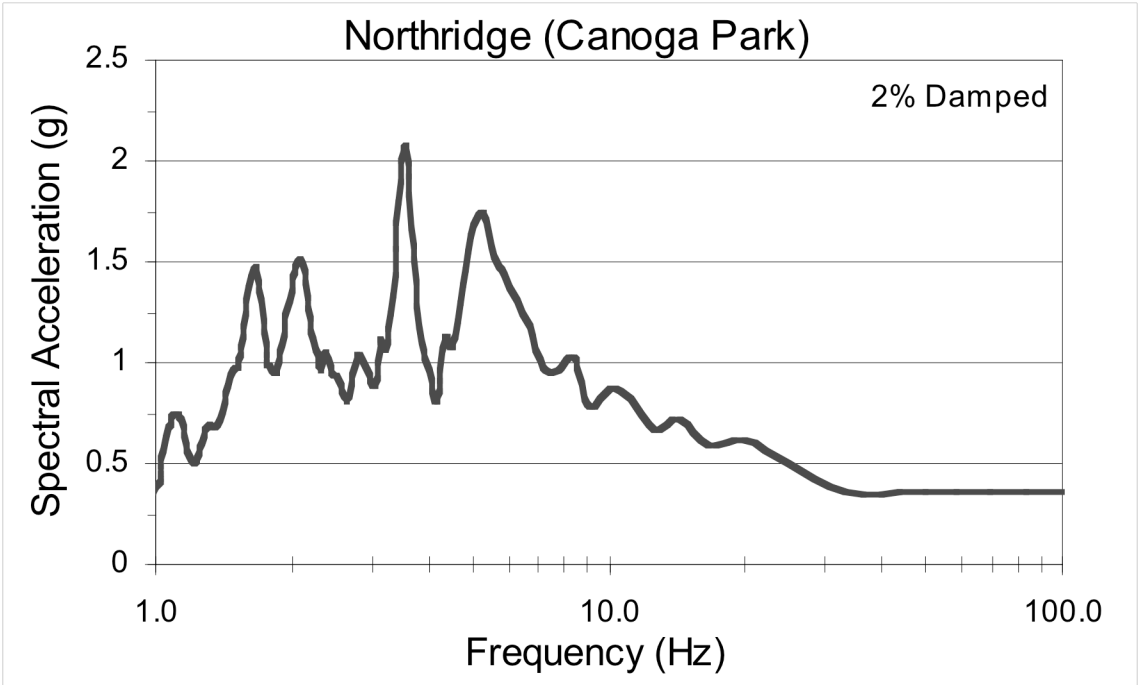

Appendix J - Absolute Acceleration Response Spectra of Ground Motions Used for Shake Table Testing.

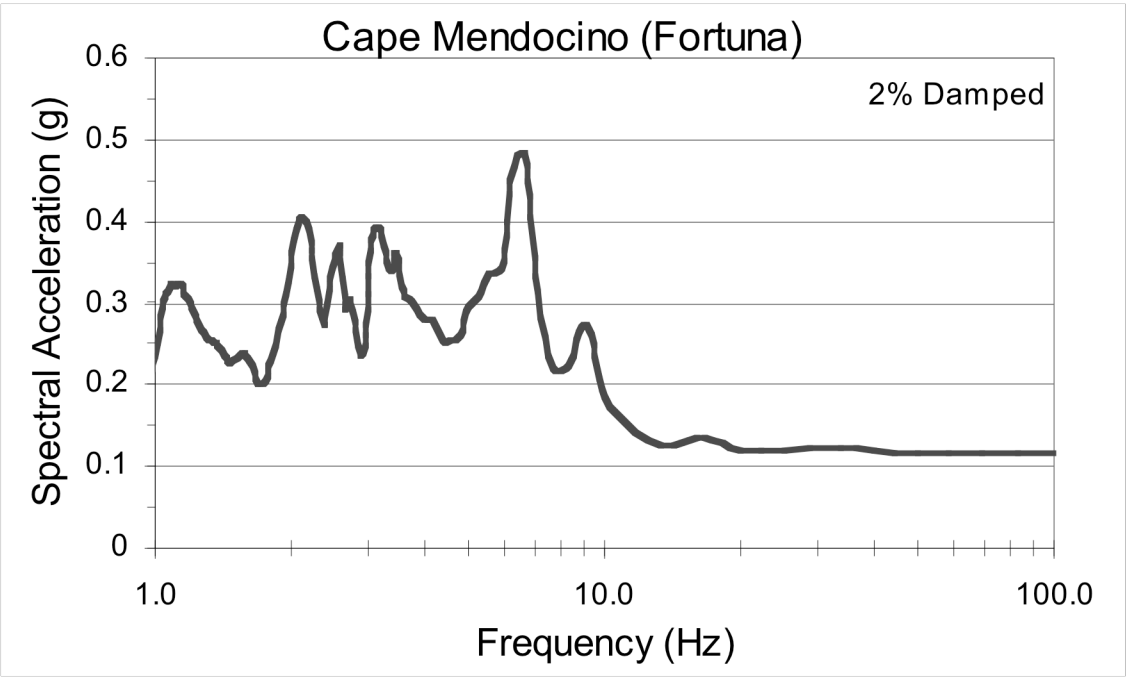

APPENDIX K – DESIRED AND FEEDBACK SHAKE TABLE RESPONSE SPECTRA

Appendix K – Desired and Feedback Shake Table Response Spectra (10% PGA)

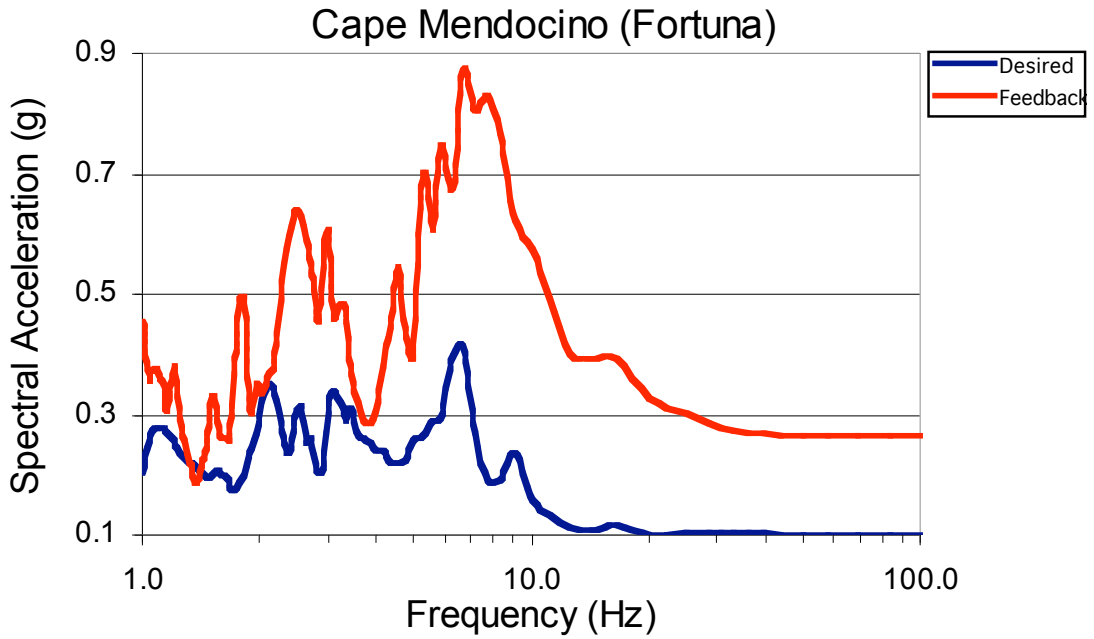

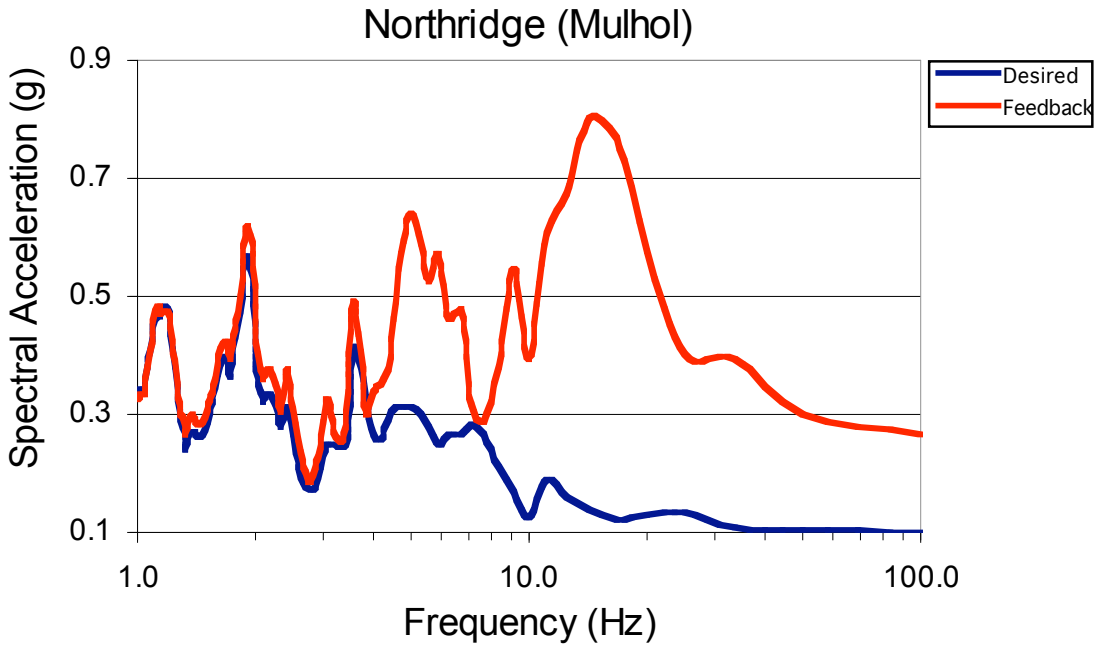

Appendix K – Desired and Feedback Shake Table Response Spectra (10% PGA)

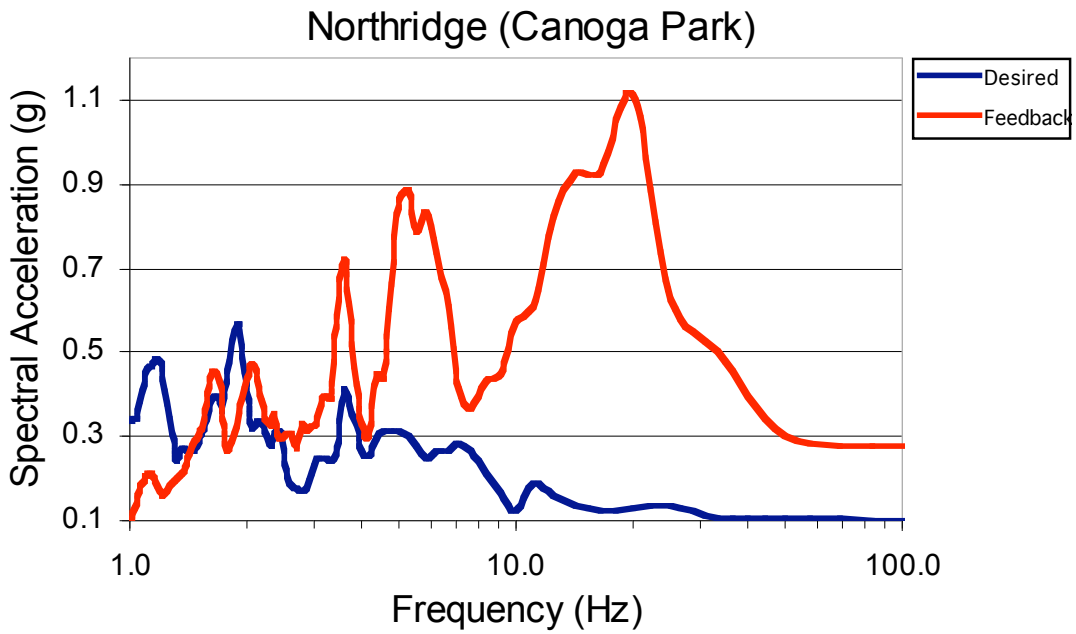

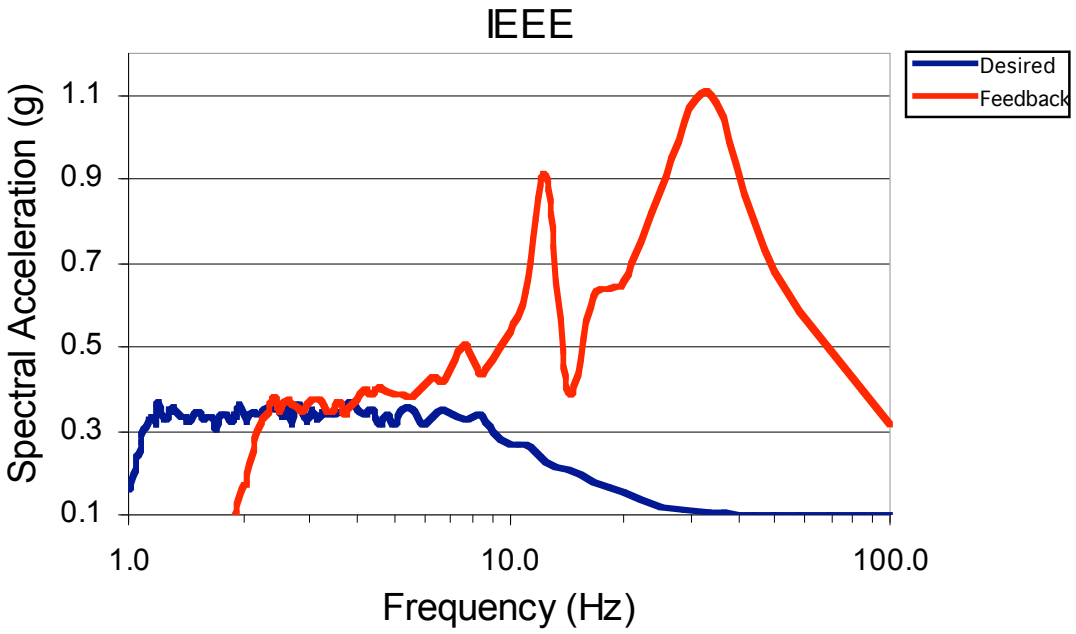

Appendix K – Desired and Feedback Shake Table Response Spectra (10% PGA)

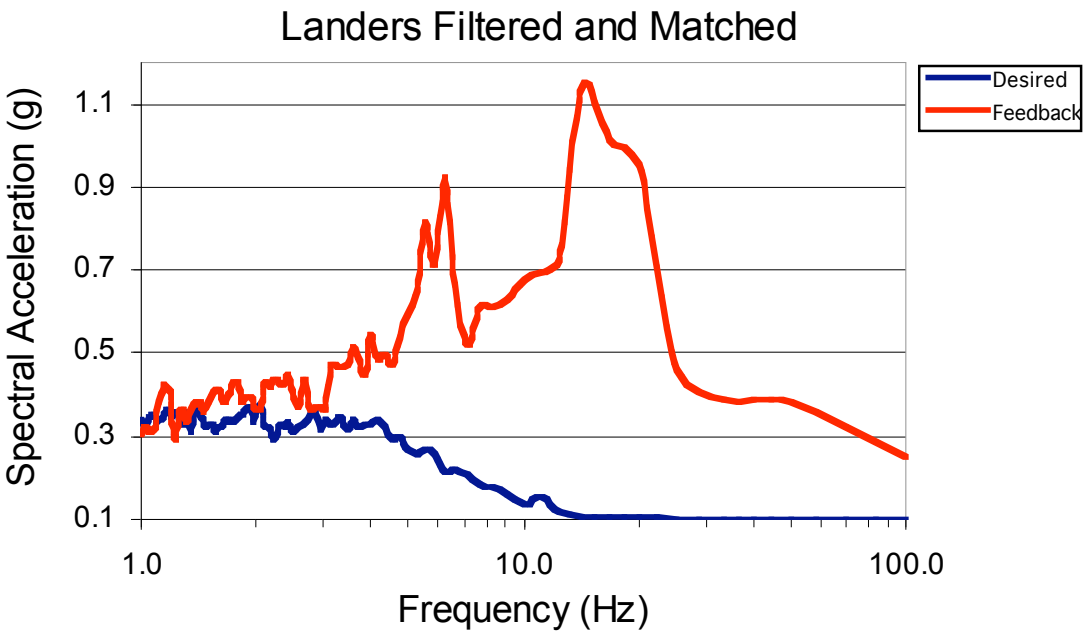

Appendix K – Desired and Feedback Shake Table Response Spectra (25% PGA)

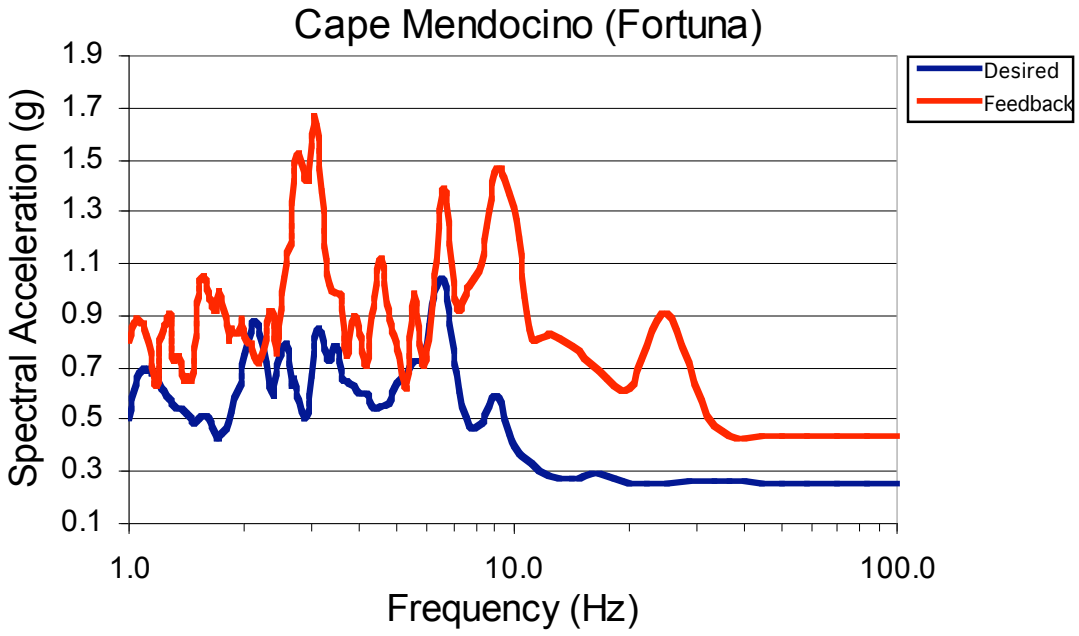

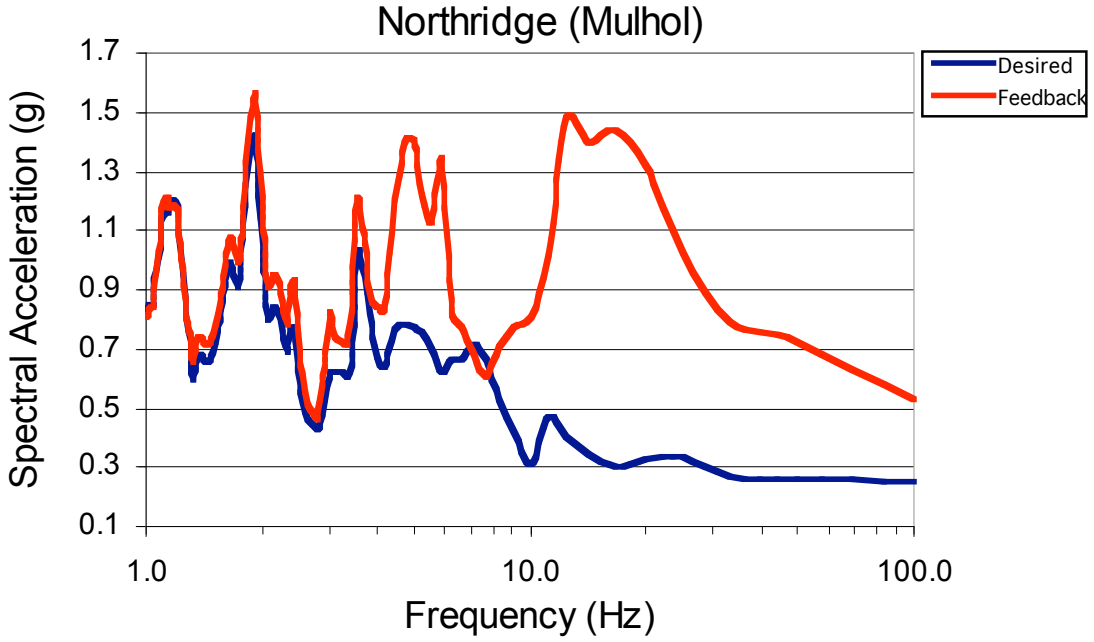

Appendix K – Desired and Feedback Shake Table Response Spectra (25% PGA)

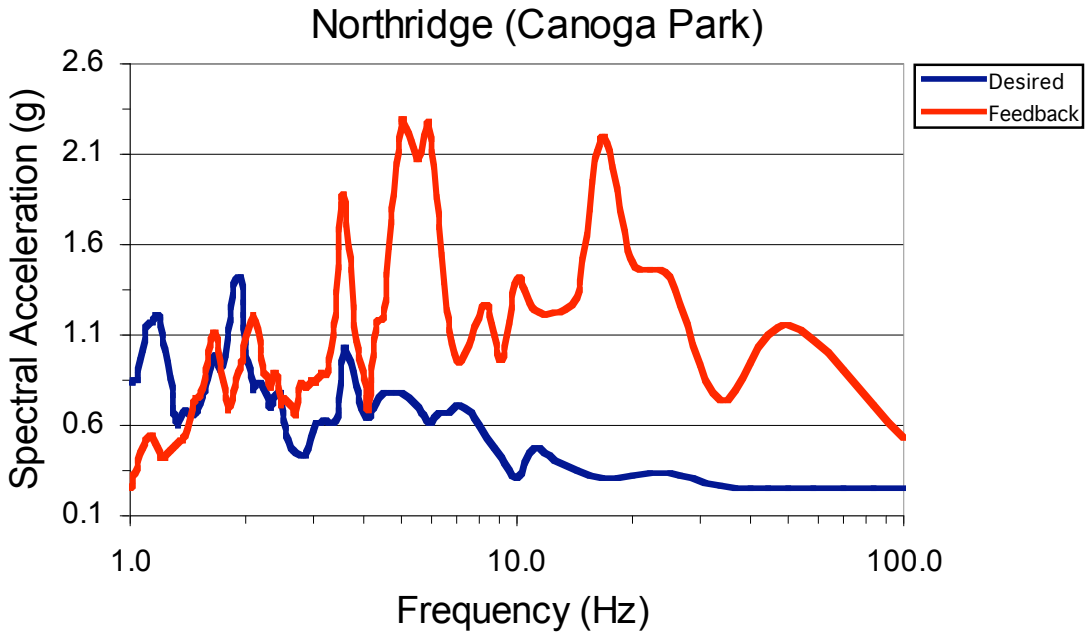

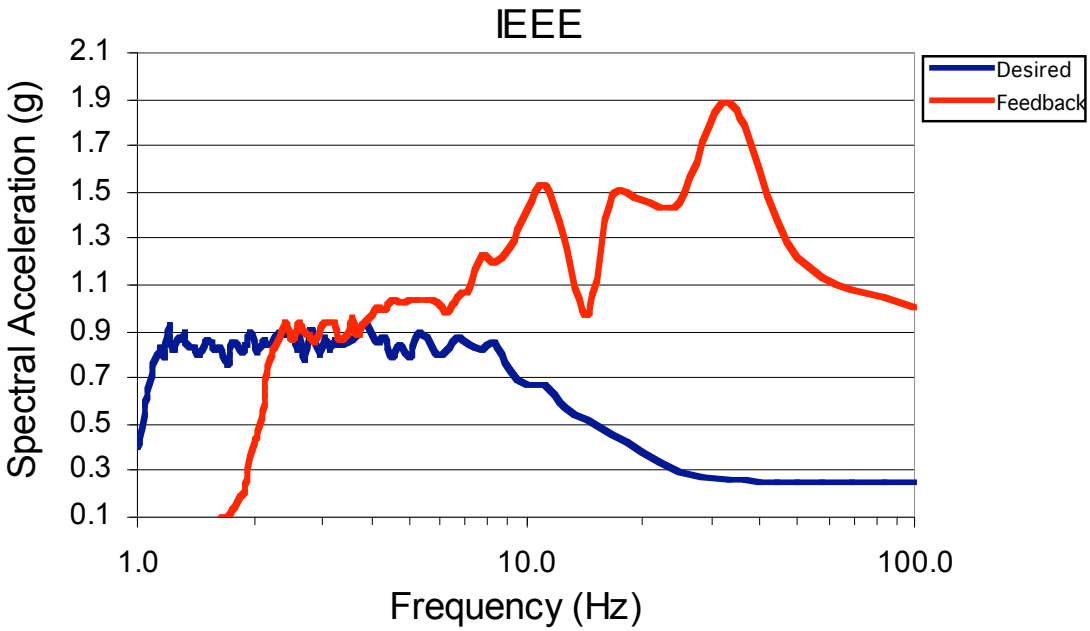

Appendix K – Desired and Feedback Shake Table Response Spectra (25% PGA)

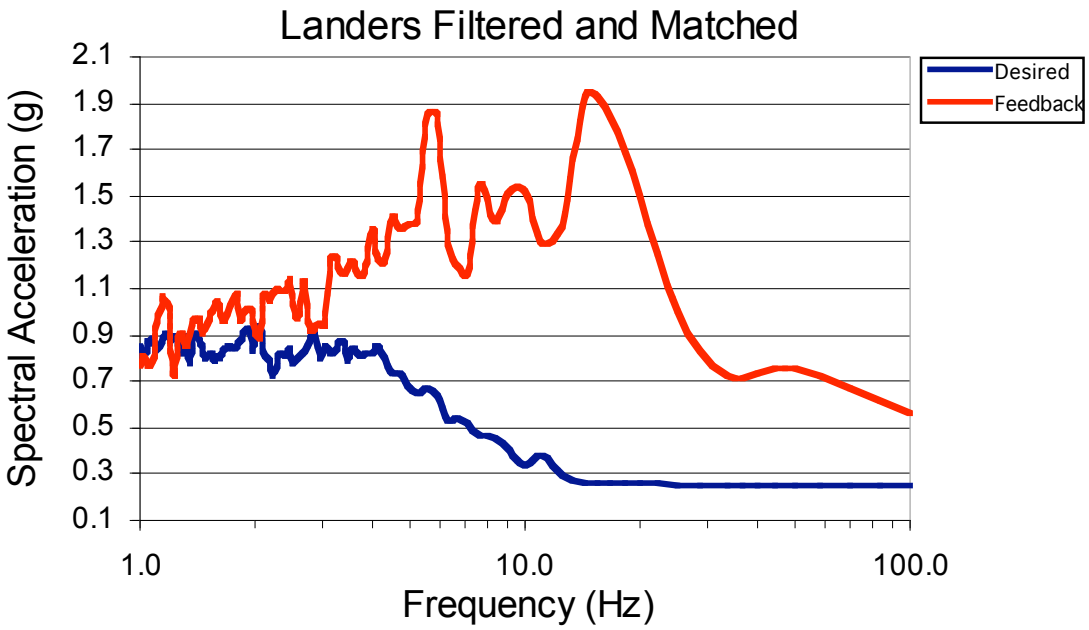

APPENDIX L – COMPARISON BETWEEN NUMERICAL AND EXPERIMENTAL RESULTS

Appendix L – Comparison of Numerical and Experimental Results

Northridge (Canoga Park)

Experimental

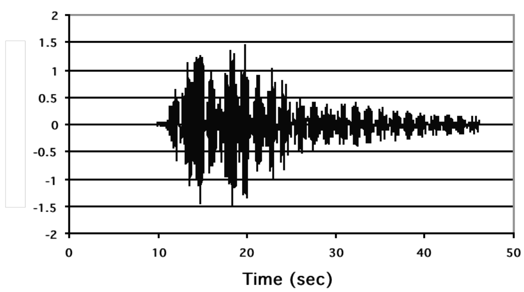

Numerical

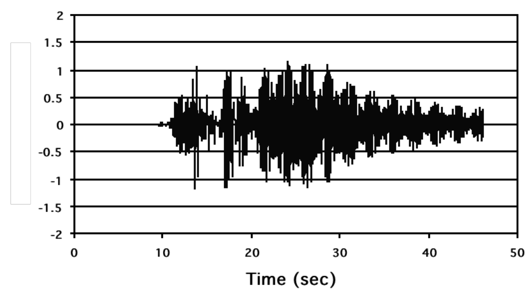

Experimental

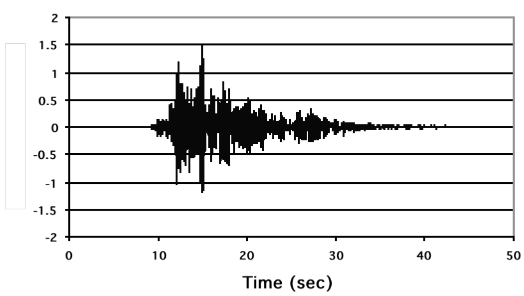

Numerical

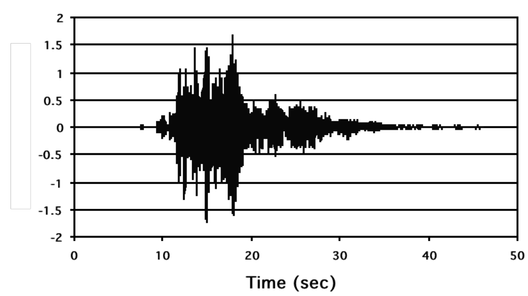

Experimental

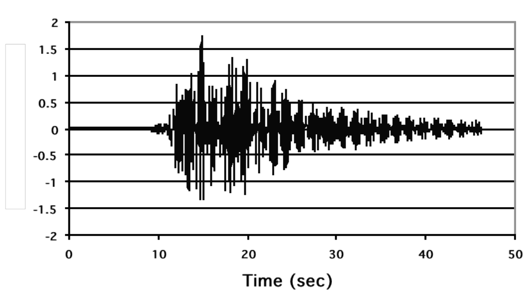

Numerical

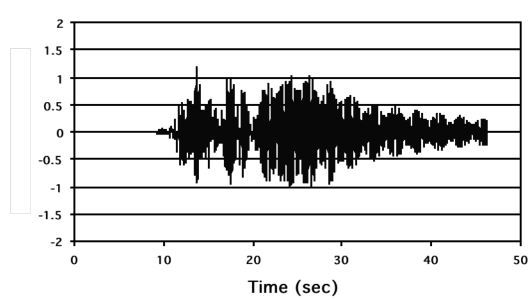

Appendix L – Comparison of Numerical and Experimental Results

Landers

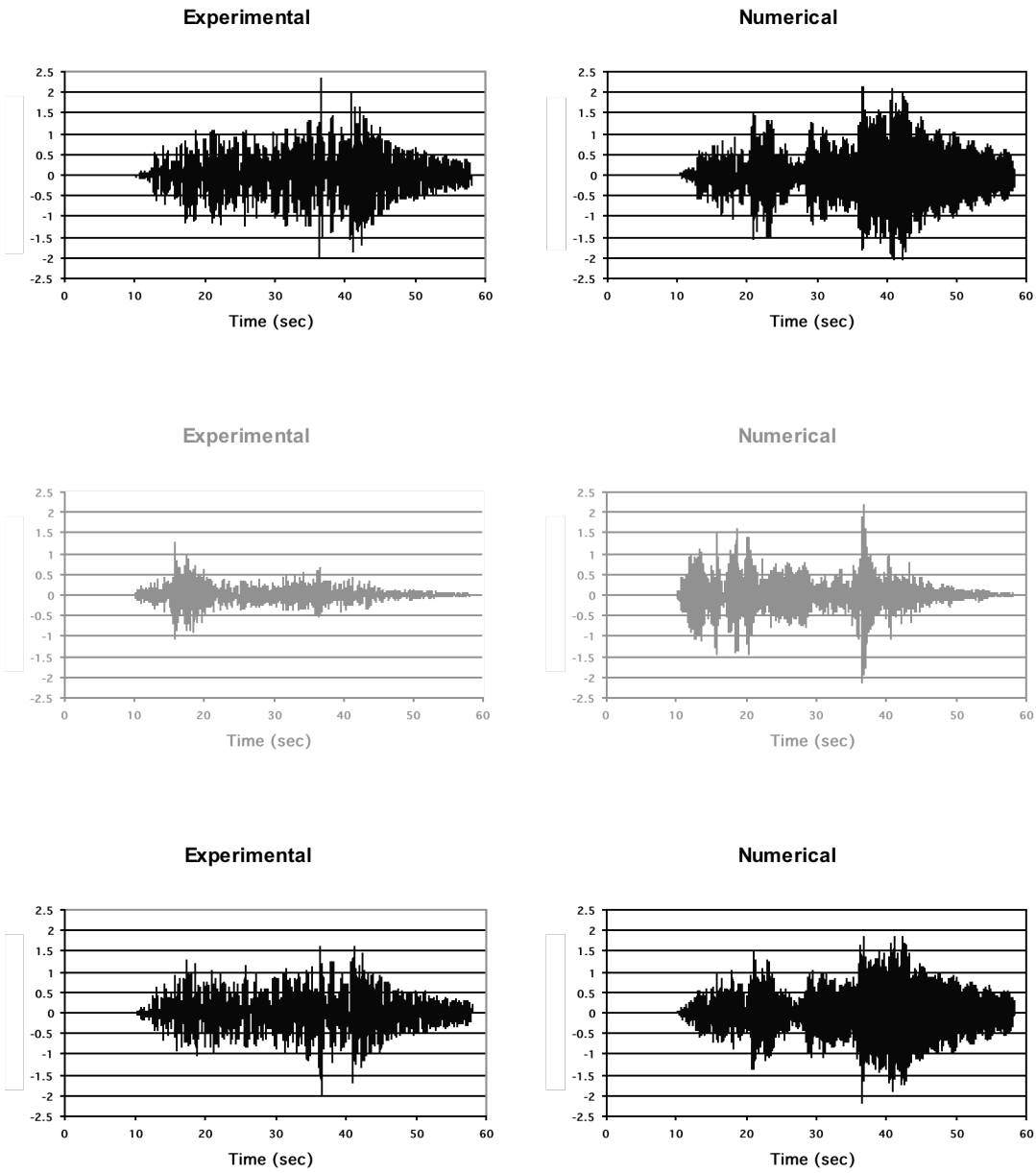

Appendix L – Comparison of Numerical and Experimental Results

IEEE